

**Earthquake Geology
of the
Northern San Andreas Fault
Near
Point Arena, California**

**Dissertation by
Carol Seabury Prentice**

**In Partial Fulfillment of the Requirements
for the Degree of
Doctor of Philosophy**

**California Institute of Technology
Pasadena, California**

1989

(submitted December 1, 1988)

This dissertation is dedicated to the
spirit of the earth
whose restless nature I want to know better

And to the memory of
Michelle Amy Strull
who spent her last summer of good health
as field assistant for this project

Acknowledgments

This work was supported by the U.S. Geological Survey's National Earthquake Hazards Reduction Program (contract numbers 14-08-0001-61370, -61098, and -22011), the Geological Society of America, and by Grants-in-Aid of Research from Sigma Xi, The Scientific Research Society.

Thank you to the Charles Scaramella family for letting me dig up their pasture, and to all the wonderful people on the coast between Elk and Jenner who let me tromp across their property, collect samples and dig holes in the ground.

Many thanks to Mendocino College, especially Bob Wallen and Jim and Linda Riley, for generously allowing me the use of its facility at Point Arena while I was working in the area.

Thanks to the Mussen family for allowing me to camp on their property near Timber Cove while conducting field work.

Field assistance from Michelle Strull, Andy Thomas, Charlie Rubin, Mitzi Vernon and Will Reed is greatly appreciated.

Thanks especially to Kerry Sieh for infinite (almost) patience, the gift of "magic eyes," and the great care and attention to detail that he has taught me to appreciate and strive to acquire.

Thanks to Lee Silver for guidance and for allowing me into his lab to separate zircons from the tuff in the Ohlson Ranch Formation, and to Bob Sharp for moral support and guidance.

Thanks to Jim O'Donnell, the world's most wonderful librarian.

Thank you to Bud Burke, Fred Fischer, Frank Bickner and the crew from Humboldt State University (the Filler Family: John Catalona, Wendy Gerstel, Danny Hagans, Kevin O'Dea) for assistance in digging, describing and interpreting the soil pits. Thanks to Gary Carver for inspiration.

Jim Ingle graciously allowed me to use his lab at Stanford University to process samples for microfossils, identified them for me, and explained their significance.

Chuck Naeser of the U.S.G.S. in Denver kindly did the fission-track analysis on the zircons from the tuff in the Ohlson Ranch Formation.

Jan Mayne drafted the final versions of many of the figures, helped to improve many of the original drawings, and was ever generous with equipment, expertise and good advise.

Work in the trenches with Steve Wesnousky helped me to retain my sense of humor and taught me much about how to keep going in the face of adversity.

Special thanks to Larry Edwards, Henry Shaw, and Ray Weldon for helping me through the first hurdle of my oral exams.

This work might never have been completed without the extra support of the U.S. Geological Survey during the final months of writing; I am especially grateful to Tom Hanks.

And thanks to Christina Gallup, Andy Gaynor, Rob Ripperdan and Janet Teshima for invaluable assistance with the final assault.

There were so many people who, during the times when I didn't know where I would find the strength to complete this work, were willing, with love and caring, to give me the support I needed and to remind me that all such strength lies within:

Luciana Astiz	Jay Namson	Bob Sharp
Andy Gaynor	Liz Olson	Kerry Sieh
Connie Gold	Anita Owen	Michelle Strull
Nancy Grulke	Beth Prentice	Janet Teshima
Marian Hill-Rocha	Will Reed	Mitzi Vernon
Astrid Howard	Sally Rigden	Dominique Weis
Joy McKinney	Linda Riley	Jeni Sue Wilburn
Jackie Miles	Jim Riley	Martha Yoder
Michele Mussen		

ABSTRACT

The northern segment of the San Andreas fault last ruptured in 1906, producing the great San Francisco earthquake. This study involves the collection and interpretation of geologic data from the segment of the northern San Andreas fault near Point Arena, California, to determine the recurrence interval and slip rate of this segment of the fault.

Holocene sediments deposited on an alluvial fan preserve a record of prehistoric earthquakes near Point Arena, California. Excavations into the fan provided exposures of the sediments across the San Andreas fault zone. At least five earthquakes were recognized in the section. All of these occurred since the deposition of a unit that is approximately 2000 years old. Because deposition in this setting was intermittent and deposition of younger units involved the erosion of underlying units, it is likely that events occurred that were not recorded in the section. Radiocarbon dating of units in the section allows constraints to be placed on the dates of the earthquakes recognized. A buried Holocene (2356-2709 years old) channel has been offset a maximum of 64 ± 2 meters. This implies a maximum slip rate of 25.5 ± 2.5 mm/yr. These data suggest that the average recurrence interval for great earthquakes on this segment of the San Andreas fault is long - between about 200 and 400 years.

Offset marine terrace risers near Point Arena and an offset landslide near Fort Ross provide estimates of the average slip rate across the San Andreas fault since Late Pleistocene time. Near Fort Ross, a landslide has been offset approximately 1.7 km across the San Andreas fault. Radiocarbon analysis of charcoal from this deposit indicates that the landslide is older than 43,700 years. This implies a slip rate of less than 39 mm/yr. Correlation of two marine terrace risers across the San Andreas fault near Point Arena suggests offsets of approximately 1.5 and 2.5 km. The U-series age of a solitary coral, altitudinal spacing and correlation with known global high sea-level stands suggest

ages of 83,000 and 133,000 years for these surfaces, indicating slip rates of about 18-19 mm/yr since Late Pleistocene time.

Tentative correlation of the Pliocene Ohlson Ranch Formation in northwestern Sonoma County with deposits 50 km to the northwest near Point Arena, provides piercing points to use in calculation of a Pliocene slip rate for the northern San Andreas fault. A fission-track age of 3.3 ± 0.8 Ma was determined for zircons separated from a tuff collected from the Ohlson Ranch Formation. The geomorphology of the region, especially of the two major river drainages, supports the proposed 50 km Pliocene offset. This implies a Pliocene slip rate of at least 12-20 mm/yr.

These rates for different time periods imply that the slip rate of the northern San Andreas fault has not changed by more than a factor of two since Pliocene time. The rates also imply that much of the Pacific-North American plate motion must be accommodated on other structures at this latitude.

TABLE OF CONTENTS

Dedication.....	ii
Acknowledgments.....	iii
Abstract.....	vi
Chapter 1: Introduction	
Organization of the dissertation.....	1
Previous work.....	2
Summary of the geology of the Gualala block.....	5
Earthquake geology.....	9
Quaternary faults of the San Andreas system in northern California.....	10
References.....	16
Chapter 2: Late Holocene Slip Rate and Paleoseismic Events on the Northern San Andreas Fault Near Point Arena	
Abstract.....	23
Introduction.....	24
Previous work.....	27
Study site.....	32
Paleoseismic events.....	40
Offset channel.....	47
Radiocarbon analyses.....	49
Unit 45.....	56
Unit 40.....	57
Unit 30.....	57
Unit 20.....	60
Channel.....	60
Unit 10.....	61
Discussion.....	62
Recurrence interval.....	62
Slip rate.....	74
Summary and conclusions.....	75
References.....	77

Chapter 3: Late Pleistocene Slip Rate on the Northern San Andreas Fault

Abstract.....	81
Introduction.....	82
Study area.....	90
Offset landslide near Fort Ross.....	90
Pleistocene marine terraces near Point Arena.....	97
Introduction.....	97
Terraces near Point Arena.....	98
Area 1.....	101
Area 2.....	110
Area 3.....	119
Age estimates of the terraces.....	120
Offset across the San Andreas fault.....	140
Stream terraces of Alder Creek.....	143
Discussion.....	145
References.....	148

Chapter 4: The Ohlson Ranch Formation, Geomorphology of the Gualala and Garcia Rivers, and a Tentative Pliocene Slip Rate Across the Northern San Andreas Fault

Abstract.....	155
Introduction.....	156
Ohlson Ranch Formation.....	156
Introduction.....	156
Age and depositional environment.....	159
Pliocene surfaces and paleoshoreline.....	166
Gualala block.....	170
Gualala ridge and Pliocene marine deposits.....	170
Evolution of drainage morphology.....	173
Pliocene slip rate.....	182
References.....	185
Appendix A: Age versus total uplift graphs for area 3.....	187
Appendix B: Correspondence.....	246
Plates 1 through 4.....	In Pocket

CHAPTER 1: INTRODUCTION

ORGANIZATION OF THE DISSERTATION

This dissertation reports the results of three projects undertaken along the San Andreas fault in northern California. This segment of the San Andreas fault, when it last ruptured, in 1906, caused the great San Francisco earthquake. The primary goals of these projects have been to determine slip rates of the northern San Andreas fault for different intervals of time and to characterize and date paleoseismic events on this segment of the fault. These data help define the seismic hazard of this segment of the San Andreas fault.

Chapter 1 serves as a review of the geology and previous work in the area and outlines the neotectonic framework of the region of California between the San Francisco Bay area and Point Arena. Chapter 2 reports the results of excavations in Holocene material that exposed evidence of prehistoric seismic activity and yielded an estimate of the Late Holocene slip rate for the San Andreas fault near Point Arena. Chapter 3 discusses Pleistocene features that are offset across the San Andreas between Fort Ross and Point Arena. Study of these features provided estimates of the fault's average slip rate since Late Pleistocene time. Chapter 4 discusses the Ohlson Ranch Formation of northwestern Sonoma County and its possible offset equivalent near Point Arena. This correlation gives an estimate of the average slip rate across the northern San

Andreas since Late Pliocene time.

PREVIOUS WORK

The area of coastal northern California between Fort Ross and Point Arena, west of the San Andreas fault, is known as the Gualala block (Wentworth, 1967) (Figure 1-1). The regional geology of this area appears on the Santa Rosa sheet of the California State Geologic Map (Wagner and Bortugno, 1982). The rocks of the Gualala block were studied briefly in the late 1800s by Becker and White, who assigned them a Cretaceous age, based on megafossils (Becker, 1885, 1888; White, 1885a, 1885b, 1891). The area was first mapped by Weaver in the early 1940s who assigned most of the rocks of the region to the Gualala group, which he considered to be Cretaceous, and recognized the Tertiary rocks near Point Arena (Weaver, 1943, 1944). Parts of the area were mapped by Dibblee in the fifties (unpublished). Irwin (1960) studied the area in reconnaissance. The most detailed mapping of the area was done by Carl Wentworth (1967), who studied the southern 3/4 of the Gualala block, from the Fort Ross area to near Schooner Gulch. The Point Arena quadrangle was mapped by Boyle (1967) and by Jahns and Hamilton (1971). Recent isotopic studies of the Late Cretaceous and Lower Tertiary formations have been done by James et al. (1986 and in press) and by Johnson and O'Neil (1988). Paleomagnetic studies of the Cretaceous and Tertiary rocks have been done by Kanter and Debiche (1985).

Figure 1-1. Map showing location of the Gualala block in northern California.

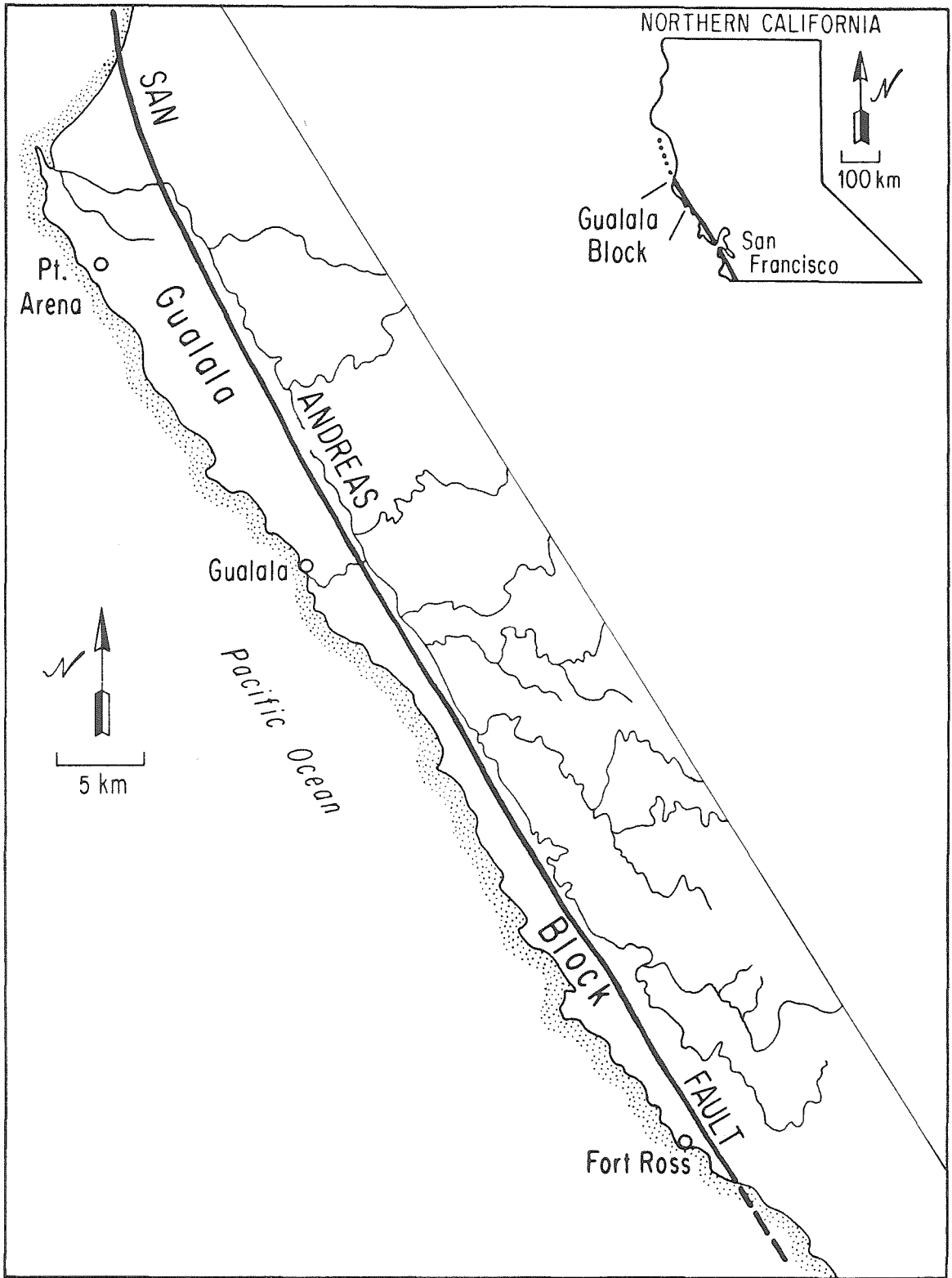


Figure 1-1

Paleontological studies of the mid-Tertiary section near Point Arena have been done by Addicott (1967) and Phillips et al. (1976). Studies of the marine terraces include the area near Fort Ross (Bauer, 1952) and near Point Arena (Valavanis, 1983). The San Andreas fault in this area was mapped by Brown and Wolfe (1972), and the problem of its Quaternary activity was addressed by Higgins, (1961).

SUMMARY OF THE GEOLOGY OF THE GUALALA BLOCK

The San Andreas fault juxtaposes rocks of very different origin along most of its length. East of the fault, in the Gualala area, are rocks of the Franciscan assemblage. These are faulted against the thick sequence of Late Cretaceous through Tertiary sedimentary (and minor volcanic) rocks of the Gualala basin, west of the San Andreas fault (Figure 1-2). Much of the following description of the Gualala block section is based on Wentworth (1967). The structurally lowest unit in this section is the small exposure of spilite near Black Point, in the core of an anticline. In fault contact with the spilite is the Gualala Formation, which consists of over 5500 feet of interbedded mudstone, arkosic sandstone, and conglomerate, deposited by turbidity currents; this formation consists of two members, the Anchor Bay member, which contains conglomerates with clasts of mafic intrusives and lacks K-feldspar-rich sandstone beds, and the Stewart's Point member which consists of K-feldspar-rich arkose and conglomerates

containing clasts of granitic rocks. Although no upper Maestrichtian fossils have been found near the top of this formation, the contact with the overlying lower Tertiary German Rancho Formation is reported to be conformable.

The Paleocene to Eocene German Rancho Formation is exposed over most of the Gualala block. This unit consists of at least 20,000 feet of K-feldspar-rich arkosic sandstone, mudstone, and conglomerate deposited by turbidity currents. The upper contact with the Iversen basalt has been reported to be concordant (Wentworth, 1967), but Boyle (1967) reported this contact to be an angular unconformity. The Iversen basalt consists of about 900 feet of very fine-grained olivine basalt and associated amygdular breccia. K-Ar dating of plagioclase crystals from the basalt yielded ages of 24.3 ± 1.3 , 22.6 ± 1.2 , and 22.8 ± 1.1 ma for this unit (Turner, 1970).

Overlying the Iversen basalt is the Miocene Skooner Gulch Formation, which consists of about 350 feet of arkosic sandstone of possible Zemorrian age (Phillips, et al., 1976). The lower portion of this unit contains clasts of the Iversen basalt indicating a hiatus of unknown duration (Boyle, 1967). This unit is gradationally overlain by the Gallaway formation, about 1300 feet of interbedded sandstone and mudstone of Saucesian and possibly Zemorrian age (Phillips, et al., 1976). Gradationally above the Gallaway formation is the Point Arena Formation (also assigned to the Monterey Formation by some workers). This unit consists of about 3000 feet of

Figure 1-2. Simplified geologic map of the Gualala block, modified from Wentworth (1967) and Wagner and Bortugno (1982). The San Andreas fault juxtaposes a thick sequence of Late Cretaceous through Tertiary sedimentary and volcanic rocks of the Gualala block against the Franciscan Formation.

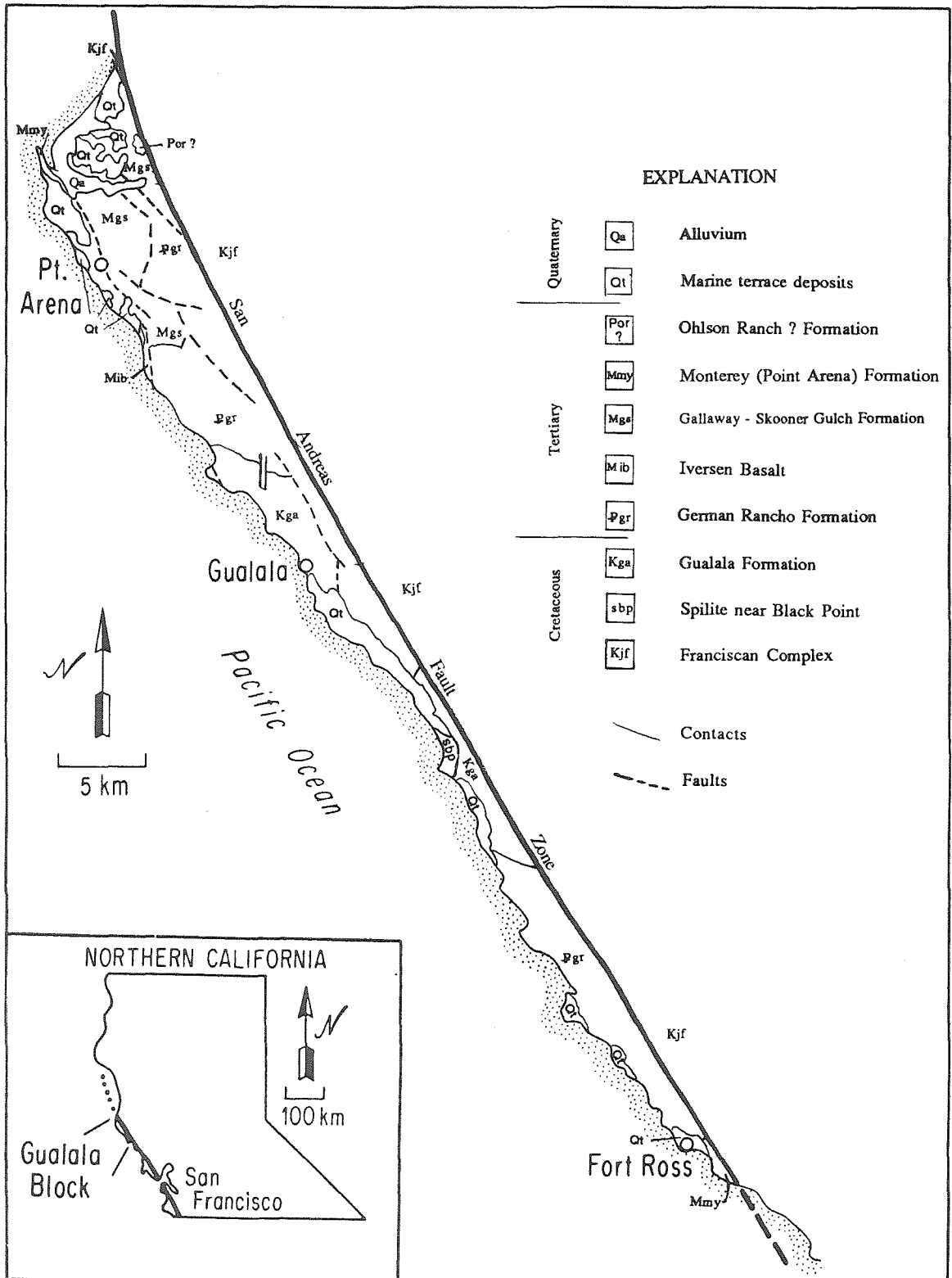


Figure 1-2

diatomaceous to porcelanaceous shale and siltstone overlain by at least 1300 feet of sandstone and sandy mudstone (Jahns and Hamilton, 1971). This unit ranges from lower to middle Miocene in age (Boyle, 1967).

Boyle (1967) mapped a small exposure, near Point Arena, of sandstone containing an Upper(?) Pliocene faunal assemblage that is probably correlative with the Ohlson Ranch Formation of Higgins (1960), on the east side of the San Andreas fault, adjacent to the southern half of the Gualala block, in Sonoma County. Further evidence supporting this correlation is discussed in Chapter 4 of this study. The most recent deposits consist of Quaternary marine terrace deposits, alluvium and landslides.

EARTHQUAKE GEOLOGY

Two types of geologic data are especially useful in evaluating the seismic hazard associated with an active fault: information about paleoseismic events, and data pertinent to the calculation of a slip rate for the fault. The collection of paleoseismic data involves recognition and documentation of the effects that past earthquakes have left in the geologic record, and placing age constraints on the timing of these events. The calculation of a geologic slip rate for a fault requires the recognition and measurement of an offset geologic feature or deposit, and the determination of its age of formation.

The San Andreas fault is the most thoroughly studied fault in California, and, perhaps, in the world. The fault displays differences in behavior along its length (e.g., The Working Group on California Earthquake Probabilities, 1988). Different segments of the fault have differing earthquake histories and slip rates, and therefore, different degrees of seismic hazard. Recent paleoseismic and slip-rate studies have led to advances in understanding the earthquake hazard associated with this fault (e.g., Hanks, 1985; Heirtzler, 1987). However, most of these studies have been conducted in southern and central California, (e.g., Sieh, 1984; Sieh and Jahns, 1984) and few paleoseismic and slip-rate studies have been conducted along the northern segment of the fault.

QUATERNARY FAULTS OF THE SAN ANDREAS SYSTEM IN NORTHERN CALIFORNIA

South of the San Francisco Peninsula, the San Andreas fault has a relatively simple geometry and is creeping as much as 32 mm/yr (Lisowski and Prescott, 1981). This creep rate gradually decreases to the northwest until, north of San Juan Bautista, the San Andreas fault is locked and has not moved since 1906. At this latitude, the San Andreas system becomes more complicated and slip is distributed across several major fault zones, including the Hayward-Rogers Creek-Maacama-Lake Mountain fault zone, the Calaveras-Concord-Green Valley fault zone, and the San Gregorio fault zone

Figure 1-3. Map of northern California showing faults of the San Andreas system. Geodetic and geologic studies show that slip on the San Andreas is currently partitioned across several fault zones in the San Francisco Bay area. How this slip is distributed north of the Bay area is not known. Fault map compiled from Herd, 1978, and Kelsey and Cashman, 1983. SAFZ: San Andreas fault zone, SGFZ: San Gregorio fault zone, CvFZ: Calaveras fault zone, HFZ: Hayward fault zone, CFZ: Concord fault zone, GVFZ: Green Valley fault zone, RCFZ: Rodgers Creek fault zone, MFZ: Maacama fault zone, BSFZ: Bartlett Springs fault zone, ER-LMFZ: Eaton Roughs - Lake Mountain fault zone.

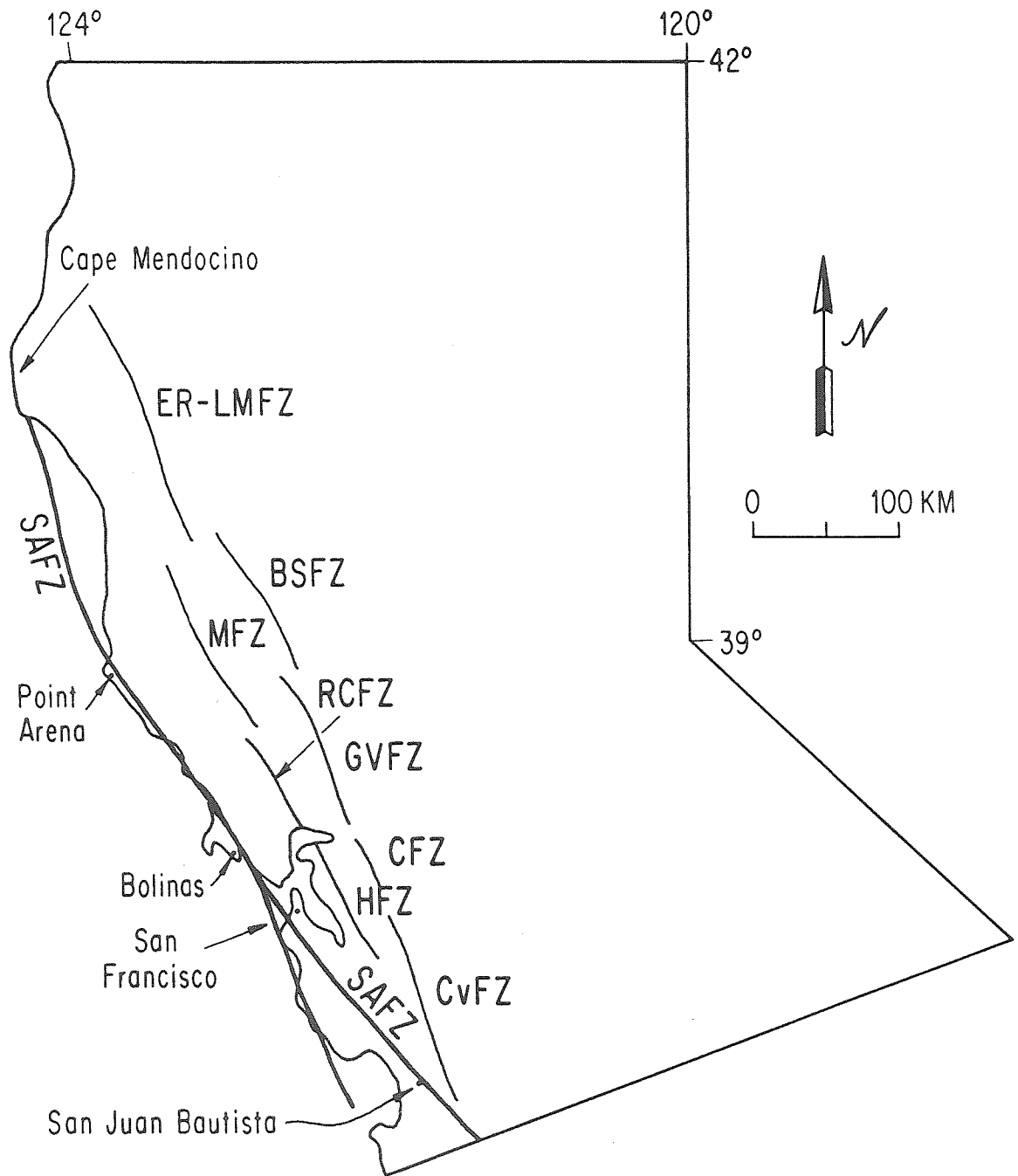


Figure 1-3

(Figure 1-3). Geodetic studies indicate that strain is accumulating at a rate of about 12.2 ± 3.9 mm/yr across the peninsular San Andreas (Prescott, et al., 1981). This study also shows that both the Calaveras and Hayward faults are creeping at 7 ± 1 mm/yr, and suggests that no strain is accumulating across either of these faults in the South Bay region. Geodetic measurements between the coast near San Francisco and the Farallon Islands (50 km offshore from San Francisco) suggest that between 11 and 18 mm/yr of slip at depth is occurring across the San Andreas fault, that a significant amount of the total relative plate motion is very broadly distributed to the east of the San Andreas north of the Golden Gate, and that no appreciable slip is taking place west of the San Andreas (Prescott and Yu, 1986).

Geologic data regarding the slip rates of these faults are much more sparse than geodetic data. Determinations of the geologic slip rate across the San Andreas fault on the San Francisco peninsula have given rates of 6-22 mm/yr (Addicott, 1969), 10-30 mm/yr (Cummings, 1968) since the late Cenozoic, and a minimum of 12 mm/yr for the last approximately 1200 years (Hall, 1984). North of San Francisco, an average rate of 37.5 mm/yr for the last 6 million years has been proposed across the San Andreas fault (Sarna-Wojcicki, 1986). A slip rate of 6-13 mm/yr has been proposed for the San Gregorio fault (Weber and Lajoie, 1977). A slip rate across the Hayward fault near Fremont of at least 4 ± 0.4 mm/yr has been

suggested by Borchardt et al., 1987. No geologic slip rate for the Calaveras system has been determined, nor have rates for continuations of the Hayward and Calaveras systems north of the San Francisco area.

Global reconstructions of the relative plate-motion between the Pacific and North American plates indicate rates of about 55 mm/yr (Minster and Jordan, 1978) to 45-51 mm/yr (DeMets, et al., 1987) for the past few million years. The discrepancy between this rate and the measured and estimated geodetic and geologic rates across the San Andreas system have long been the subject of discussion, with suggestions that the "missing slip" might be taken up in the Basin and Range region or along faults offshore, or by folding instead of slip across faults.

North of the Golden Gate not enough slip-rate data are available to understand how the plate motion is distributed across the faults in this region. The suggested slip rate of 37.5 mm/yr across the San Andreas north of the Golden Gate is based on correlation of a 6-Ma tephra found in cores from the Delgada Fan, with a tephra in the Wilson Grove formation north of San Francisco (Sarna-Wojcicki, 1986), and is not well constrained. No other slip rate studies have been done in this area.

The historical record of large earthquakes in the area is very short. No large earthquakes have occurred on the San Andreas fault since 1906. Prior to 1906, earthquakes probably associated with motion on the northern San Andreas fault

occurred in 1838 and 1865 on the San Francisco peninsula and in 1898 near Point Arena, but little is known about the extent or amount of displacement associated with these events (Topozzada, et al., 1981). Earthquakes on the Hayward fault occurred in 1836 and 1868. The Calaveras fault has not produced any large earthquakes historically, though several moderate events have occurred in recent years.

Prior to this study, only one study of paleoseismic events has been available for the San Andreas fault north of San Francisco. This study, done at Dogtown, near Point Reyes, identified several events prior to 1906, but problems with radiocarbon dating did not allow the ages of these events to be determined (Hall and Hay, 1984; Cotton, et al., 1982). More information about prehistoric seismic activity and slip rate on the northern San Andreas fault is critical in the evaluation of the seismic hazard of this segment of the fault.

REFERENCES

- Addicott, W.O., 1967, Age of the Skooner Gulch Formation, Mendocino County, CA: U.S.G.S. Bull. 1254-C.
- Bauer, F.H., 1952, Marine Terraces Between Salmon Creek and Stewarts Point, Sonoma County, California: unpublished M.A. thesis, Department of Geography, University of California, Berkeley.
- Borchardt, G., Lienkamper, J.J., and Schwartz, D.P., 1987, Holocene slip rate of the Hayward fault at Fremont, California: EOS, Trans. Am. Geophys. Union v. 68, n.44, p. 1506.
- Boyle, M.W., 1967, Stratigraphy, sedimentation, and structure of an area near Point Arena, California: unpublished M.S. thesis, Univ. of Calif., Berkeley.
- Brown, R.D., and Wolfe, E.W., 1972, Map showing recently active breaks along the San Andreas fault between Point Delgada and Bolinas Bay, California: U.S.G.S. Misc. Geol. Investigations Map I-692.

Cotton, W.R., Hall, N.T., and Hay, E.A., 1982, Holocene behavior of the San Andreas fault at Dogtown, Point Reyes National Seashore, California: Final Tech. Rept. for U.S.G.S. Contract No. 14-08-0001-19841, Sept.

DeMets, C., Gordon, R.G., Stein, S., Argus, D.F., 1987, A revised estimate of Pacific-North America motion and implications for western North America plate boundary zone tectonics: Geophys. Res. Letters, v. 14, n. 9, pp. 911-914.

Hall, N.T., and Hay, E.A., 1984, Problems in the application of ^{14}C dates to slip rate determinations on the San Andreas fault: Earthquake Notes, Abs., Seis. Soc. Am., 79th mtg., p. 8.

Hall, N. T., 1984, Holocene history of the San Andreas fault between Crystal Springs Reservoir and San Andreas Dam, San Mateo County, California: Seis. Soc. Am. Bull., v. 7, pp. 281-299.

Hanks, T.C., 1985, The National Earthquake Hazards Reduction Program - scientific status: U.S. Geol. Survey Bull. 1659, 40 pp.

Heirtzler, J.R., ed., 1987, U.S. National report to International Union of Geodesy and Geophysics, 1983-1986; Contributions in seismology: Reviews of Geophysics, v. 25, n. 6, pp. 1131-1133.

Higgins, C.G., 1960, Ohlson Ranch Formation, Pliocene, Northwestern Sonoma County, California: Univ. Calif. Pubs. Geol. Sci., v. 36, n. 3, pp. 199-232.

Higgins, C.G., 1961, San Andreas fault north of San Francisco, California: GSA Bull., vol. 72, pp. 51-68.

James, E.W., Kimbrough, D.L., and Mattinson, J.M., 1986, Evaluation of pre-Tertiary displacements on the northern San Andreas fault using U-Pb zircon dating, initial Sr and common Pb isotopic ratios: GSA Abstracts with Programs, v. 18, n. 2, p.121.

Johnson, C.M., and O'Neil, J.R., 1988, Constraints on pre-Tertiary movement on the San Andreas fault system: stable and radiogenic isotope and trace element data from Jurassic gabbros: Geol. Soc. Am., Abstracts, v. 20, n. 7, pp. A381.

Kanter, L.R., and Debiche, M., 1985, Modeling the motion histories of the Point Arena and Central Salinia terranes: in: Tectonostratigraphic terranes of the Circum-Pacific Region, Howell, D.G., ed., pp 227-238.

Lisowski, M., and Prescott, W.H., 1981, Short range distance measurements along the San Andreas fault in Central California, *Bull. Seis. Soc. Am.*, v. 71, n. 5, pp 1607-1624.

Prescott, W.H., Lisowski, M., and Savage, J.C., 1981, Geodetic measurement of crustal deformation on the San Andreas, Hayward, and Calaveras faults near San Francisco, California: *J.G.R.*, v.86, pp. 10853-10869.

Prescott, W.H., and Yu, S.-B., 1986, Geodetic measurement of horizontal deformation in the northern San Francisco Bay region, California: *J.G.R.*, v.91, n. B7, pp. 7475-7484.

Minster, J.B., and Jordan, T.H., 1978, Present-day plate motions: *J. Geophys. Res.*, v. 83, n. B11, pp. 5331-5354.

Phillips, F.J., Welton, B., and Welton, J., 1976, Paleontologic studies of the middle Tertiary Skooner Gulch and Gallaway formations at Point Arena, California, in The Neogene Symposium, Paleontology, Sedimentology, Petrology, Tectonics, and Geologic History of the Pacific Coast of North America; Fritsche, A.E, Terbest, H., and Wornatdt, W.W., eds., Pacific Section SEPM, pp. 137-154.

Sieh, K.E., 1984, Lateral offsets and revised dates of large prehistoric earthquakes at Pallett Creek, southern California: J. Geophys. Res., v. 89, pp. 7641-7670.

Sieh, K.E., and Jahns, R.H., 1984, Holocene activity of the San Andreas fault at Wallace Creek, California: Geol. Soc. Am. Bull., v. 95, pp. 883-896.

Topozada, T.R., Real, C.R., and Parke, D.L., 1981, Preparation of isoseismal maps and summaries of reported effects for pre-1900 California earthquakes: Cal. Div. Mines and Geol. Open File Report 81-11 SAC.

Turner, D.L., 1970, Potassium-Argon dating of Pacific coast Miocene foraminiferal sages, in: Radiometric Dating and Paleontologic Zonation; O.L. Bandy, ed.: GSA Spec. Pap. 124, pp 91-129.

- Valavanis, D.S., 1983, Abrasion Platform Morphology of the Lowest Marine Terrace, Arena Cove to Alder Creek, Mendocino County, California: unpublished M.A. thesis, Department of Geography, California State University, Hayward.
- Wagner, D.L. and Bortugno, E.J., 1982, Geologic Map of the Santa Rosa Quadrangle: CDMG Regional Geologic Map Series, Map no. 2A (geology).
- Weaver, C.E., 1943, Point Arena-Fort Ross region [California]: Cal Div. Mines and Geol. Bull. 118, p. 628-632.
- Weaver, C.E., 1944, Geology of the Cretaceous (Gualala Group) and Tertiary formations along the Pacific coast between Point Arena and Fort Ross, California: Wash. (State) Univ. Pub. in Geology, V. 6, n. 1, 29 pp.
- Weber, Gerald B. and Lajoie. K. R., 1977, Late Pleistocene and Holocene tectonics of the San Gregorio fault zone between Moss Beach and Point Ano Nuevo, San Mateo County, California, GSA Abstracts with Programs, 9(4), p. 524.
- Wentworth, C.M., 1967, The Upper Cretaceous and Lower Tertiary rocks of the Gualala block, northern Coast ranges, California: Ph.D. dissertation, Stanford University.

Working Group on California Earthquake Probabilities (D.C. Agnew, C.R. Allen, L.S. Cluff, J.H. Dieterich, W.L. Ellsworth, R.L. Keeney, A.G. Lindh, S.P. Nishenko, D.P. Schwartz, K.E. Sieh, W. Thatcher, R.L. Wesson), 1988, Probabilities of large earthquakes occurring in California on the San Andreas fault system: U.S. Geological Survey Open File Report 88-398, 62 pp.

CHAPTER 2: LATE HOLOCENE SLIP RATE AND PALEOSEISMIC EVENTS ON THE NORTHERN SAN ANDREAS FAULT NEAR POINT ARENA

ABSTRACT

Excavations in a Holocene alluvial fan cut by the northern San Andreas fault have exposed an offset channel, allowing the determination of a maximum slip rate for the late Holocene epoch. Data from these excavations have also provided evidence of prehistoric seismic activity along the fault. The site of the excavations is in an abandoned river valley near the town of Manchester in Mendocino County. The section exposed by the excavations consists of a dark grey clay overlain by one to two meters of coarse fluvial sand and gravel. This section is cut by faults of at least five, or, perhaps, six, ages. The most recent fault represents the 1906 earthquake. Radiocarbon analyses of detrital charcoal and wood indicate that all five or six faulting events have taken place within the past 2000 years. A channel incised into the grey clay and buried by the fluvial gravels has been offset a maximum of 64 ± 2 meters. Radiocarbon analysis of two samples from the material filling the channel gives an age of 2356-2709 years. This implies a maximum Holocene slip rate of 25.5 ± 2.5 mm/yr. These data suggest that the average recurrence interval for great earthquakes on this segment of the San Andreas fault is long - between about 200 and 400 years.

INTRODUCTION

On April 18, 1906, the San Andreas fault ruptured along a 430-km length, from near San Juan Bautista to offshore Cape Mendocino (Figure 2-1). This rupture produced the great San Francisco earthquake (Figure 2-1) (Lawson, 1908). Damage to San Francisco and other northern coastal communities was substantial. Because the population of the San Francisco Bay area has grown tremendously since 1906, the destructive potential of a repeat of the 1906 earthquake has greatly increased. Forecasts of the likelihood of a repeat of this event within the next few decades are needed.

The historical record is too short to provide the information necessary to understand what to expect from the northern San Andreas in the near future. Little is known about the behavior of the northern San Andreas prior to 1906; an earthquake of high intensity in San Francisco was reported to have been associated with rupture along the San Andreas south of San Francisco in 1838, but there is no information about amount of offset and little can be said about the length of rupture (Louderback, 1947). Other large nineteenth century earthquakes in northern California occurred in 1865 and 1898 (Figure 2-1) (Topozada, 1981). Information about the prehistoric behavior of the northern San Andreas fault is needed to help evaluate the probability of a great earthquake along this segment of the fault in the next few decades. Geologic data useful in evaluating the seismic hazard posed

Figure 2-1. Map of northern California showing major fault zones of the San Andreas system. Suggested epicenters of large nineteenth century earthquakes that may have been associated with the San Andreas fault are indicated by large dots (from Topozada, 1981). Length of surface rupture of the San Andreas fault during the 1906 San Francisco earthquake (about 430 km; Lawson, 1908) is shown with hachures. The historic record in California is too short to enable determination of the recurrence interval of earthquakes as large as that of 1906.

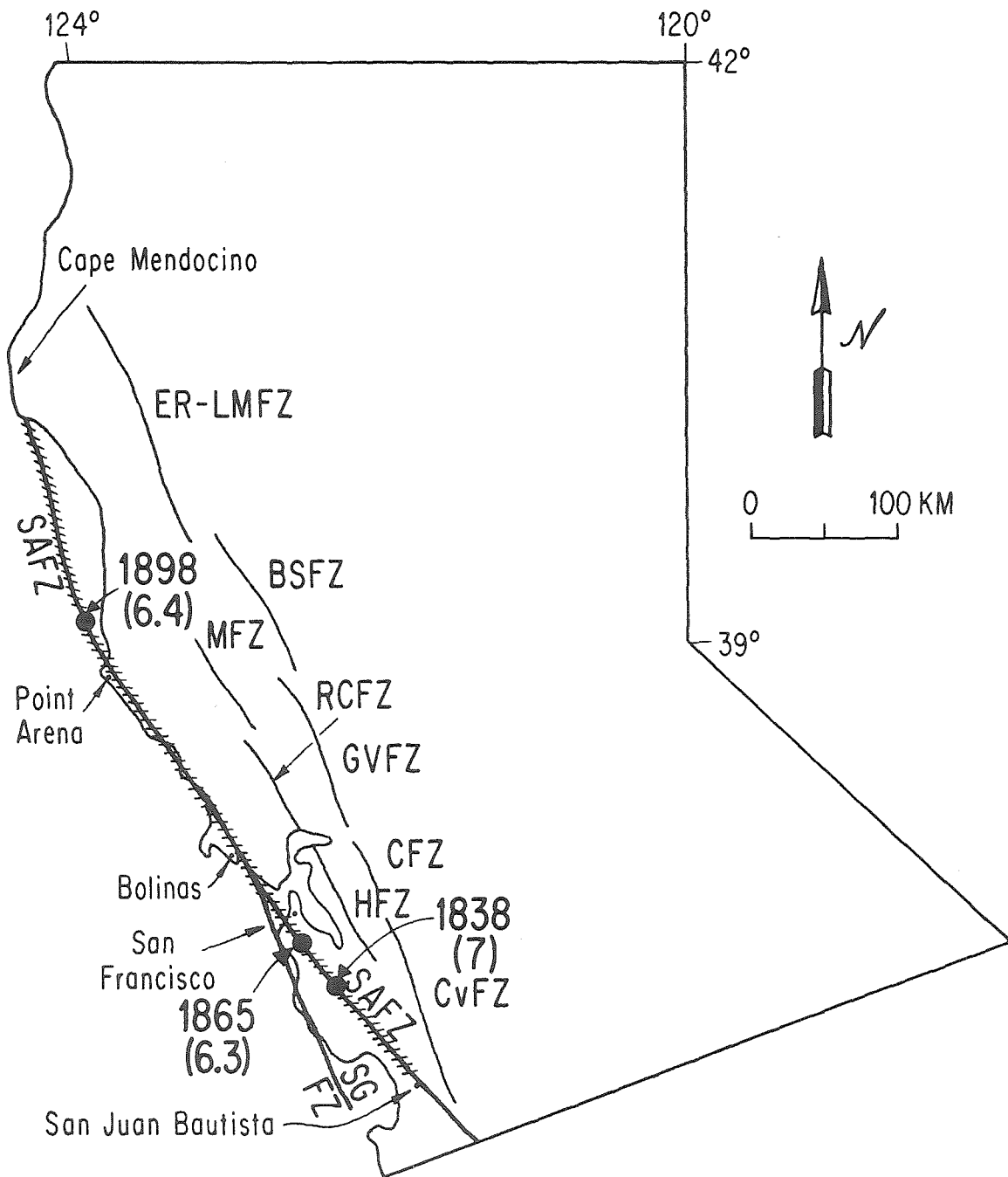


Figure 2-1

by an active fault include fault slip-rate and paleoseismic data (e.g., Schwartz, 1987). This chapter summarizes the results of a study undertaken near Point Arena to gather slip-rate and paleoseismic data for the northern San Andreas fault.

PREVIOUS WORK

Several geologic and geodetic studies of the slip rate and one paleoseismic study on the northern San Andreas fault have been undertaken in recent years (Figures 2-2 & 2-3). A paleoseismic study on the northern San Andreas fault was conducted at Dogtown, north of Bolinas, but was inconclusive due to problems with radiocarbon dates and high sedimentation rates (Cotton, et al., 1982; Hall and Hay, 1984; Hall, personal communication, 1985).

South of San Francisco, near San Andreas Lake, a minimum Holocene slip rate of 12 mm/yr was determined from 44 feet (13.4 m) of offset accumulated on a channel that was incised across the fault after 1130 ± 160 radiocarbon years B.P. (Hall, 1984). From this slip rate and the assumption that the 1906 event is characteristic at this site, a maximum recurrence interval of 224 ± 25 years was calculated. This slip rate is in agreement with the geodetic strain rate determined by Prescott et al., (1981). In contrast to this low rate, a study north of San Francisco led to the estimation of a long term rate of 37.5 mm/yr, based on the correlation of a six-million-year tephra recovered from the Delgada fan off

Figure 2-2. Map of northern California showing faults of the San Andreas system. Numbers are current slip rates based on geodetic data (in mm/yr); bold numbers indicate fault creep rate. Rates from Prescott et al., 1981. Fault map compiled from Herd, 1978, and Kelsey and Cashman, 1983. SAFZ: San Andreas fault zone, SGFZ: San Gregorio fault zone, CvFZ: Calaveras fault zone, HFZ: Hayward fault zone, CFZ: Concord fault zone, GVFZ: Green Valley fault zone, RCFZ: Rodgers Creek fault zone, MFZ: Maacama fault zone, BSFZ: Bartlett Springs fault zone, ER-LMFZ: Eaton Roughs - Lake Mountain fault zone. Geodetic studies show that currently, slip on the San Andreas is partitioned across several fault zones in the San Francisco Bay area. How this slip is distributed north of the bay area is not known.

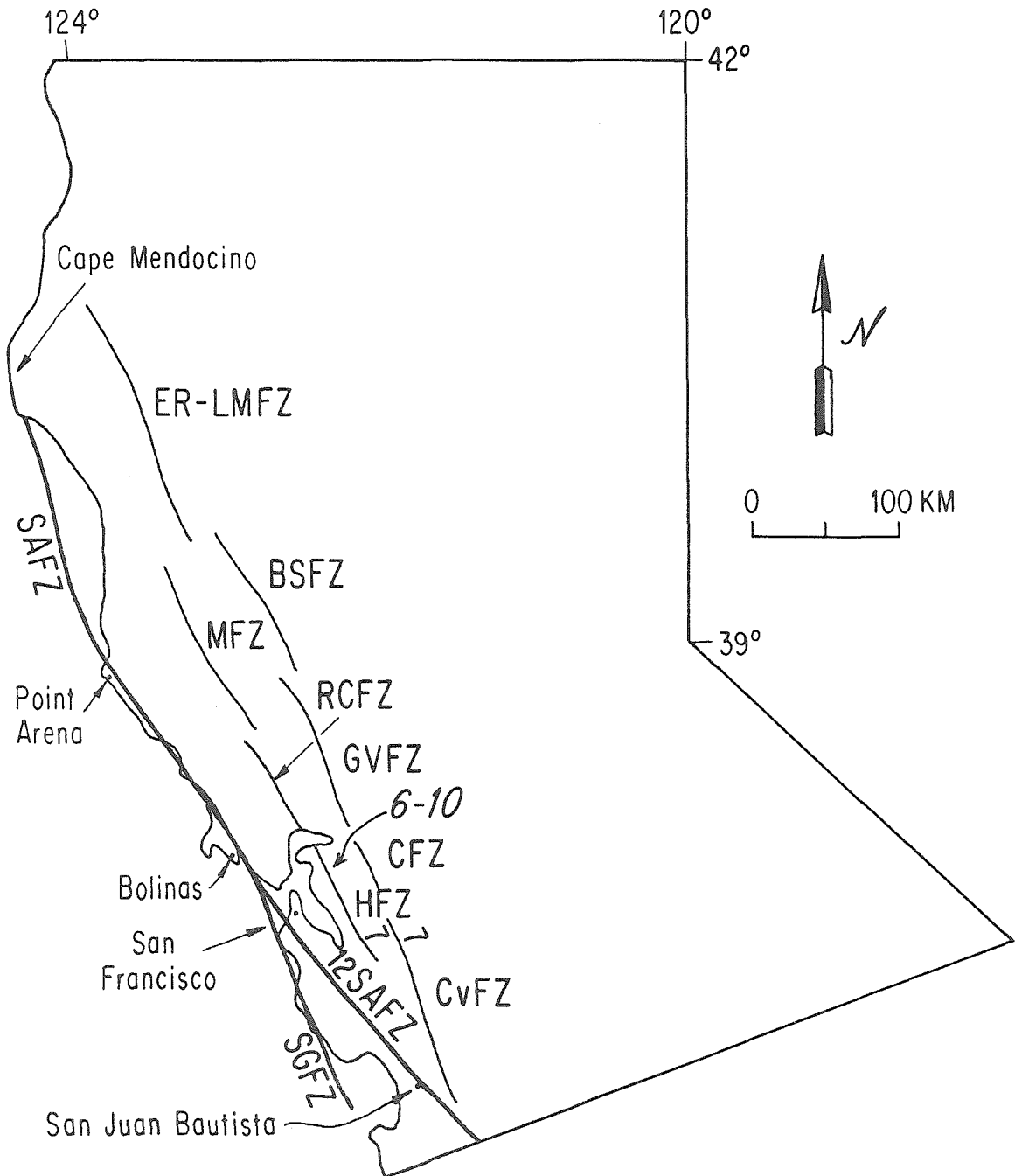


Figure 2-2

Figure 2-3. Map of northern California showing proposed geologic slip rates of faults in northern California in mm/yr. Rates from Hall, 1984, Sarna-Wojcicki, 1986, and Weber and Lajoie, 1977. Fault map compiled from Herd, 1978, and Kelsey and Cashman, 1983. SAFZ: San Andreas fault zone, SGFZ: San Gregorio fault zone, CvFZ: Calaveras fault zone, HFZ: Hayward fault zone, CFZ: Concord fault zone, GVFZ: Green Valley fault zone, RCFZ: Rodgers Creek fault zone, MFZ: Maacama fault zone, BSFZ: Bartlett Springs fault zone, ER-LMFZ: Eaton Roughs - Lake Mountain fault zone. Rate determined for San Andreas north of San Francisco Bay for the last 6 Ma is over three times the 1200 year rate determined for this fault on the San Francisco peninsula. If both are correct, either the fault has slowed down in recent years or the slip rate is much higher north of the Golden Gate. The San Gregorio fault joins the San Andreas between these two areas, and may add a component of slip to the San Andreas north of the juncture.

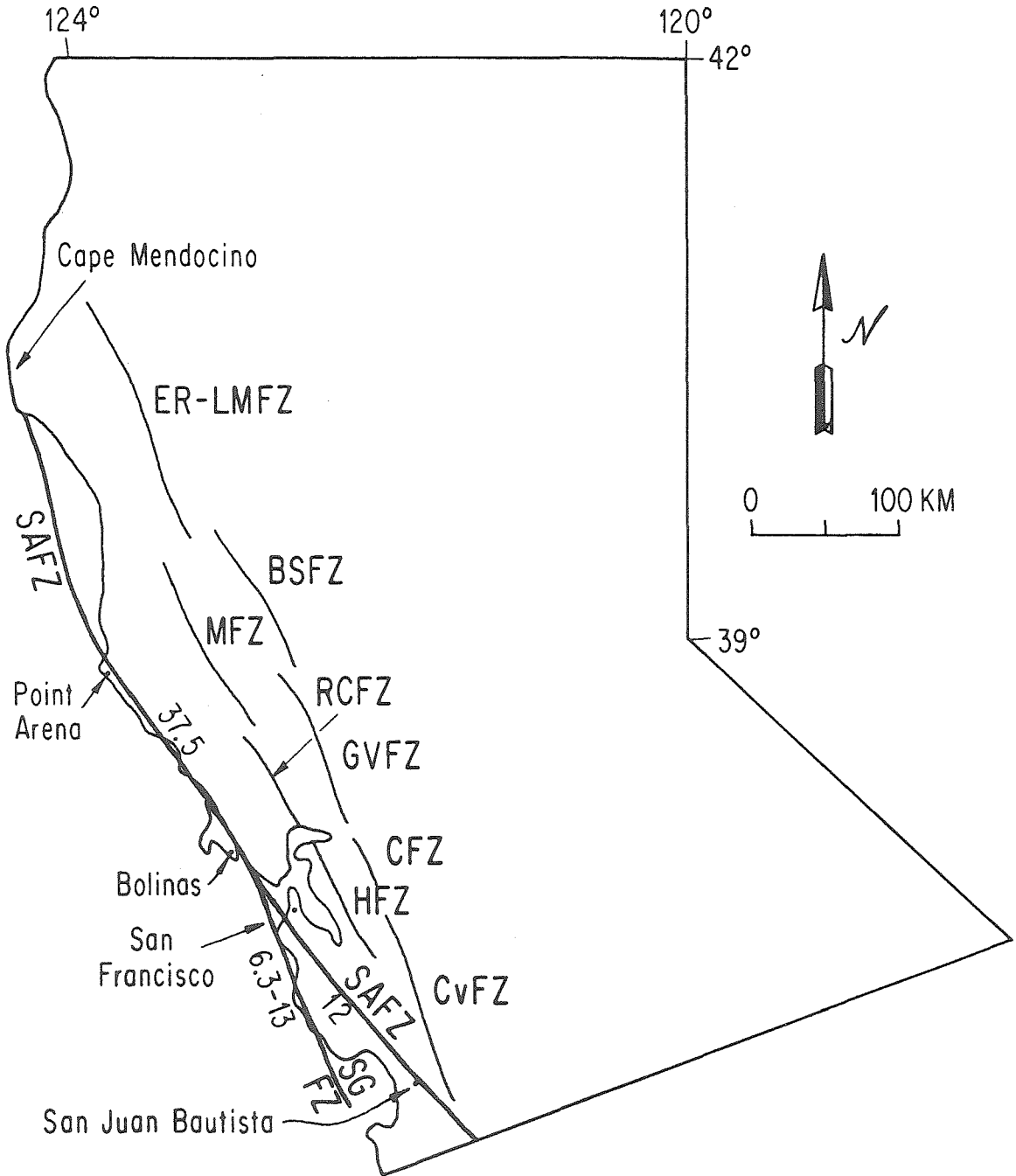


Figure 2-3

the coast of Cape Mendocino with a tephra in the Wilson Grove Formation north of San Francisco (Sarna-Wojcicki, et. al., 1986). If the interpretations from both studies are correct, either the San Andreas is moving three times faster north of San Francisco than south, or the fault has slowed down a great deal in geologically recent times.

STUDY SITE

A search for a suitable site to study the Holocene slip rate and paleoseismicity of the northern San Andreas fault was conducted using aerial photographs and geologic field maps along the segment of the fault between Fort Ross and Point Arena (Figure 2-4). Because much of the fault zone lies along the heavily forested drainages of the Gualala and Garcia Rivers (Brown and Wolfe, 1972), suitable localities for paleoseismic work were difficult to find. For most of this distance the fault lies along the steep western slope of the Gualala and Garcia river valleys, so sediments have not accumulated across the fault in many areas.

The site I chose to excavate is located near the town of Manchester, in Mendocino county (Figure 2-4). The excavation site lies in an abandoned river valley cut off from its source by dextral slip along the San Andreas fault (Figure 2-5). The valley bottom was marshy until it was drained by an artificial channel earlier this century.

Two potential excavation sites were identified within this

Figure 2-4. Map showing the Gualala block and location of excavation site near Point Arena. The fault in this area last ruptured during the 1906 earthquake. About 5 meters of slip was measured near the study site soon after the earthquake (Lawson, et al., 1908).

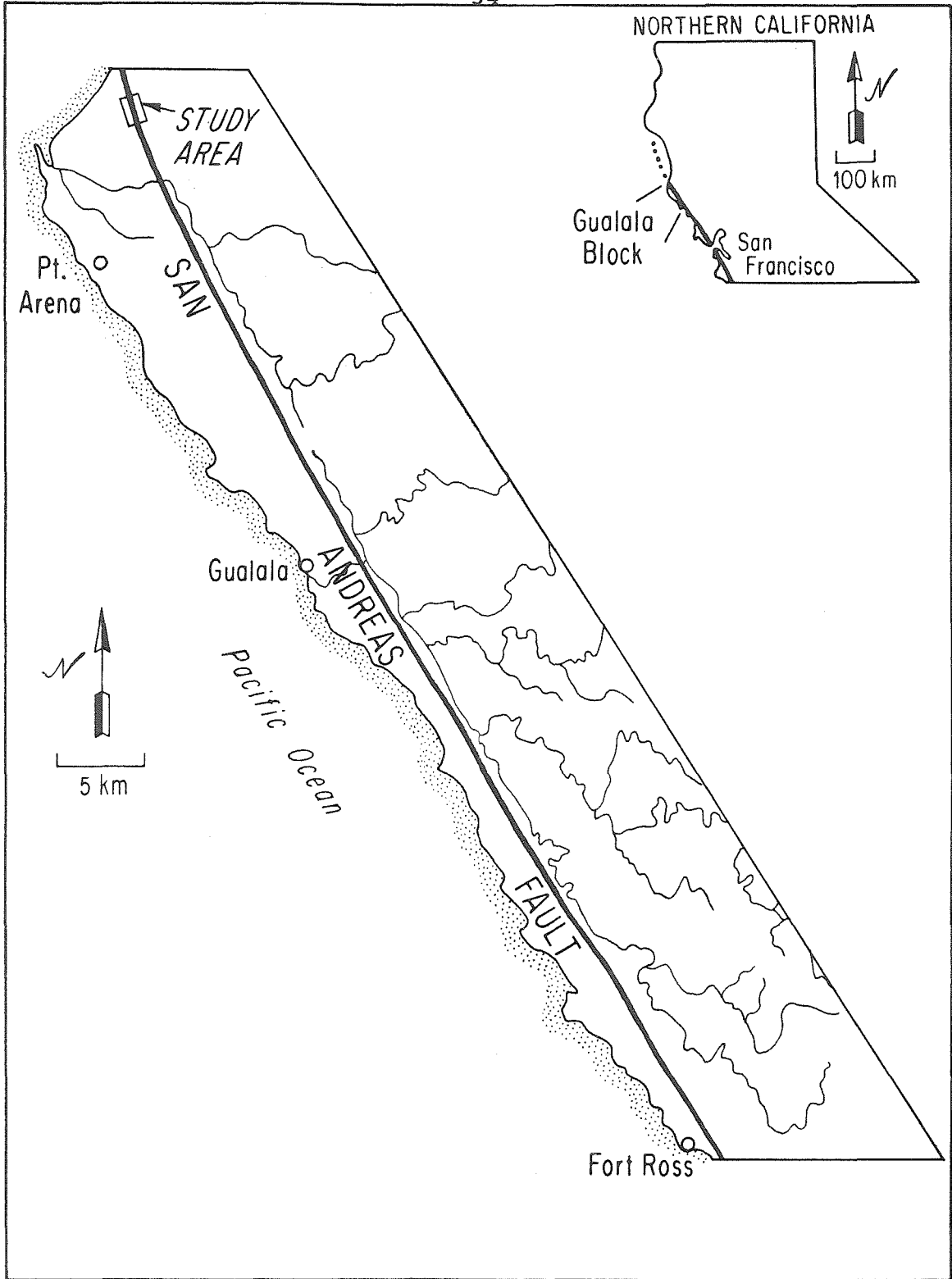


Figure 2-4

abandoned valley (Figure 2-5). At the first site a shutter ridge lies in front of a small tributary drainage entering the valley from the east. This juxtaposition has caused alluvium to accumulate upstream from the ridge. I had hoped that the ponded sediments at this site would contain a record of prehistoric earthquakes. The stream supplying sediment to the site is small and its drainage basin contains no redwood trees. I had hoped to avoid radiocarbon dates of detrital wood and charcoal from ancient redwoods. (Since redwood trees can live for several thousand years, detrital charcoal and wood derived from them can be much older than the strata containing them). However, the excavation cut at this first site showed that the sedimentation rate is so low that burrowing and other surficial disturbances (bioturbation) have homogenized the sedimentary layers before deep burial. Hence, the site proved to be unsuitable for paleoseismic investigation.

Approximately 300 meters to the north of the first excavation site, a stream entering the valley from the east has built a small fan across the fault (Figures 2-5 & 2-6). The fault at this site is expressed as a low scarp formed during the 1906 earthquake. Excavations revealed a late Holocene section consisting of a massive, very poorly sorted, sandy, pebbly, dark grey clay overlain by one to two meters of very coarse fluvial gravels and sands (Figure 2-7). The massive to poorly bedded, very coarse gravels are separated by several finer-grained, silty, sand beds (units 20, 30, and

Figure 2-5. Map showing setting of excavation site. Site is located in an abandoned river valley. Abandonment of the river valley created a marsh which was artificially drained earlier this century. The first excavation was dug where a very small tributary stream enters the valley. This location was chosen in the hope that the small drainage supplying sediment would not supply charcoal derived from ancient redwood trees, since none are present in its watershed. However, the sedimentation rate was so slow at this site that the section has been completely bioturbated, making it unsatisfactory for paleoseismic study. Excavations at the second location, on the fan built by a larger stream, revealed a section that has recorded 5 or 6 earthquakes and an offset buried channel.

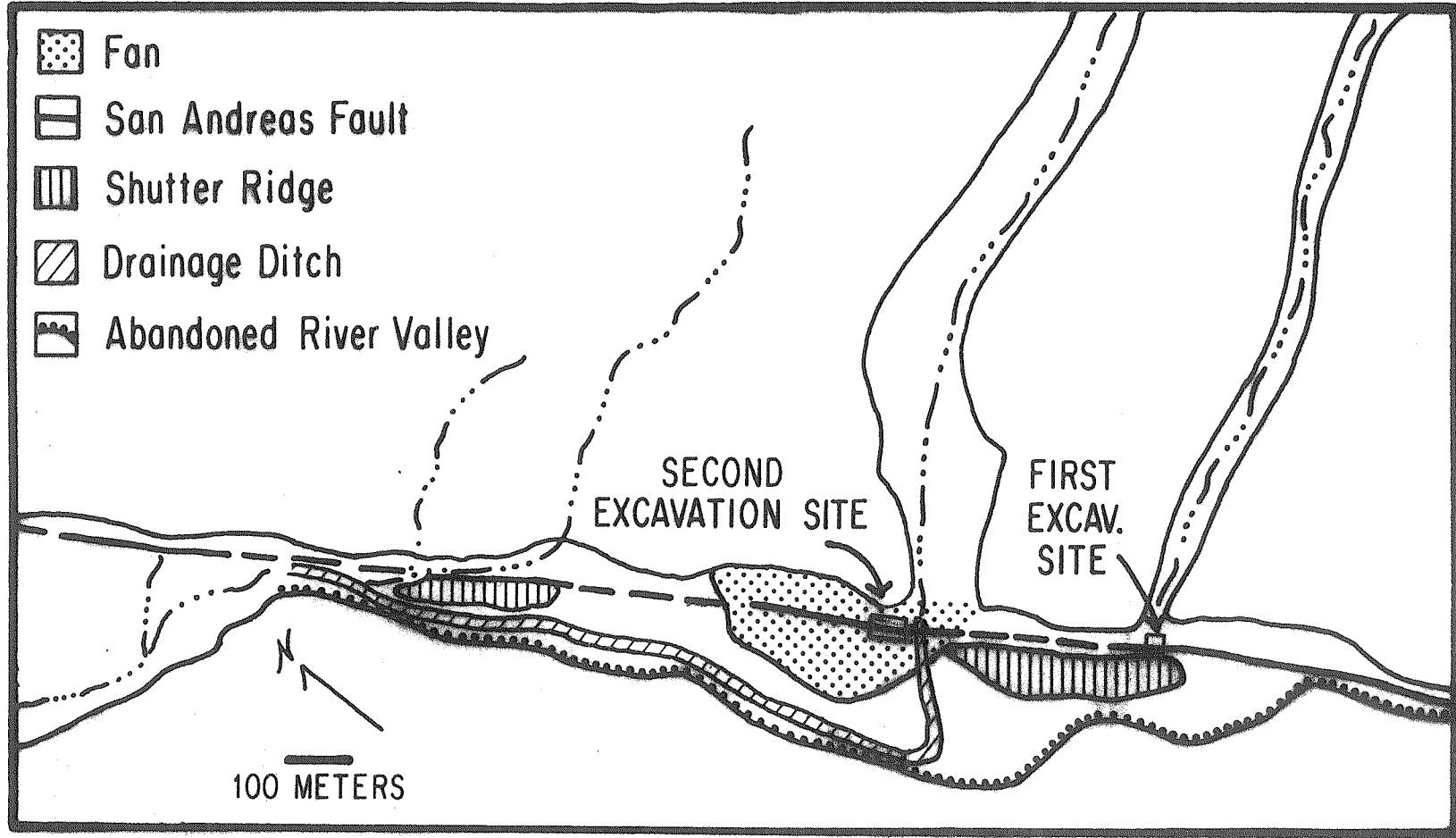


Figure 2-5

Figure 2-6. Topographic map showing locations of all excavations from which data was collected. Excavations were in an alluvial fan built out over the abandoned valley by a tributary stream. The continuous, heavy line that bisects the map represents the 1906 fault trace, visible across the site as a low scarp. The stream supplying sediment to the fan was diverted into a drainage ditch earlier this century. Logs of excavations 86-1, 2 and 3 are shown on plate 1; logs of excavations 6, 7, 9, and 14 are shown on plate 2.

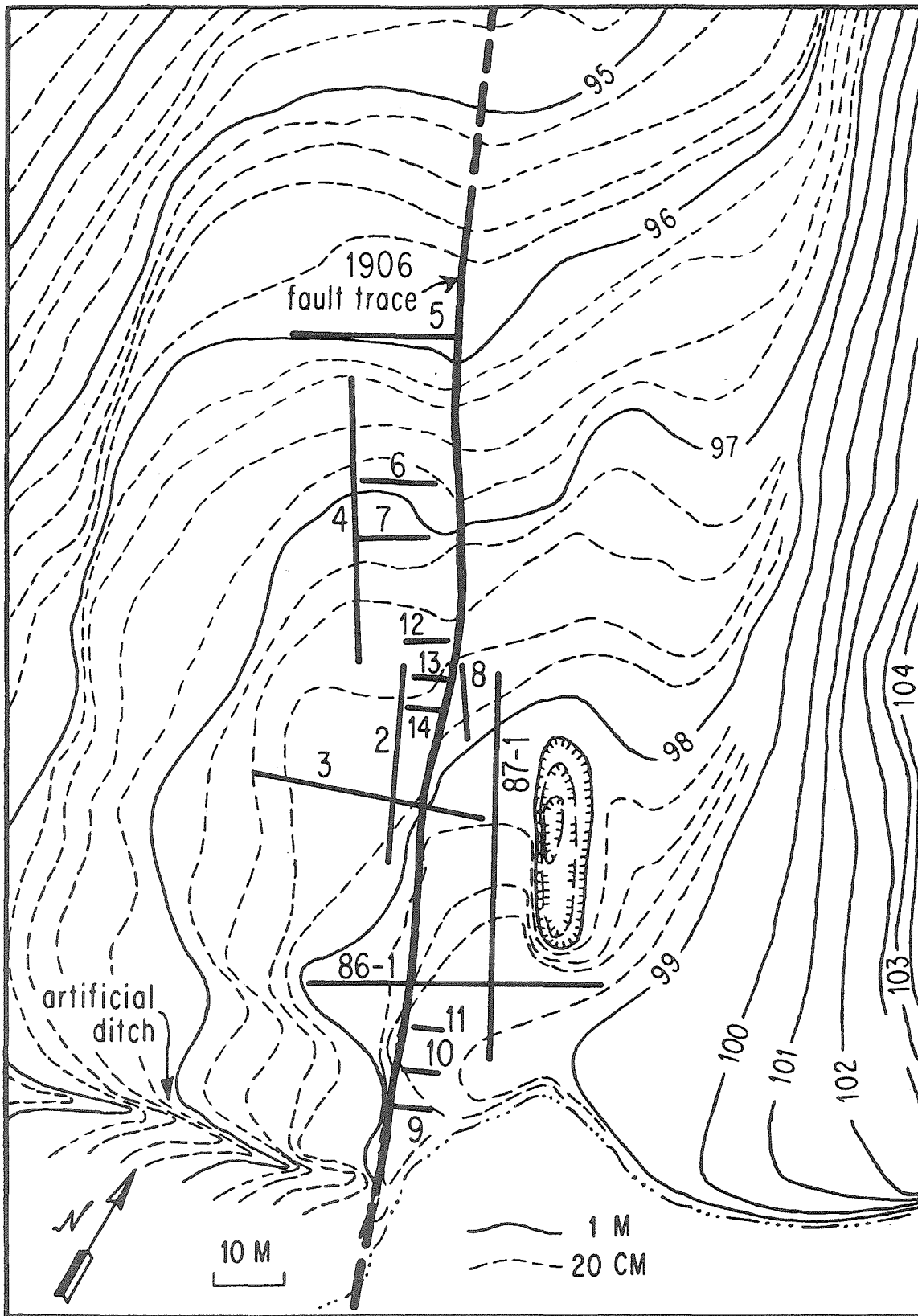


Figure 2-6

40) that are traceable in excavations throughout the site.

The uppermost gravel (unit 50) is a historical deposit: a brick and a square nail were found in these sediments (Figure 2-8). Since this unit is faulted, it must have been deposited before 1906 (no creep has been detected along this segment of the fault (Nason, 1971)). The ages of the units shown in Figure 2-7 were determined by radiocarbon analysis and are discussed in detail below.

PALEOSEISMIC EVENTS

Five or six faulting events have been recognized in the sediments exposed by the excavations. Evidence for these is recorded in the logs of exposures 2a, 2b, 3a, 3b, and 86-1, which are shown on Plate 1. More events may have occurred during the period represented by the sediments: first, these sediments are alluvial, and deposition has been intermittent; also, deposition of some younger units has involved the erosion of underlying units. This implies that any one of the documented faulting events could actually represent several events. In addition, because the main fault zone is quite complicated (see especially exposures 3a and 3b) events may be obscured. This is particularly likely because of the coarse and massive nature of the faulted sediments.

The evidence for these events is discussed below. The events are labeled F, J, N, R, V, and Z from oldest to youngest, with event Z being the 1906 earthquake. Individual

Figure 2-7. Generalized stratigraphic column of the section exposed by the excavations. Section consists of about 2 meters of very coarse fluvial gravels and interbedded silty sand units overlying massive, pebbly, sandy, dark grey clay. Several fine-grained units were laterally extensive and could be traced throughout the site. Six slip events cut unit 20, which radiocarbon analyses indicate was deposited between B.C. 89 and A.D. 212. The most recent event breaks unit 50 and represents the 1906 earthquake. A brick and square nail found in this deposit show that it was deposited between about 1850 and 1906. Ages of other units are summarized in Table 2. Relationships of slip events to dated sedimentary deposits are shown in Figure 2-9.

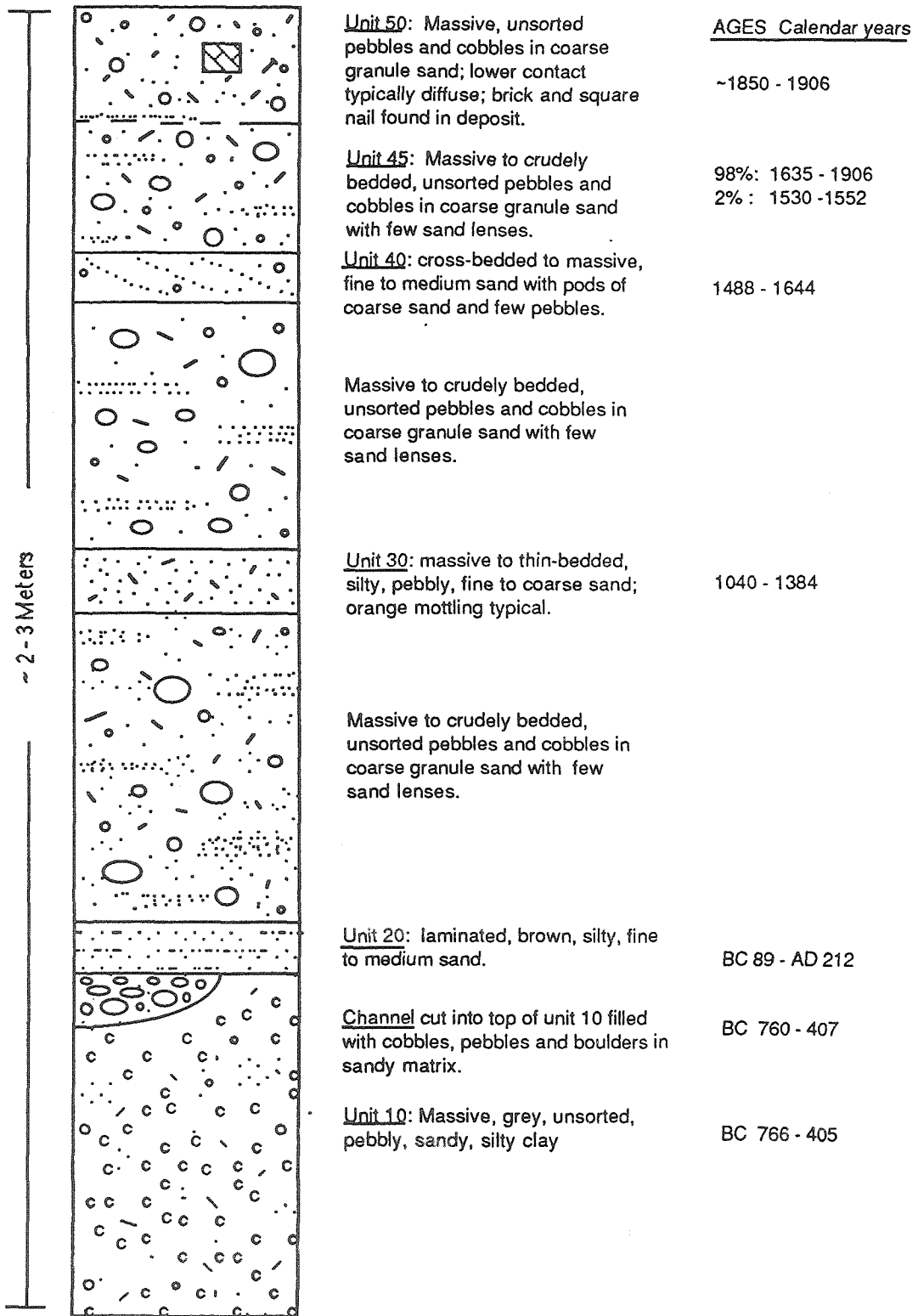


Figure 2-7

Figure 2-8. Photograph of brick found in unit 50. Sample was collected in excavation 2 (see Plate 1, exposure 2a). This region was settled in the mid-1800s, so unit 50 was deposited sometime between then and 1906.

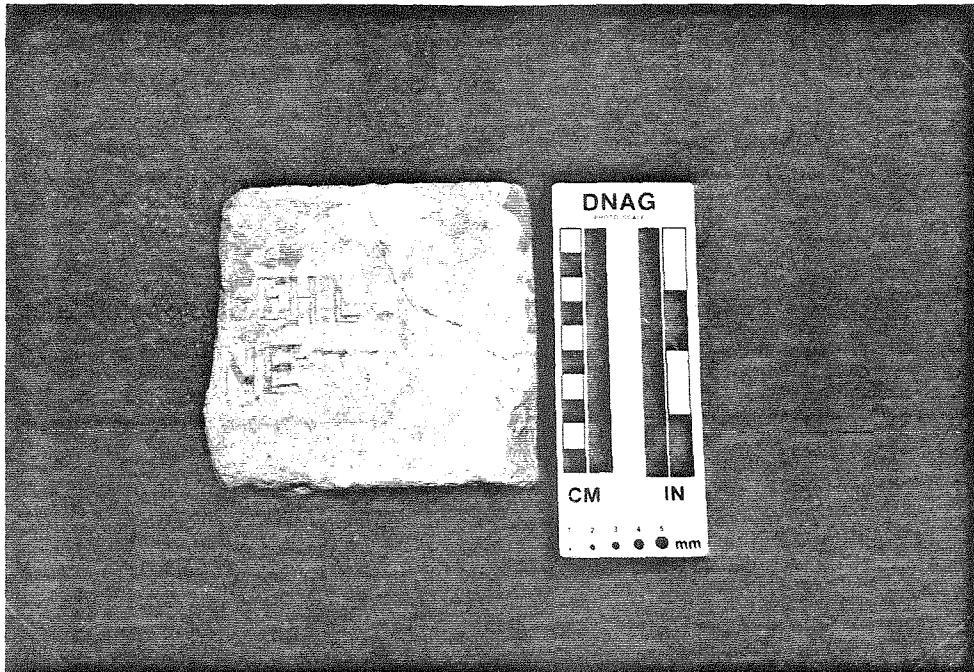


Figure 2-8

faults and fissures discussed in the following text are labeled on the drawings. The labels have three parts: the first is the letter designation of the event, the second is the exposure in which the fault occurs, and the third is the individual number of the feature, with lower numbers being farther to the left. For example, Z-3b-1 refers to a piece of evidence associated with event Z in exposure 3b, nearest the left side of the log.

Unit 50, the historical unit, is clearly faulted. Several of the faults cutting this unit can be traced to the ground surface and are associated with a low scarp on the ground surface (Z-861-1, Z-3a-1, Z-3b-1). These faults represent the 1906 earthquake (event Z) at this site. Some of the faults and one fissure that break unit 50 can not be followed to the ground surface (X-2a-1 and X-2a-2, X-2b-1 through X-2b-4, X-3b-1 and X-3b-2); however, only one of these faults (X-2b-3) appears to be truncated, and since unit 50 is so coarse and massive, it is impossible to be certain whether these faults represent an event prior to 1906 or are faults related to the 1906 earthquake. The fault that appears to be truncated within unit 50 (X-2b-3) may represent an earthquake that occurred before 1906, but after deposition of the lower portion of unit 50. This would be an event in between events Z and V. This is the only suggestion of such an event, however, so the evidence is not strong enough to propose that such an event did, in fact, occur.

Unit 50 truncates an older set of faults that represent an earthquake that occurred before 1906. This event is named event V, and evidence for it consists of one fissure (V-2b-1) and several faults (V-2a-1 through V-2a-3, V-2b-2 through V-2b-5).

Event R is represented by faults that break unit 40 but appear to be truncated within the gravel beneath the lower unit 50 contact (R-2a-1 through R-2a-3, R-2b-1). Because of the coarse, massive nature of the gravels and the uncertainty of the position of the base of unit 50 in this part of the exposure, these faults could have slipped during event V rather than during a different seismic event. The available evidence in these exposures suggests, but does not prove, the occurrence of event R as an event distinct from event V.

Unit 40 truncates a set of faults that represent event N. (N-2a-1, N-3a-1) Since these faults break unit 30 and are overlain by Unit 40, this earthquake occurred between the times that units 30 and 40 were deposited. The relationships in exposure 2a suggest that unit 40 was deposited fairly soon after this event, since this unit appears to drape a scarp produced by event N (N-2a-1).

Events F and J both post-date deposition of unit 20 and pre-date deposition of unit 30 (J-861-1, F-861-1, F/J-3a-1). The map of exposure 86-1 shows both of these faults; exposure 3a shows one of these events clearly, and it is uncertain whether this fault represents event F or J.

In all, evidence for at least five paleoseismic events that post-date the deposition of unit 20 exists in the three excavations represented on Plate 1. Evidence for at least six events exists, if R and V are separate events. The latest of these, event Z, is the 1906 earthquake. Prior to 1906, one or two events (R & V) post-date the deposition of gravels in unit 45. Event N occurred between the time that units 30 and 40 were deposited, and events F and J predate deposition of unit 30 and postdate deposition of unit 20.

OFFSET CHANNEL

The grey clay (unit 10) forms a very regular, monotonously smooth, level to very gently dipping horizon below the fluvial gravels in most of the excavations (Plates 1 & 2). However, several excavations exposed the edges of a channel cut into unit 10 (Plate 2, exposures 6, 7, 14a & 9b; Plate 1, exposures 3a & 3b).

The western edge of this channel was located in several excavations. In exposure 14, on the southwest side of the San Andreas, this edge of the channel is seen only in the northwest wall of the excavation (Exposures 14a, Plate 2). It is not present in the southeast wall of this excavation (Exposure 14b) because it has been offset along the fault. This edge of the channel intersects the fault zone (fault A, Plate 2, Map View) within the one meter width of the excavation.

On the northeast side of the fault zone, the edge of this channel is again exposed adjacent to the fault zone, in exposure 9 (fault B, Plate 2, Map View). Again, the channel edge is only seen on one wall of the excavation, because it intersects the fault zone between the two walls of the trench and has been offset along the fault. The location of the channel edge is projected on the map on Plate 2 to show the trend of the feature as it approaches the San Andreas. No other similar features were observed in the numerous other excavations in the area (Plate 2, Map View), so this feature appears to be unique, and the correlation across the fault is probably correct.

Unfortunately, the low angle at which the channel approaches the San Andreas makes it a less-than-ideal offset reference line. This is because its original course within the fault zone is not known. Some portion of the 64 ± 2 meters of observed separation is probably due to initial geometry of the channel across the fault zone. This geometry is not known, but if the trend of the channel exposures in excavations 5 through 7 and 14 is projected straight across the zone, the separation is reduced to about 58 meters (Map View B, Plate 2; the three closely-spaced dotted lines represent three possible projections). Even taking this into consideration, the separation is probably greater than the true offset because the channel on the eastern side of the fault zone is only exposed in one excavation, so its trend approaching the fault

zone is unknown and cannot be projected in a similar manner. In addition, it is very possible that the channel flowed along the fault zone for some unknown distance, adding to the difference between separation and offset. In any case, the true offset must be less than the separation.

RADIOCARBON ANALYSES

It is important to determine the ages of the paleoseismic events and the offset channel to understand the behavior of the northern San Andreas fault at this site. Ideally, we would like to know the exact year of each earthquake and the exact year that the channel was cut to determine the recurrence interval and slip rate of the fault. However, it is not possible to determine the timing of these events directly. What can be determined are the ages of units that bracket the events. Radiocarbon dating is the best dating tool available for Holocene materials and useful in this case since abundant organic material is preserved in the section.

Radiocarbon dating of sediments has several potential pitfalls. In northern California a major problem is that charcoal and wood collected from a stratigraphic horizon can be much older than the stratum in which it was deposited, because redwood trees have life-spans ranging up to several thousand years. (This problem is not unique to northern California, see, for example, Blong and Gillespie, 1978). Samples may also be younger than the horizon from which they

are collected. There are two reasons for this: 1) rodents can introduce new organic material into a stratum by burrowing and 2) the sample may represent the roots of a tree or shrub that grew in the sediment after deposition.

The latter two problems were avoided at this site by not collecting organic material from rodent burrows or material having obvious root-like characteristics. The former problem, however, is difficult to avoid. I found it impossible to assess, prior to radiocarbon analysis, whether a detrital charcoal or wood sample was substantially older than the stratum in which it was incorporated. In order to determine whether or not this was a problem, I looked for discordant radiocarbon dates between samples from the same stratum.

Two methods of radiocarbon dating are widely used today: conventional decay counting and direct measurement using the accelerator mass spectrometer (AMS) technique. Conventional radiocarbon dating can be more precise, but requires larger samples (tens of grams vs. tens of milligrams). A sample large enough for conventional analysis will typically contain many fragments of charcoal and wood. If the fragments of charcoal and wood within a sedimentary layer are derived from trees of various ages, then the radiocarbon age will be an intermediate value between the youngest and oldest fragment present in the sample.

To test for age variation among the pieces of wood and charcoal collected from a particular sedimentary horizon,

several small samples were analyzed separately by the AMS method. In the cases where these showed little age variation, the more precise conventional date of the large sample is taken as a close approximation of the age of the unit in question.

A total of 23 analyses were performed, five by the conventional counting method and 18 using the AMS technique (Table 2-1). The samples fall into six groups: samples from units 10, 20, 30, 40, and 45, and samples from the channel. The radiocarbon dates of the samples from each of these groups are discussed separately below, from youngest to oldest.

Table 2-1 lists all the samples, their uncorrected radiocarbon ages, their calibrated ages in calendar years and years before present, and the fraction of the likelihood function that falls within each age range (Sieh and others, in press). Those designated with QL numbers are conventional analyses done by M. Stuiver at the University of Washington; the rest are AMS analyses from the University of Arizona (AA) and Beta Analytic (ETH). The C14 ages were calibrated using the University of Washington Quaternary Isotope Lab Radiocarbon Calibration Program Rev. 2.0 (Stuiver and Reimer, 1986). Table 2 is a summary of the age estimates of the units derived from these data and relationships observed in the excavations.

Table 2-1. Table listing radiocarbon ages of samples collected from excavations near Point Arena. Under the column heading "LAB NO.", each sample is listed by sequential number (as they are discussed in the text) and by the number assigned by the laboratory responsible for the analysis. Samples with labels beginning with AA were analyzed at the National Science Foundation Accelerator Facility for radioisotope Analysis at the University of Arizona. QL samples were analyzed at the Quaternary Research Center of the University of Washington. ETH samples were analyzed through Beta Analytic at the accelerator at ETH, in Switzerland.

Under the heading "C14 AGE", radiocarbon ages are reported using standard conventions (e.g., Taylor, 1987, p.4). Errors in this column are one standard deviation.

Under the "CALENDAR YR" and "YRS BP" headings the calibrated ages are listed in calendar years and years before present, respectively. All C14 ages are calibrated using the calibration program of Stuiver and Reimer, 1986. No lab error multiplier was used. Date ranges reported span the 2 sigma error.

Under the "LIKELIHOOD" column the likelihood that the age of a sample lies within the given range is expressed as a fraction of 1.

Samples were averaged when appropriate; these are listed at the end of the table under Averages. Sample locations are noted on Plates 1 and 2.

TABLE 1

LAB NO.	C14 AGE	CALENDAR YR	YRS BP	LIKELIHOOD	COMMENTS
1) AA 3053	90±65	AD 1797-1947 1756-1780 1668-1753	3-153 170-194 197-282	.64 .05 .31	Charcoal from fissure produced by event V, i.e. post-dates event V.
2) AA 3047	165±75	AD 1636-1955 1531-1544	0-314 406-419	.99 .01	Charcoal from sand lense immediately below unit 50 contact, i.e. pre-dates event V. 99% probability is in range 0-314 ybp.
3) AA 3050	125±60	AD 1794-1949 1666-1784	1-156 166-284	.59 .40	Charcoal from sand lense unbroken by event R.
4) AA 3058	170±75	AD 1635-1955 1530-1552	0-315 398-420	.98 .02	Charcoal from gravel lense broken by event R.
5) QL 4210	300±30	AD 1492-1650	300-458	1.0	Charcoal and wood (mix of 6 & 7) from unit 40. Post-dates event N, pre-dates R/V.
6) AA3052	295±100	AD 1917-1955 1831-1877 1719-1814 1430-1700	0-33 73-119 136-231 250-520	.05 .03 .16 .75	One piece of partially burned wood from unit 40.
7) AA 3051	400±65	AD 1418-1639	311-532	1.0	One piece of charcoal from unit 40.
8) QL 4211	1170±30	AD 967-976 917-964 796-904 776-794	974-983 986-1033 1046-1154 1156-1174	.02 .18 .69 .11	Charcoal from unit 30 (mix of 9 & 11). Pre-dates event N; post-dates events F & J.
9) AA 3055	1150±70	AD 764-1000 708-750 688-703	950-1186 1200-1242 1247-1262	.92 .06 .02	Charcoal from unit 30 (one piece from 8).
10) AA 3057	1055±85	AD 775-1162	788-1175	.99	One piece of wood from unit 30.

TABLE 1 (cont'd)

LAB NO.	C14 AGE	CALENDAR YR	YRS BP	LIKELIHOOD	COMMENTS
11) AA 3054	780±65	AD 1371-1384 1150-1304 1118-1140 1040-1096	566-579 646-800 810-832 854-910	.02 .88 .03 .07	Charcoal from unit 30 (one piece from sample 8)
12) QL 4209	1930±40	AD 200-212 149-172 BC 3-AD 133 42-8 69-60 89-81	1738-1750 1778-1801 1817-1952 1957-1991 2009-2018 2030-2038	.02 .03 .86 .07 .01 .02	Wood and charcoal from unit 20.
13) ETH 2728	2265±90	BC 545-95 758-686	2044-2494 2635-2707	.96 .04	Wood from unit 20.
14) ETH 2729	2195±90	BC 84-18 410-86	1967-2033 2035-2359	.04 .95	Charcoal from unit 20.
15) ETH 2730	2080±90	BC 374-AD 72	1878-2313	1.0	Charcoal from unit 20.
16) ETH 2731	2710±90	BC 1187-663	2612-3136		Charcoal from unit 20.
17) QL 4213	2420±30	BC 563-405 592-566 657-637 760-683	2354-2512 2515-2541 2586-2606 2632-2709	.60 .06 .04 .29	Branch from channel.
18) AA 3056	2480±75	BC 474-412 789-478	2361-2423 2427-2738	.16 .84	One piece of charcoal from channel.
19) QL 4208	2030±30	AD 42-48 BC 116-AD 28 BC 166-144	1902-1908 1922-2965 2093-2115	.02 .92 .06	Charcoal and wood (mix of 22 & 23) from grey clay (unit 10).
20) AA 3059	3045±80	BC 1462-1060 1504-1477	3009-3411 3426-3453	.98 .02	Charcoal from unit 10.
21) AA3060	2540±85	BC 826-409	2358-2775	1.0	One piece of charcoal from unit 10..
22) AA 3048	505±75	AD 1597-1619 1282-1517	331-353 433-668	.02 .98	Wood from unit 10 - root that is younger than the unit (one piece from 19).
23) AA 3049	2355±75	BC 295-230 661-352 766-675	2179-2244 2610-2301 2715-2624	.08 .71 .20	One piece of charcoal from unit 10.

TABLE 1 (cont'd)

AVERAGES

UNIT	SAMPLE	C14 AGE	AVE C14	CALENDAR YRS	LIKELIHOOD
5) 40 6) 40 7) 40	QL-4210 AA-3052 AA-3051	300±30 295±65 400±65	316±26	AD 1488-1644	1.0
17) Ch 18) Ch	QL-4213 AA-3056	2420±30 2480±75	2428±28	BC 593-407 657-635 760-682	.65 .05 .30
21) 10 23) 10	AA-3060 AA-3049	2540±85 2355±75	2436±56	BC 661-405 766-675	.73 .27

Unit 45

Four samples were collected from the gravel between units 40 and 50 (1 through 4 in Table 1). Not enough datable material was available to do more than one AMS analysis of each sample, so the precision is poor for all of these. Calendric age ranges for these samples are from three to four hundred years to the present. All of these samples must be older than 1906 because the sediments show evidence of deformation during the 1906 earthquake. The horizons dated by these samples were deposited between AD 1530 and 1906, most likely after 1635.

Sample 1 (Table 1) was collected from a fissure associated with event V (Plate 1, V-2b-1). The age of the material filling this fissure must very closely post-date event V, because an open fissure would fill rapidly in the wet climate of northern California. The radiocarbon analysis of the charcoal collected from this unit indicates that it was deposited after 1668 AD.

Sample 2 was collected from a sand lens immediately below the unit-50 contact. This deposit, which pre-dates event V, formed after 1526 A.D. The likelihood that it formed after 1636 is 99%.

Sample 3 is from a sand lens unbroken by event R. Because this unit could have been deposited any time after 1666 AD, this radiocarbon analysis does not solve the problem of

whether event R is really a different earthquake than event V.

Sample 4 was collected from a unit broken by a fault associated with event R. The unit was deposited after 1530 AD and most likely after 1635.

These analyses provide constraints on the date(s) of event(s) R/V. Event V occurred after 1531 and most likely after 1636 (after deposition of sample 2); if event R is a separate earthquake, then it occurred after 1530 and most likely after 1635 (after deposition of sample 4).

Unit 40

Sample 5, collected from unit 40, was dated by the conventional method. Samples 6 and 7 were individual pieces of charcoal and wood selected from this sample and dated by the AMS technique. All three dates are compatible, so the higher-precision conventional date of sample 5, 1492-1650 AD, is a maximum age for unit 40. The average of the three samples gives a nearly identical date range: 1488-1644. Event N occurred before a date within this range.

Unit 30

Samples 8 through 11 were collected from unit 30. Of the three AMS ages determined for individual pieces of wood and charcoal (9-11), one, sample 11, is much younger. One way to interpret this set of data is to average the three concordant

Table 2-2. Interpretations of ages of units based on radiocarbon data.

TABLE 2
AGE ESTIMATES OF UNITS

UNIT	MAX RANGE	MOST LIKELY RANGE	COMMENTS
50	~1850-1906	Same	Brick and nail found in deposit; broken by 1906 faulting.
45	AD 1524-1906	AD 1635-1906	Gravels between units 40 and 50. Broken by event(s) R/V.
40	AD 1490-1653	Same	At least one, possibly two earthquakes between deposition of this unit and 1906.
30	AD 1045-1378	AD 1150-1204 (.88)	At least two, possibly three earthquakes between deposition of this unit and 1906.
20	BC 88-AD 206	BC 2-AD 133 (.86)	At least four, possibly five earthquakes between deposition of this unit and 1906.
Chan.	BC 763-403	BC 592-405 (.65) BC 759-681 (.30)	Maximum offset 64 m.
10	BC 790-400	BC 660-400 (.73) 766-675 (.27)	

dates (8, 9, & 10), and consider sample 11 to be a spurious analysis. However, samples 9 and 11, which do not have overlapping age ranges, were individual pieces of charcoal taken from sample 8. This could be interpreted to mean that the charcoal in sample 8 had a wide age range. If this is the case, then the age determination for sample 11 is a maximum age range for unit 30: 1040-1384 AD. The likelihood is very high (88%) that the date is in the range from 1150-1304 AD. This implies that event N most likely occurred after a date within the range 1150-1304 AD, and that event J most likely occurred before a date within this range.

Unit 20

Samples 12 through 16 were collected from unit 20. Again, the dates indicate a range in the ages of individual pieces of wood and charcoal within the unit, and the youngest age (sample 12) is taken as a maximum for this unit: BC 89-AD 212, with an 86% likelihood that the date is within the range BC 3-A.D. 133. This indicates that events F and J occurred after BC 89, and probably after BC 3

Channel

Samples 17 and 18 were collected from the sediment filling the channel cut into unit 10. Sample 17 was collected from the southwest side of the fault in trench 14; sample 18 was collected from the northeast side of the fault in trench 9

(Plate 2). The two samples give compatible ranges: BC 760-405 for sample 17 and BC 789-412 for sample 18, and therefore, the average of these, BC 760-407 is taken as the age of the channel-filling sediment. Sample 17 was a small branch of wood, and because it is unlikely that it was much older than the sediments in which it was deposited, this age is probably close to the true age of the deposit.

Unit 10

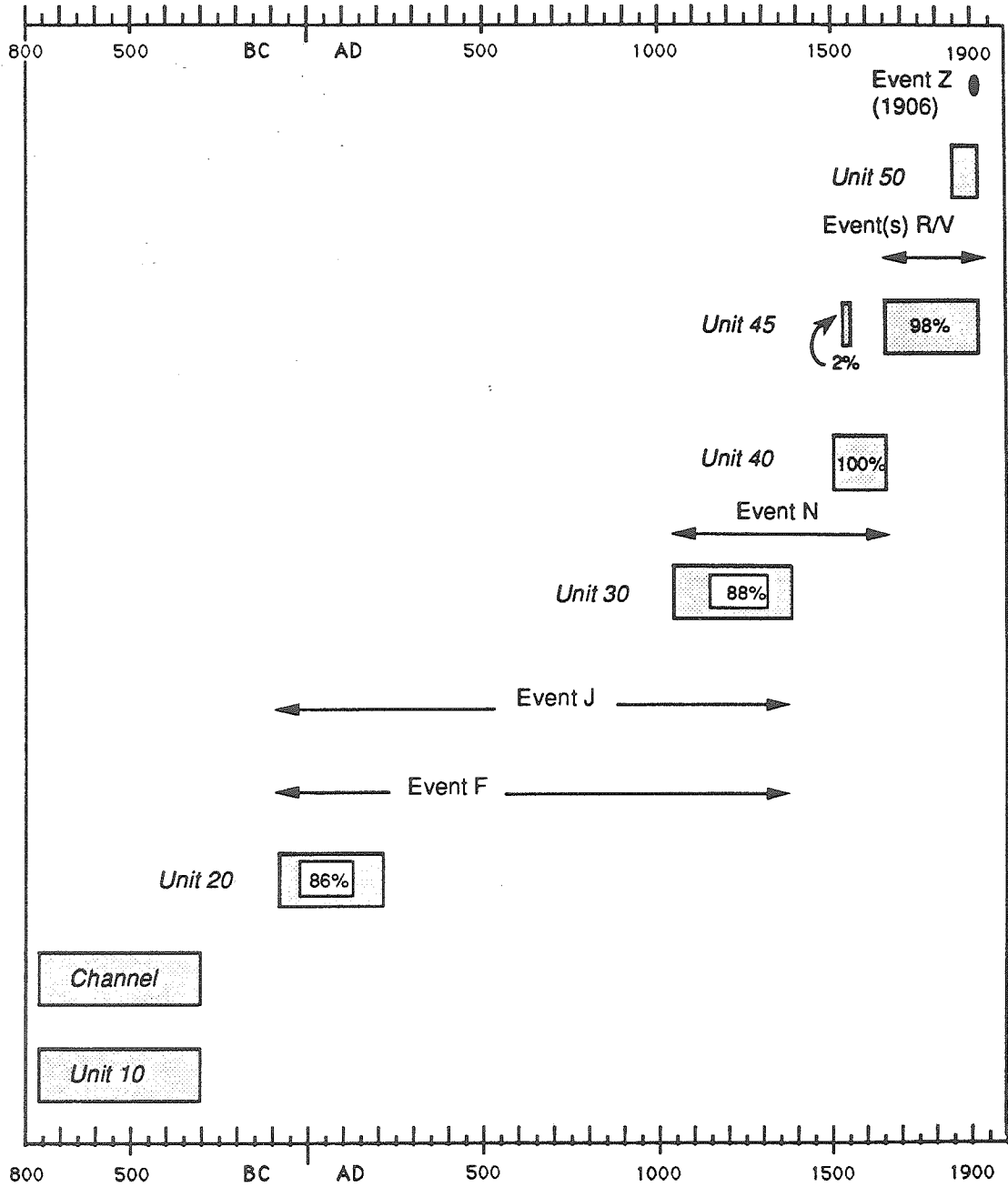
Five samples from the grey clay underlying the fluvial gravels (unit 10) were analyzed. Sample 22 was a twig-shaped piece of wood that was thought to be a branch; however the anomalously young age for this sample indicates that it was a root mistakenly identified as a twig. This material was taken from sample 19; sample 19 was a large sample of mixed wood and charcoal sent for conventional analysis. The contamination caused by roots is apparent in the radiocarbon age of sample 19: BC 116-AD 28, intermediate between the ages of samples 22 and 23 that were taken from sample 19. Samples 23 and 21 yielded overlapping age ranges, BC 766-230 and BC 826-409. The fifth sample, 20, gave an age of BC 1504-1060, much older than the others. Since the age ranges of samples 22 and 23 overlap, the weighted average of these, BC 766-405, is taken as the maximum age range for unit 10. This strongly suggests that the age of the channel cut is not more than a few 100 years greater than the age of the channel fill.

DISCUSSION

Recurrence interval

Figure 2-9 summarizes the relationships between the paleoseismic events described above and the dated units. Events F and J occurred between the times of deposition of units 20 and 30, between BC 89 and AD 1384, with the highest likelihood between BC 3 and AD 1304. Event N occurred between the times of deposition of units 30 and 40, between 1040 and 1644, most likely between 1150 and 1644. Event(s) R/V occurred between the time that unit 45 began to be deposited and the time of deposition of unit 50, most likely between 1635 and 1906, though there is a small possibility that unit 45 formed as long ago as 1530. Two historical earthquakes could be the cause of the faults associated with event(s) R/V: the 1898 earthquake assigned to the San Andreas fault offshore to the northwest of Point Arena, and the 1838 earthquake on the San Francisco peninsula. There is no indication that the 1838 rupture extended as far north as Point Arena, but this possibility can not be ruled out completely. While it is possible that surface rupture in 1898 occurred in Point Arena, again there is no report of any, and the intensities reported for this earthquake suggest a magnitude of 6.4 (Topozada, et al., 1981), which is probably not large enough to have been associated with surface rupture as far away as Point Arena (Mark, 1977; Slemmons and Chung, 1982). While event(s) R/V

Figure 2-9. Chart summarizing relationships between dated units and paleoseismic events recognized in the exposures. Horizontal axis shows time in calendar years, vertical axis has no significance. The horizontal width of a box indicates the age range of the unit (2 sigma error); Smaller, nested boxes with percentages indicate the most likely age ranges. Horizontal arrows represent the age ranges of paleoseismic events. Events F and J occurred between the times of deposition of units 20 and 30, so could have occurred any time within the interval BC 89 and AD 1384. Event N occurred between the times of deposition of units 30 and 40, between AD 1040 and 1644. Event(s) R/V occurred before the deposition of unit 50 (between about 1850 and 1906) and most likely after 1635. Event Z occurred in 1906.



CALENDAR YEARS
Figure 2-9

could represent one or both of these earthquakes, this is not very likely.

These data imply that either the recurrence interval of earthquakes along this stretch of the fault is irregular, or that slip events were not recorded within the section. Recent work in southern California shows that the time period between earthquakes at the Pallett Creek site is irregular (Sieh and others, in press), so this may be the case in northern California as well. However, the nature of the section near Point Arena is such that it is just as likely that slip events are unrecognized: the sediments of the section are very coarse, deposition was episodic, and the deposition of some of the younger units was accompanied by erosion of underlying units. It is not possible with the data available to determine which of these possibilities is the case.

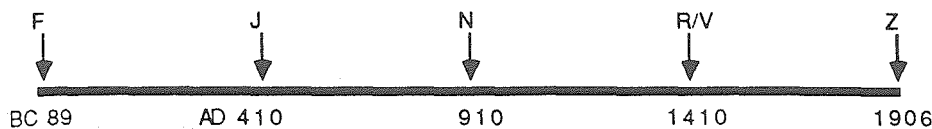
If the assumption that great earthquakes occur at regular intervals along any given segment of a fault is accepted, and the hypothesis that slip events have gone unrecognized in the section is correct, then several different possible scenarios can be constructed to estimate the recurrence interval of the northern San Andreas fault using the data collected from these excavations. Two sets of possible recurrence intervals can be deduced from the dates and relationships observed in the excavations. The first set assumes that faults assigned to event R represent the same earthquake as faults associated with event V - in other words that events R and V are actually

the same earthquake. This means that a minimum of 5 earthquakes have occurred since the deposition of unit 20. The longest recurrence interval that is possible given this situation is illustrated in Figure 10 A: if unit 20 was deposited in BC 89 (its maximum age within 2 sigma error) and event F happened immediately after deposition, then the time interval between BC 89 and 1906 (2000 years) contains 4 recurrence intervals of about 500 years in length. In this case, event J would have occurred around AD 410, N in AD 910 and R/V in 1410. However, the radiocarbon age data for unit 45 imply that this scenario is wrong - event R/V happened after deposition of unit 45, no earlier than AD 1530, and probably no earlier than AD 1635 (Tables 1 and 2). Also, event N occurred after the deposition of unit 30, no earlier than AD 1040. So, if the recurrence interval is regular, then events must be missing from the section, and the interval must be less than 500 years.

At the other extreme, unit 20 could have been deposited as late as AD 212, and an earthquake not recorded in the section could have occurred immediately before its deposition, meaning that a full recurrence interval elapsed between deposition of unit 20 and the occurrence of event F (Figure 10, case B). In this case the interval between AD 212 and 1906 (1700 years) contains 5 recurrence intervals each 340 years in length. This scenario implies the occurrence of an earthquake around 1566 AD, which is possible because R/V occurred after deposition

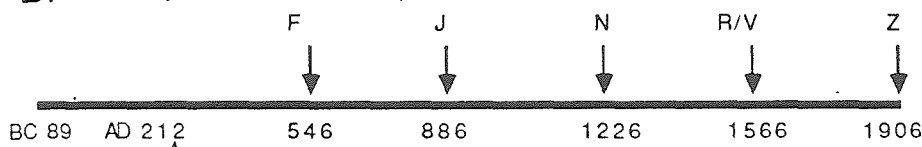
Figure 2-10. Figure showing possible scenarios of earthquake occurrence if uniform recurrence is assumed. R/V is considered to be a single event in this set of models. The horizontal lines represent time in calendar years; arrows represent dates of earthquakes predicted by the models - downward-pointing arrows represent earthquakes that can be assigned to events seen in the excavations, upward-pointing arrows represent events predicted by the models but not recorded at the Point Arena site.

A. 500 year recurrence; not possible



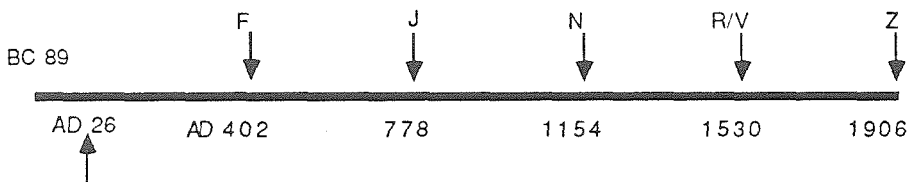
CALENDAR YEARS

B. 340 year recurrence; possible



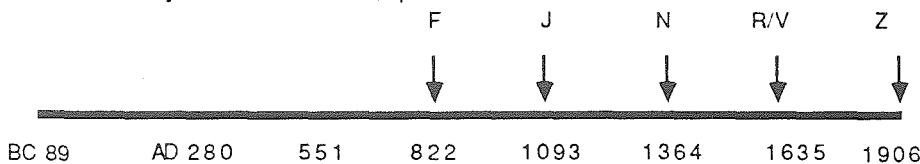
CALENDAR YEARS

C. 376 year recurrence; possible



CALENDAR YEARS

D. 271 year recurrence; possible



CALENDAR YEARS

SYMBOLS

↓ event seen in section

↑ unrecorded or unrecognized event

Column showing units, maximum age ranges, and timing of events

Event Z (1906)

50 Historical 1906 to mid-1800's

Event R/V

45 1906-1530

40 1644-1488

Event N

30 1384-1040

Events F and J

20 212-BC 89

Ch BC 407-BC 760

10 BC 405-BC 766

Figure 2-10

of unit 45 and unit 45 was deposited after AD 1530. However, this case is unlikely because there is a 98% chance that unit 45 was deposited after AD 1635, so event R/V most probably occurred after AD 1635.

A different approach is taken in cases C and D in Figure 10. Event R/V must have occurred sometime after AD 1530, the earliest date possible for deposition of unit 45. Thus, the maximum interval between events R/V and Z is 376 years. This recurrence interval suggests that earthquakes should have occurred around AD 1530, AD 1154, AD 778, and AD 402 (case C, Figure 10). This case is also possible given the available constraints, but unlikely since event R/V probably happened after 1635.

Case D in Figure 10 illustrates the results of adopting the most likely earliest date of event R/V: AD 1635, the earliest probable date of deposition of unit 45. The interval between AD 1635 and 1906, 271 years, is then the longest probable recurrence interval between events R/V and Z. Using this recurrence interval, earthquakes should have occurred around AD 1364, AD 1093, AD 822, AD 551 and AD 280. This is also possible given the data available: event N could have occurred in AD 1365, J in AD 1094 and F in AD 823. The two earlier events implied in this case (in AD 552 and 281) may have occurred and simply not been recorded in the section. This is quite possible, given the nature of the sediments at this site.

Figure 11 illustrates the possibilities if events R and V were two different earthquakes. Case A, as in case A in Figure 10, assumes the earliest possible date of deposition of unit 20, BC 89, and that event F occurred immediately after unit 20 was deposited. In this case the amount of time between BC 89 and 1906, 1995 years, contains five intervals, each 399 years in length. In this scenario, earthquakes should have occurred in AD 310, AD 709, AD 1108 and AD 1507. As in case A in Figure 10, this is not possible because events R and V both occurred after AD 1530.

The other extreme, as in case B in Figure 10, is illustrated in Figure 11, case B. If unit G were deposited in AD 212 and an earthquake prior to event F occurred immediately before deposition and was not recorded, then the time between AD 212 and 1906 (1694 years) contains 6 intervals, each 282 years long. In this case earthquakes would have occurred in AD 491, AD 775, AD 1058, AD 1341 and AD 1624. This is also not possible, because event R could not have occurred as early as AD 1341. Also, event N occurred after deposition of unit 30, and although it may have occurred in 1058 (because the maximum date range for unit 30 is AD 1040-1384) this is unlikely because there is an 88% chance that unit 30 was deposited between AD 1150-1304.

If both events R and V occurred after AD 1530, as required by the available data, then the interval between AD 1530 and 1906 (376 years) contains two earthquake recurrence intervals

Figure 2-11. Figure showing possible scenarios of earthquake occurrence if uniform recurrence is assumed. R and V are considered to be separate events in this set of models. The horizontal lines represent time in calendar years; arrows represent dates of earthquakes predicted by the models - downward-pointing arrows represent earthquakes that can be assigned to events seen in the excavations, upward-pointing arrows represent events predicted by the models but not recorded at the Point Arena site.

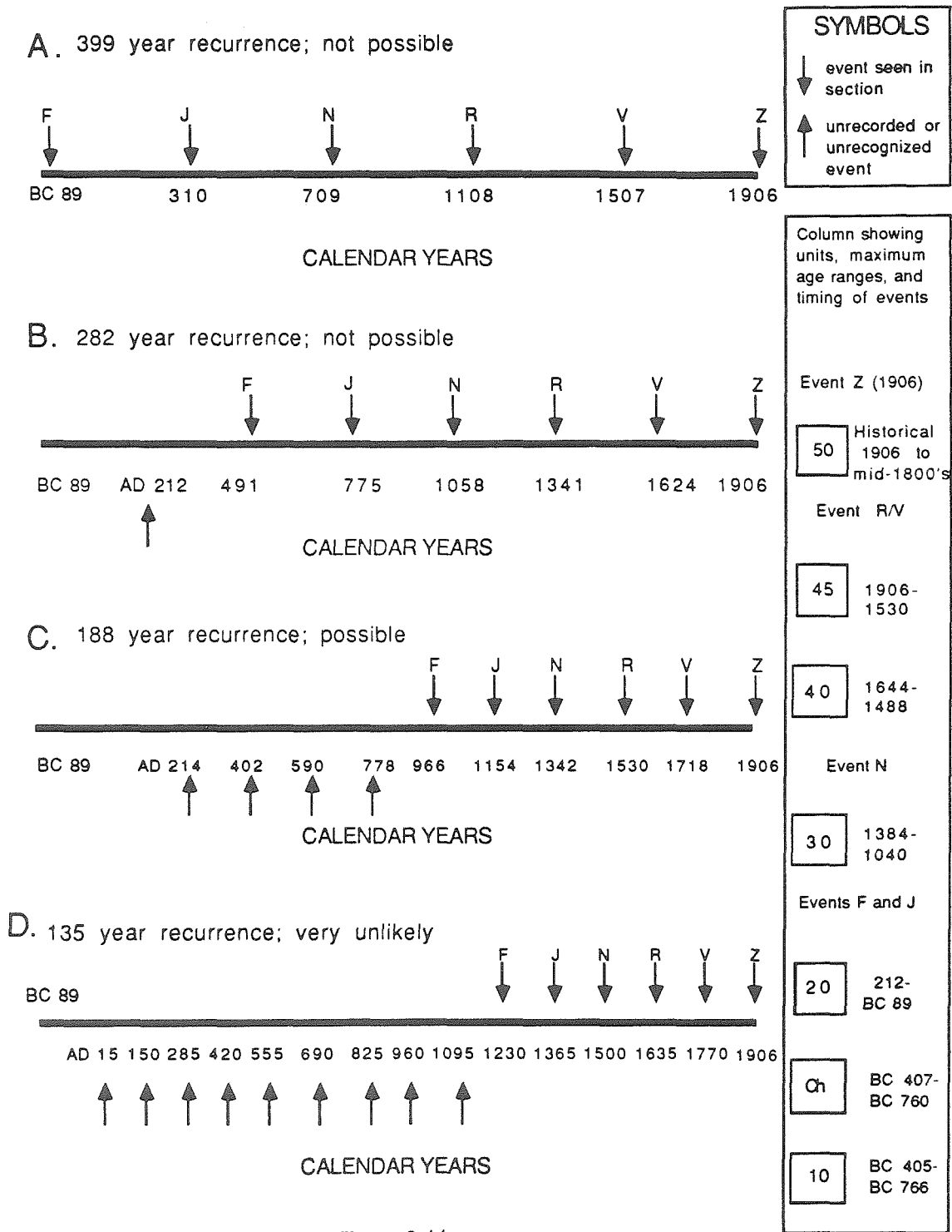


Figure 2-11

of at most 188 years each. This case is illustrated in case C of Figure 11, which shows earthquakes in AD 1718, 1530, 1342, 1154, 966, 778, 590, 402 and 214. Events N, J and F could have occurred in 1342, 1154 and 966, respectively, and the four earlier earthquakes could have occurred and gone unrecorded or unrecognized in the section.

The case that yields the shortest recurrence interval is illustrated in Figure 11 case D. The most likely earliest date of deposition of unit 45 is AD 1636, and both events R and V (if they are separate earthquakes) occurred after deposition of this unit and before 1906. This case illustrates a 135 year recurrence interval, with earthquakes in AD 1770, 1635, 1500, 1365, 1230, 1095, 960, 825, 690, 555, 420, 285, 150, and 15. While not impossible given the data, this case suggests that at least 9 earthquakes, unrecorded or unrecognized in the section, have occurred. It seems unlikely that this many events would be missing.

Of the 8 cases presented in Figures 10 and 11, only four, 10 B, C, D and 11 C fit the available data reasonably well. This suggests that the average recurrence interval for earthquakes at this site is between about 200 years (if events R and V represent two separate earthquakes, case 11 C) and 380 years. All of the possible cases imply that unrecorded or unrecognized earthquakes occurred during the time interval recorded by the entire section exposed in the excavations. Only one of the cases built around the interpretation that

events R and V are separate earthquakes is possible (Figure 11 C), and this case is unlikely since there is a 99% chance that event R did not occur as early as 1530. If earthquake recurrence intervals are uniform along this segment of the fault, then this suggests that faults assigned to events R and V are really the result of a single earthquake.

It is interesting to note that a study of old trees along this segment of the fault suggests the possible occurrence of an earthquake between 1400 and 1650 AD (LaMarche and Wallace, 1972). This could well be event N, or, less likely, event R/V.

Slip rate

The offset channel cut into the grey clay (unit 10) provides an opportunity to place a constraint on the late Holocene slip rate of the fault in this area. The two samples analyzed for radiocarbon dating were collected from opposite sides of the fault zone in trenches 6 and 9 (Plate 2). The similarity of the two ages supports the suggested correlation. The separation of the channel edge across the fault zone is 64 ± 1 meters. The geometry of the channel edge projected in map view, as shown in Plate 2, strongly suggests that some portion of this separation is due to the original path of the channel through the fault zone, rather than tectonic offset, because the channel approaches the fault at such a low angle. Thus, the measured separation of 64 meters is a maximum displacement of the channel. If the trend of the channel in

excavations 5 through 7 and 14 is projected across the fault zone, then the separation is reduced to about 58 meters (Plate 2, Map View B). The age of the channel fill (2356 to 2709 years bp), and the age of the grey clay it is cut into (2354 to 2715 years bp), are indistinguishable. This indicates that the channel itself was probably cut sometime during the interval 2354-2709 years before present. These data yield a maximum average late Holocene slip rate of 25.5 ± 2.5 mm/yr; if the maximum separation is only 58 ± 1 meters, as suggested by projecting the channel edge across the fault zone, then the maximum average slip rate is 23 ± 2 mm/yr.

Five meters (sixteen feet) of offset was measured near this site after the 1906 earthquake (Lawson, 1908). Assuming that strain accumulates uniformly, and that slip associated with the 1906 earthquake is characteristic at this site, the minimum average recurrence interval is about 200 years. This is in agreement with the paleoseismic data, which suggest a maximum recurrence interval between about 200 and 380 years.

SUMMARY AND CONCLUSIONS

At least five events have occurred near Point Arena on the San Andreas fault during the past 2000 years. All of these have occurred since the deposition of a unit that has a radiocarbon date range of BC 89 to AD 212. The most recent earthquake, event Z, occurred in 1906. These data can be used

to construct a variety of cases for possible earthquake recurrence intervals. If more earthquakes occurred than were recognized in the section, then uniform recurrence intervals from about 200 to 380 years are possible (but 270 to 380 years is a more likely range for the recurrence interval at this site). If the events recognized in the section are the only events that have occurred during this time interval, then the recurrence intervals have not been uniform.

The late Holocene maximum average slip rate determined from an offset buried channel is about 25.5 ± 2.5 mm/yr. This slip rate combined with the amount of slip at this site measured after the 1906 earthquake (about 5 m) suggests at least a 200 year interval between earthquakes, which is in agreement with the best interpretations of the paleoseismic data.

If the entire segment that ruptured during the 1906 earthquake ruptured during each of the earthquakes recorded near Point Arena, then these data strongly suggest a long recurrence interval between 1906-sized events in the San Francisco area. Although these conclusions are tentative, and more paleoseismic and slip-rate data are needed to assess the hazard posed by the northern San Andreas fault, a repeat of the 1906 earthquake in the next century seems unlikely.

REFERENCES

- Blong, R.J., and Gillespie, R., 1978, Fluvially transported charcoal gives erroneous ^{14}C ages for recent deposits: *Nature*, V. 271, pp. 739-741.
- Brown, R.D., and Wolfe, E.W., 1972, Map showing recently active breaks along the San Andreas fault between Point Delgada and Bolinas Bay, California: U.S.G.S. Misc. Geol. Investigations Map I-692
- Cotton, W.R., Hall, N.T., and Hay, E.A., 1982, Holocene Behavior of the San Andreas fault at Dogtown, Point Reyes National Seashore, California: Final Tech. Rept. for U.S.G.S. Contract No. 14-08-0001-19841.
- Hall, 1984, Holocene history of the San Andreas fault between Crystal Springs Reservoir and San Andreas Dam, San Mateo County, California: *B.S.S.A.*, v. 74, n. 1, pp. 281-299.
- Hall, N.T., and Hay, E.A., 1984, Problems in the application of ^{14}C dates to slip rate determinations on the San Andreas fault: *Earthquake Notes, Abs., Seis. Soc. Am.*, 79th meeting, p. 8.

LaMarche, V.C., and Wallace, R.E., 1972, Evaluation of effects on trees of past movements on the San Andreas fault, northern California: Geol. Soc. Am. Bull., v. 83, pp. 2665-2676.

Lawson, A.C., et al., 1908, The California earthquake of April 18, 1906, Report of the State Earthquake Investigation Commission: Carnegie Inst. Wash. Publ. 87, 451 pp.

Louderback, G.D., 1947, Central California earthquakes of the 1830's: B.S.S.A., v.37, pp. 33-74.

Mark, R.K., 1977, Application of linear statistical models of earthquake magnitude versus fault length in estimating maximum expectable earthquakes: Geology, v.5, pp. 464-466.

Nason, R.D., 1971, Investigation of fault creep slippage in northern and central California: Ph.D. dissertation, University of California, San Diego, 231 pp.

- Prescott, W.H., Lisowski, M., and Savage, J.C., 1981, Geodetic measurement of crustal deformation on the San Andreas, Hayward, and Calaveras faults near San Francisco, California: J.G.R., v.86, pp. 10853-10869.
- Sarna-Wojcicki, A., Meyer, C.E., and Slate, J.L., 1986, Displacement of a ca. 6 Ma tuff across the San Andreas fault system, northern California: EOS, v. 67, n. 44, p. 1224.
- Schwartz, D. P., 1987, Earthquakes of the Holocene: Reviews of Geophysics, v. 25, n. 6, pp. 1197-1202.
- Sieh, K.E., Stuiver, M. and Brillinger, D., 1988, A more precise chronology of earthquakes produced by the San Andreas fault in southern California: in press.
- Slemmons, D.B., and Chung, D.H., 1982, Maximum credible earthquake magnitudes for the Calaveras and Hayward fault zones, California, in: Earthquake Hazards in the Eastern San Francisco Bay Area, Cal. Div. Mines and Geol. Special Pub. 62, pp. 115-124.

Stuiver, M. and Reimer, P.J., 1986, A computer program for radiocarbon age calibration: Radiocarbon, v. 28, pp. 1022-1030.

Topozada, T.R., Real, C.R., and Parke, D.L., 1981, Preparation of isoseismal maps and summaries of reported effects for pre-1900 California earthquakes: Cal. Div. Mines and Geol. Open File Report 81-11 SAC.

Weber, G., and Cotton, W., 1980, Geologic investigation of the recurrence intervals and recency of faulting along the San Gregorio fault zone, San Mateo County, California: Final Tech. Rept. for U.S.G.S. Contract no. 14-08-001-16822.

CHAPTER 3: LATE PLEISTOCENE SLIP RATE ON THE NORTHERN SAN ANDREAS FAULT

ABSTRACT

Offset marine terrace risers near Point Arena and an offset landslide near Fort Ross in northern California provide estimates of the average slip rate across the San Andreas fault since Late Pleistocene time. Near Fort Ross, a landslide has been offset approximately 1.7 km across the San Andreas fault. Radiocarbon analysis of charcoal from this deposit indicates that the landslide is older than 43,700 years. This implies that the average slip rate has been less than 39 mm/year across this segment of the fault. Correlation of two marine terrace risers across the San Andreas fault near Point Arena suggests offsets of approximately 1.5 and 2.5 km. The U-series age of a solitary coral, altitudinal spacing and correlation with known global high-sea-level stands suggest ages of 83,000 and 133,000 years for these surfaces, respectively, indicating an average slip rate of about 18-19 mm/yr since the Late Pleistocene. This rate is in agreement with the suggested Holocene maximum rate of about 23 mm/yr (Chapter 2, this work). If slip accumulates uniformly at this

rate, the 5 meters of slip that occurred in this area during the 1906 earthquake would take 250-280 years to accumulate. This slip rate implies that over half of the Pacific-North American plate motion is not accommodated on the San Andreas fault and must be occurring on other structures.

Correlation and age estimates for a flight of 5 marine terraces suggest uplift rates of 0.25 mm/yr north of Point Arena, about 0.5 mm/yr south of Point Arena, southwest of the San Andreas fault, and 0.75 mm/yr on the block adjacent to and northeast of the San Andreas. Deformation of marine terraces away from the principal zone of dextral slip includes reverse faulting and backtilting of surfaces near Point Arena. This suggests that compression perpendicular to the San Andreas is being accommodated by the growth of folds and reverse faults that trend subparallel to the fault.

INTRODUCTION

South of San Francisco the San Andreas fault undergoes a behavioral transition from creep at rates as high as 32 mm/yr (Burford and Harsh, 1980; Lisowski and Prescott, 1981) to dormancy punctuated by large coseismic ruptures (Prescott et al., 1981). This transition occurs near the southern end of the fault rupture of 1906, near San Juan Bautista (Figure 3-1). Along the creeping segment, the San Andreas fault zone is relatively simple, and activity is confined to a narrow zone (Lisowski and Prescott, 1981). North of the creeping segment,

Figure 3-1. Map of northern California showing faults of the San Andreas system. Numbers are current slip rates based on geodetic data (in mm/yr); bold numbers indicate fault creep rate. Geodetic studies show that slip on the San Andreas is currently partitioned across several fault zones in the San Francisco Bay area. How this slip is distributed north of the Bay area is not known. Rates from Prescott et al, 1981. Fault map compiled from Herd, 1978, and Kelsey and Cashman, 1983. SAFZ: San Andreas fault zone, SGFZ: San Gregorio fault zone, CvFZ: Calaveras fault zone, HFZ: Hayward fault zone, CFZ: Concord fault zone, GVFZ: Green Valley fault zone, RCFZ: Rodgers Creek fault zone, MFZ: Maacama fault zone, BSFZ: Bartlett Springs fault zone, ER-LMFZ: Eaton Roughs - Lake Mountain fault zone.

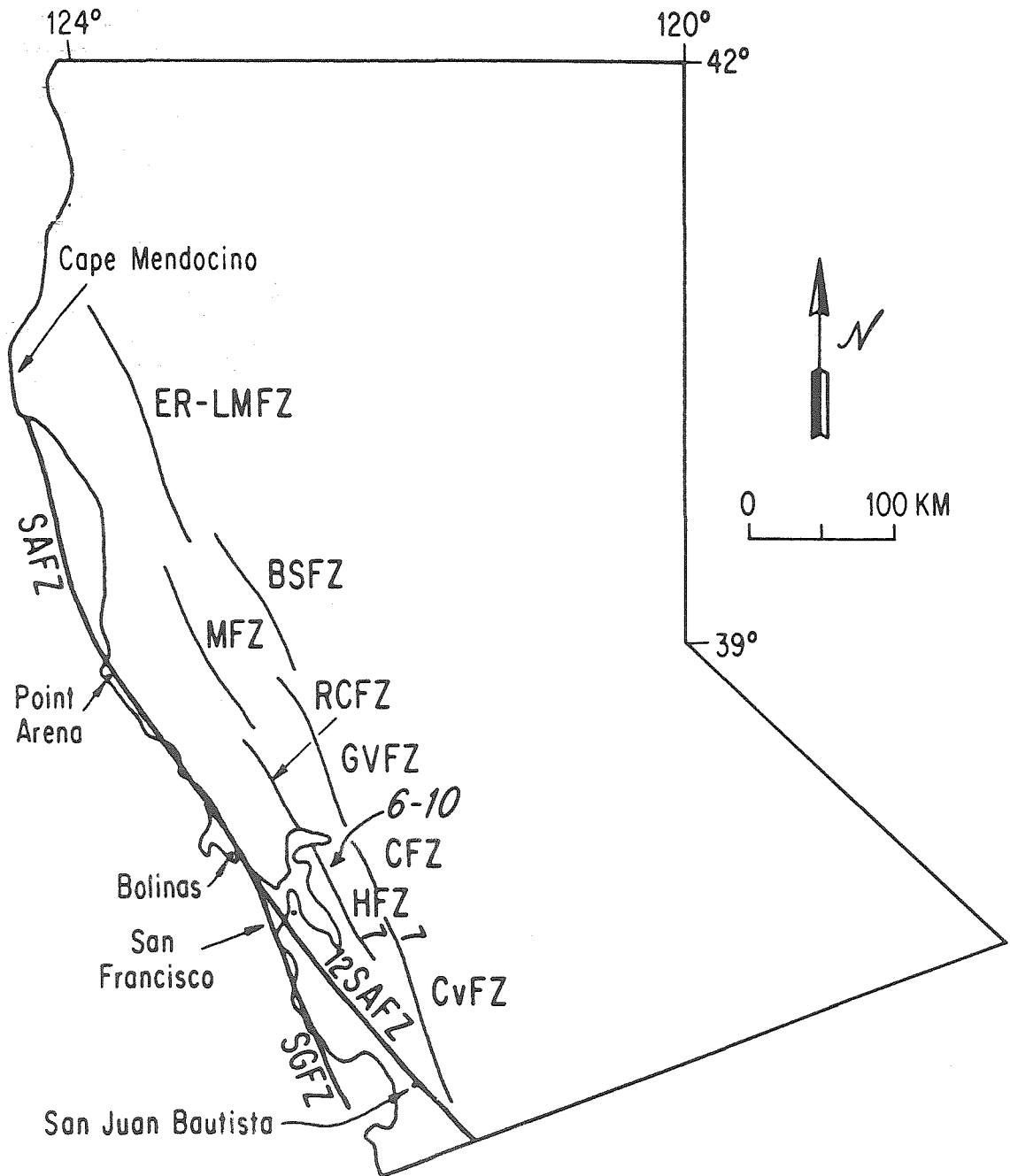


Figure 3-1

Figure 3-2. Map of northern California showing proposed geologic slip rates of faults in northern California in mm/yr. Rate determined for San Andreas north of San Francisco Bay for the last 6 Ma is over three times the 1200 year rate determined for this fault on the San Francisco peninsula. If both are correct, either the fault has slowed down in recent years or the slip rate is much higher north of the Golden Gate. The San Gregorio fault joins the San Andreas between these two areas and may add a component of slip to the San Andreas. Rates from Hall, 1984, Sarna-Wojcicki, 1986, and Weber and Lajoie, 1977. Fault map compiled from Herd, 1978, and Kelsey and Cashman, 1983. SAFZ: San Andreas fault zone, SGFZ: San Gregorio fault zone, CvFZ: Calaveras fault zone, HFZ: Hayward fault zone, CFZ: Concord fault zone, GVFZ: Green Valley fault zone, RCFZ: Rodgers Creek fault zone, MFZ: Maacama fault zone, BSFZ: Bartlett Springs fault zone, ER-LMFZ: Eaton Roughs - Lake Mountain fault zone.

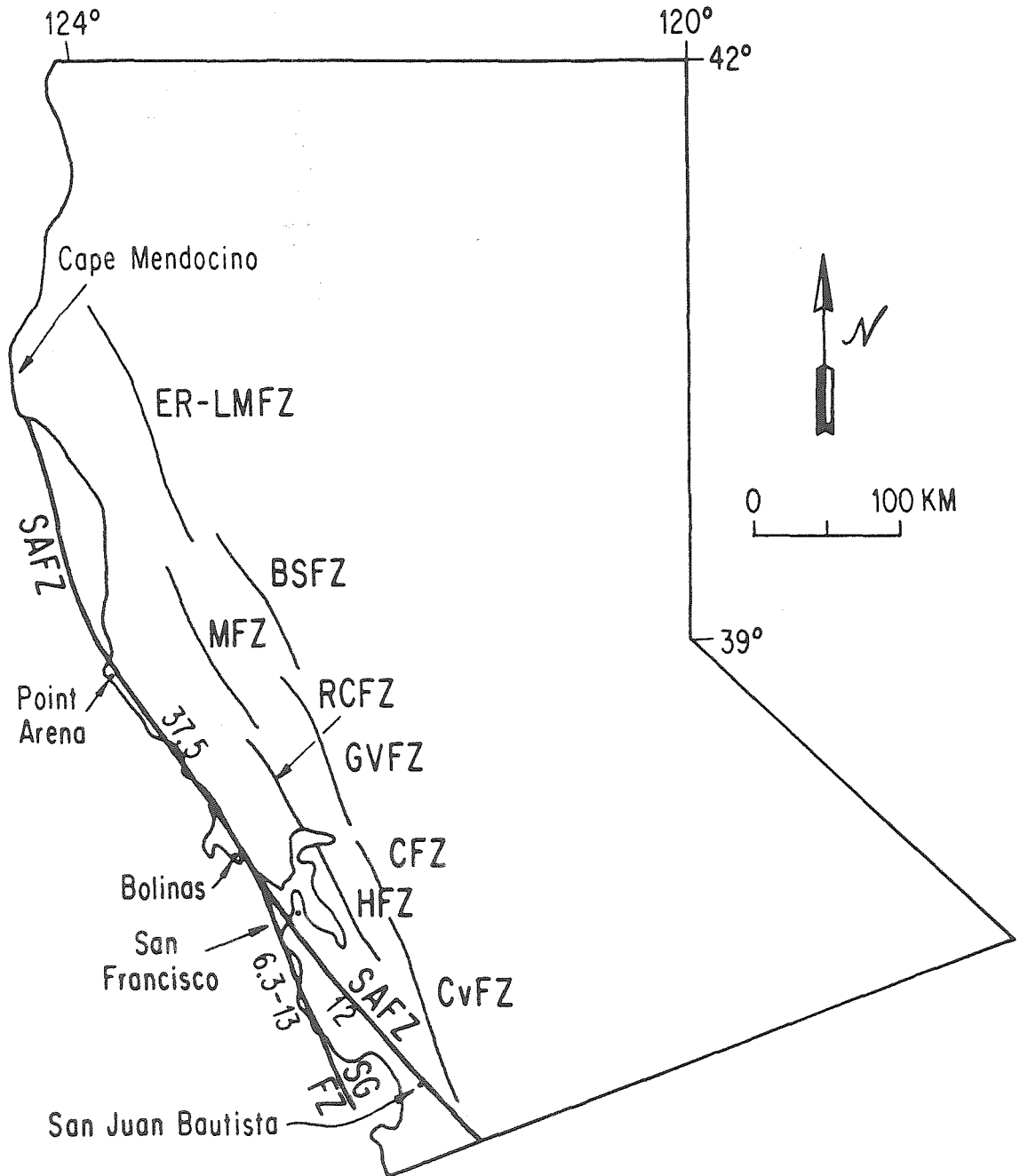


Figure 3-2

the plate boundary is a broad zone that includes several major strike-slip faults, all of which accommodate some portion of the plate-boundary motion (Figures 3-1 and 3-2). How slip is distributed across these fault zones has been the subject of several recent geodetic and geologic studies. Understanding the distribution of slip across the various faults is important in evaluating the seismic hazard posed by each of the faults and in estimating the recurrence time of great earthquakes.

A minimum average slip rate of about 12 mm/yr for the last 1200 years was determined from a geologic study near San Andreas Lake, south of San Francisco (Hall, 1984). This rate is similar to that inferred from geodetic data collected by Prescott et al. (1981) on the San Francisco peninsula. A slip rate across the Hayward fault near Fremont of at least 4 ± 0.4 mm/yr has been suggested by Borchardt et al., 1987. Geologic estimates of slip rate have not been proposed for the Calaveras fault north of its bifurcation with the Hayward fault, but geodetic data indicate that the modern slip rate is about 7 mm/yr on each of the two faults (Prescott et al., 1981). This is in agreement with observations of creep on the Hayward fault of 6-10 mm/yr (Nason, 1971; Savage and Burford, 1973). The geologic slip rate of the San Gregorio fault has been estimated at 6.3 - 13 mm/yr (Weber and LaJoie, 1977), but no geodetic data are available for this fault on the southern San Francisco peninsula. These data, together with

measurements of the slip rate on the creeping segment of the San Andreas fault suggests that much of the slip that occurs on the creeping segment is transferred to other faults in the San Francisco Bay area. While some of this slip is accommodated by creep, much of it is accumulating as elastic strain.

North of the San Francisco area little is known about the distribution of slip across the plate boundary. The San Gregorio fault apparently intersects the San Andreas near Bolinas (Figures 3-1 & 3-2), and although there appears to be another structure west of the San Andreas north of the intersection of the San Gregorio (Wagner and Bortugno, 1982), little is known about it, and available geodetic data suggest that little or no elastic strain is accumulating west of the San Andreas fault in this region (Prescott and Yu, 1986). There are a number of active faults north of the Golden Gate and east of the San Andreas (Figures 3-1 & 3-2). Faults associated with the modern plate boundary east of the San Andreas north of San Francisco include the Rodgers Creek, Maacama and Green Valley faults (Figures 3-1 & 3-2). Modeling of geodetic data indicates that much of the relative plate motion is being taken up east of the San Andreas fault north of San Francisco Bay, but the data do not allow resolution of the issue of whether this motion is confined to slip along the faults present in the area or if a significant portion of the slip is going into anelastic deformation over a broad region

(Prescott and Yu, 1986).

Little geologic information is available for the faults comprising the plate boundary north of San Francisco Bay. A study by Fox (1983) shows that late Tertiary rocks immediately east of the San Andreas fault are little deformed, but the late Tertiary rocks in the vicinity of the more easterly faults are intensely deformed. This suggests that a portion of the motion between the Pacific and North American plates is being accommodated over a broad region. However, this can not be quantified because no slip-rate data are available for any of the faults east of the San Andreas.

A suggested correlation of a 6 Ma tephra recovered from the offshore Delgada fan near Cape Mendocino with a tephra in the Wilson Grove Formation north of San Francisco is the basis for a proposed 37.5 mm/yr slip rate for the northern San Andreas fault since latest Miocene time (Sarna-Wojcicki, et al., 1986). If both this slip rate and the 12 mm/yr rate determined for the last 1200 years on the San Francisco Peninsula by Hall (1984) are correct, then either the San Andreas fault north of the Golden Gate is moving 3 times faster than it is just south of San Francisco, or the fault has slowed down considerably in recent time. These different slip rates imply dramatically different degrees of seismic hazard posed by the San Andreas to the San Francisco area.

Because of the importance of knowing the Quaternary slip rate of the San Andreas fault north of San Francisco, I have

used Pleistocene features and deposits to constrain the slip-rate for the northern San Andreas fault, north of San Francisco.

STUDY AREA

The area of coastal northern California between Fort Ross and Point Arena and west of the San Andreas fault is known as the Gualala block (Wentworth, 1967; Figure 3-3). Pleistocene deposits in this area include marine and fluvial terrace deposits and landslides. Near Point Arena and Fort Ross, at the northern and southern ends of the Gualala block, the San Andreas fault intersects a flight of Pleistocene marine terraces, and, near Fort Ross, a large landslide that was deposited across the fault (Figure 3-3). These features have been offset across the San Andreas fault. Estimates of the ages and offsets of these features enables calculation of an average Late Pleistocene slip rate across the San Andreas fault in this area.

OFFSET LANDSLIDE NEAR FORT ROSS

The headscarp of a large landslide is prominent on aerial photographs northeast of the San Andreas fault, about 1.5 km east-southeast of Fort Ross (Figure 4). Portions of this slide are still active, especially during heavy winter rainfall. However, most of the motion occurred at some time in the past. While much of the slide mass is on the northeast side of the

Figure 3-3. Map of the Gualala block showing locations of offset marine terrace risers near Point Arena and offset landslide near Fort Ross. Age and offset estimates of these features allow the calculation of slip rates for the northern San Andreas fault. The fault in this area last ruptured during the 1906 earthquake.

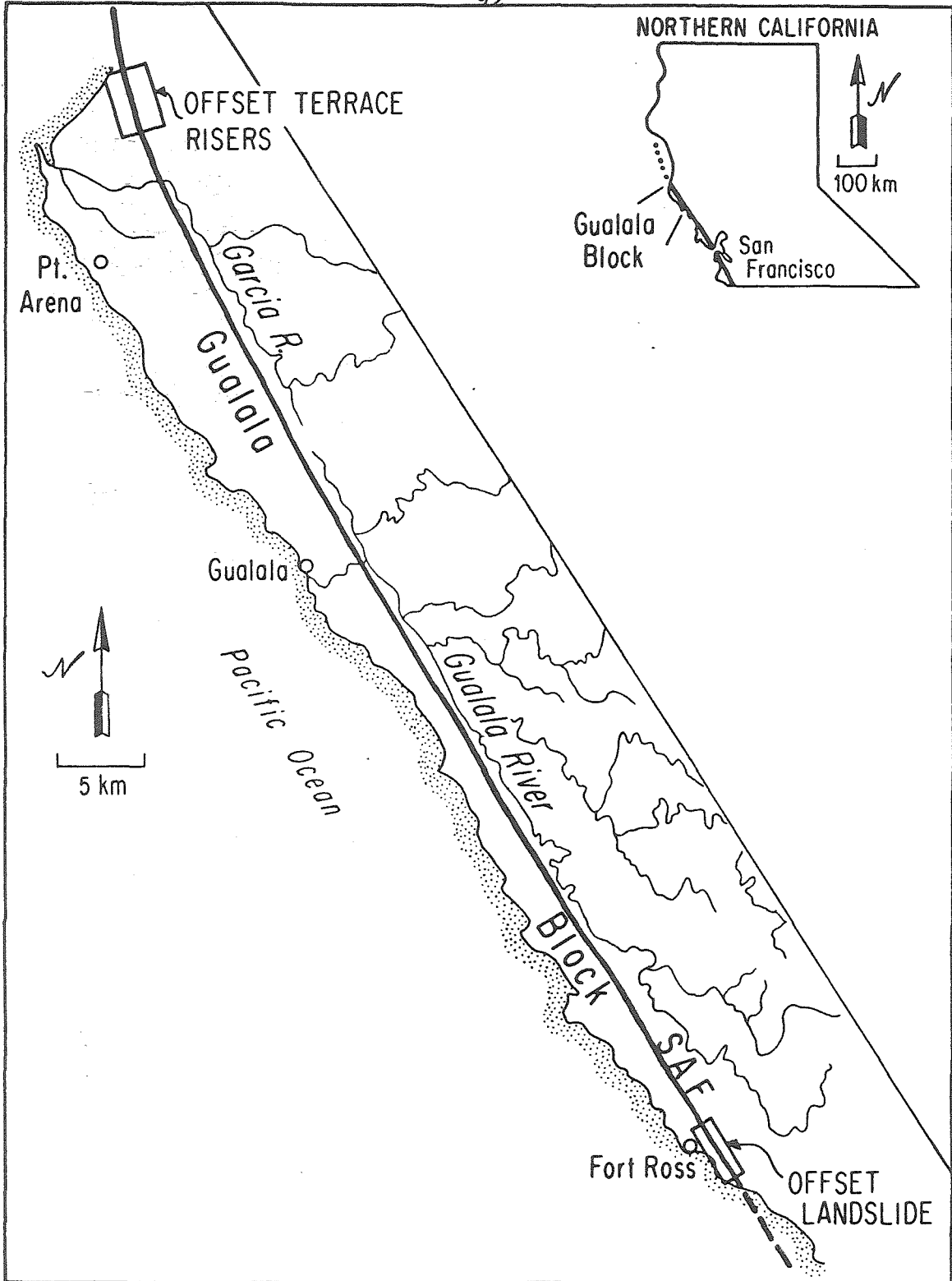


Figure 3-3

fault, it is clear that when the slide occurred it came across the fault zone. Also, the size of the headscarp suggests that the original slide was much larger than the volume of debris currently present immediately below it. The original toe of the slide, which was on the southwest side of the fault, has been offset by motion on the San Andreas. The slide is positioned such that ongoing motion across the fault removes the toe, so portions of the slide have continued to be unstable. Typically, small slumps occur during the wet winter months and often move out over the highway.

A landslide deposit approximately 0.5 km north of Fort Ross, on the southwestern side of the fault, is the only candidate to be the offset toe of the landslide discussed above (Figure 3-4). The surface of this deposit is hummocky, and exposures of the material in the small streams that dissect it are composed of Franciscan debris, which indicates that this mass originated northeast of the fault. No source for this material is evident in the hills immediately above this deposit; the closest headscarp of adequate size is the feature previously described, about 1.5 km east-southeast of Fort Ross, on the northeast side of the fault. A charcoal sample collected from within this deposit and near its base (Figure 3-4) was submitted for AMS radiocarbon analysis. Results of this analysis indicate that the material is beyond

Figure 3-4. Map of headscarp and offset toe of large landslide near Fort Ross. Age of slide deposit is greater than 43,700 years (beyond the range of radiocarbon dating). Offset is approximately 1.7 km; average slip rate since late Pleistocene time is therefore no greater than about 39 mm/yr.

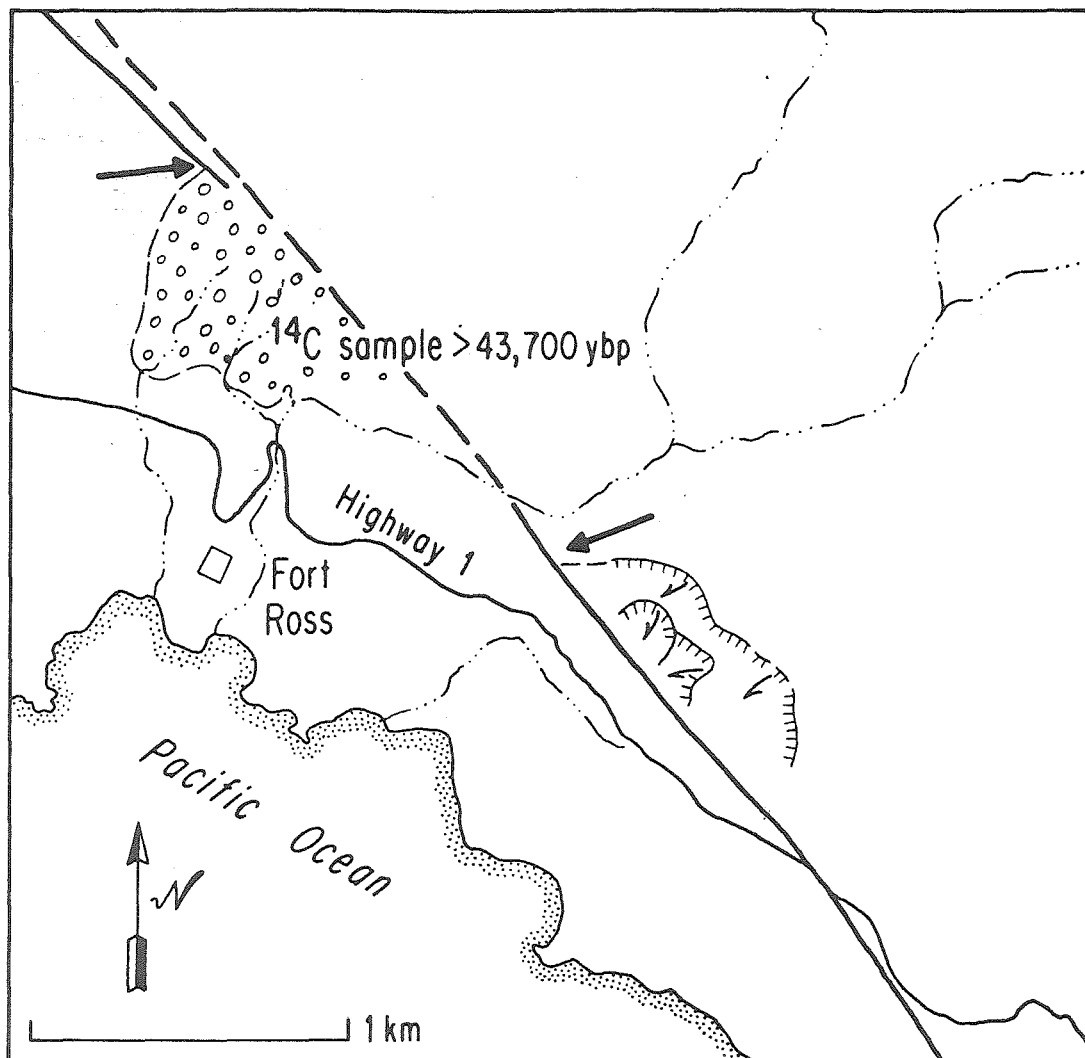


Figure 3-4

the range of radiocarbon dating: older than 43,700 years. ¹

Precise determination of the amount of offset of this feature is difficult. Because material has continued to be deposited as the toe of the slide has been offset, the northwest edge of the deposit is best suited to use as a piercing point. However, exposures in this region are poor, making definition of the edge of the deposit somewhat uncertain. Also uncertain is the amount of erosion that may have affected the deposit: the deposit may have at one time extended farther to the northwest if material has been eroded off the northern edge. However, assuming no significant erosion has occurred, the mapped northern edge of the deposit represents the best estimate of the position of the slide mass at the time the landslide first occurred.

On the northeast side of the fault, the headscarp does not extend all the way to the fault. Projection of the headscarp to the fault provides the best estimate of a piercing point to match with the northern edge of the deposit on the southwest side of the fault (Figure 3-4). Estimated error associated with this projection is about 0.2 km. The best estimate of the amount of offset is about 1.7 km; the offset is probably not less than 1.6 km, and not more than 1.9 km if this correlation is correct.

¹Sample AA-1577, analyzed at the National Science Foundation Accelerator Facility for Radioisotope Analysis, University of Arizona, 1986.

The minimum age of the landslide (43,700 years) and the best estimate of the offset (1.7 km) allow calculation of a maximum slip rate for this segment of the San Andreas fault. The slip rate is less than about 39 mm/yr. This determination confirms that the motion between the Pacific and North American plates is not all accommodated by slip on the San Andreas fault, but does not resolve the question of whether the slip rate is 37 mm/yr or 12 mm/yr.

PLEISTOCENE MARINE TERRACES NEAR POINT ARENA

Introduction

Although the offset landslide gives a maximum Pleistocene slip rate for this segment of the fault, I felt it was important to search for other features that might allow better constraint of the Pleistocene slip rate. The best such feature in this area is the flight of marine terraces that intersects the San Andreas fault zone near Point Arena.

There are two previous studies of the geology of the Point Arena area that include discussions of the marine terraces: a consultant's report (Jahns and Hamilton, 1971) and an unpublished Master's thesis (Valavanis, 1983). The former is a general study of the geology of the region, in which particular attention was paid to the tectonic setting of a proposed nuclear plant site. The latter study focuses on the geometry of the lowest terrace platform, using seismic refraction profiling. Contrary to my findings, both of these

studies conclude that no deformation of the youngest marine terraces, other than dextral offset across the San Andreas fault, has occurred. Neither study attempted to correlate terraces across the San Andreas fault or to quantify the displacements of these terraces across the fault zone.

Terraces Near Point Arena

Figure 3-5 is a representative profile across the Gualala block. The block is characterized by a northwest-trending linear ridge that lies between the San Andreas fault and the ocean (Gualala Ridge). The flat to gently rolling summit of this ridge reaches a maximum elevation of about 450 meters. It drops off steeply to the east into the drainages of the Gualala and Garcia Rivers. The western slope descends more gradually in a flight of five marine terraces to the modern shoreline. Because the marine terraces intersect and have been offset across the San Andreas fault near Point Arena, estimates of their ages and amounts of offset can be used to determine a Late Pleistocene slip rate for this segment of the fault.

To use the flight of terraces to determine fault slip rates, I mapped the terraces in the region, correlated them across the fault zone, made estimates of their offsets and estimated their ages. Plate 3 is a map of the terraces and other Quaternary deposits in the Point Arena area, prepared from study of aerial photographs and field mapping.

Figure 3-5. Topographic profile across the Gualala block south of Point Arena (area 1). Profile line is shown on Figure 3-6 and Plate 3. The five marine terraces recognized in the area are indicated.

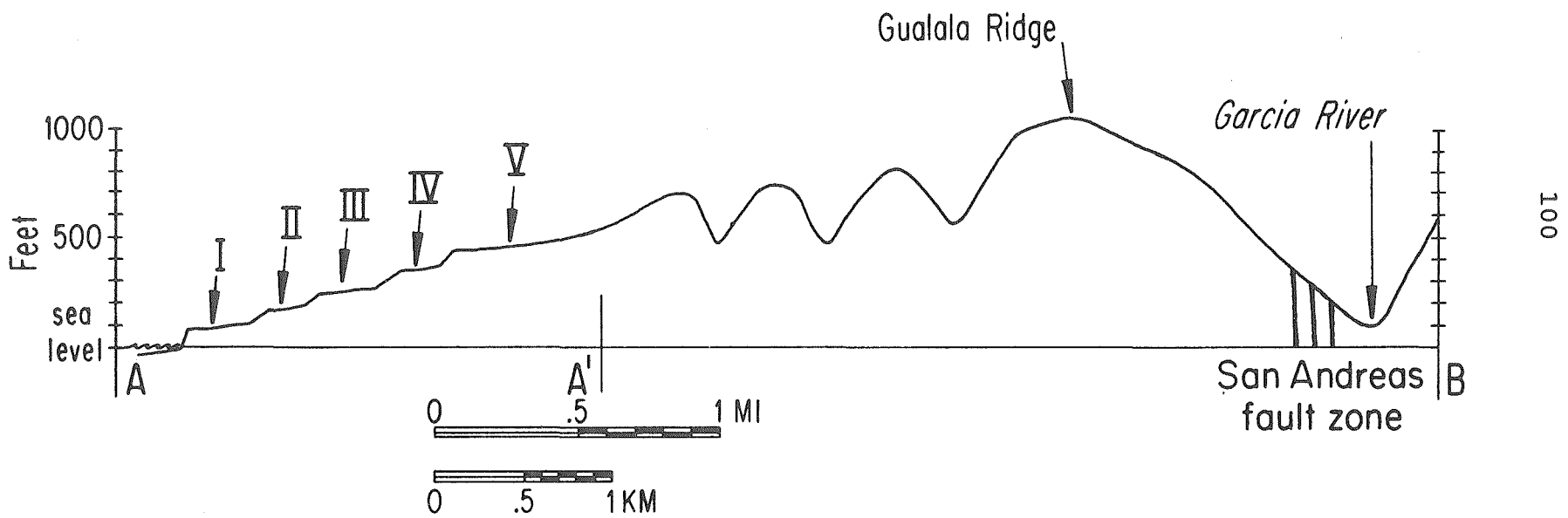


Figure 3-5

Because the terraces have been faulted and tilted throughout the area mapped, the correlation of surfaces is difficult. In most cases relative geomorphic position and elevation were the criteria used to discriminate the terraces. Three areas that are geomorphically and tectonically distinct will be discussed separately: 1) the area on the southwest side of the San Andreas south of the Garcia River, 2) the area on the southwest side of the San Andreas north of the Garcia River, and 3) the northeast side of the San Andreas fault (Figure 3-6). The major uncertainties in terrace correlation occur between these regions.

Area 1

Five distinct terrace levels were recognized in the coastal area southwest of the San Andreas fault between Iversen Point and Point Arena, south of the Garcia River (Figure 3-6, Plate 3). These are indicated on Figure 3-5 as levels I through V. Terraces I and III-V are fairly extensive and easy to trace to the Garcia River (Plate 3). Terrace II is represented by only a few remnants that have been correlated on the basis of their geomorphic position between terraces I and III.

The lower three terraces clearly have been tectonically deformed by both faulting and tilting. A thrust fault that places Miocene bedrock over the Pleistocene deposits of

Figure 3-6. Map showing the three geomorphically distinct areas: Area 1, south of the Garcia River mouth on the southwest side of the San Andreas fault, area 2, north of the Garcia River on the southwest side of the San Andreas fault, and, area 3, northeast side of the San Andreas fault. The presence of dunes, lagoons, and the accumulation of fluvial sediments in area 2 suggest that it is rising more slowly than the surrounding regions. This area is topographically lower than areas 1 and 3, and terrace elevations are also lower. Terraces in area 3 are at a higher elevation, suggesting higher rates of uplift. Greatest uncertainty in terrace correlation is between these areas. Profile line for Figure 3-5 shown. P7, P8, P11, P12, and P17 are photo points of Figures 3-7, 3-8, 3-11, 3-12, and 3-17, respectively.

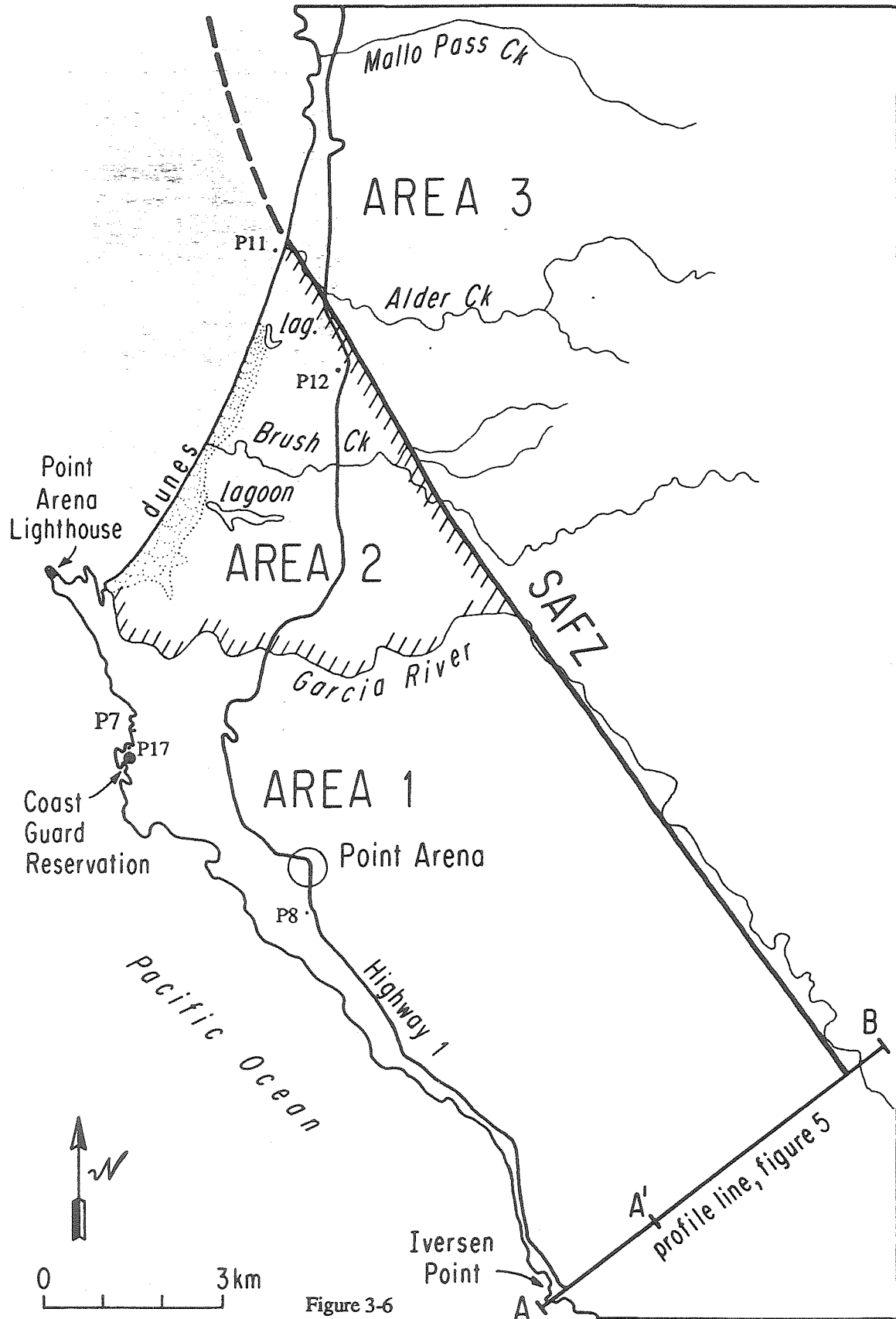


Figure 3-6

terrace I is shown in Figure 3-7. This is one of two such thrusts observed within a few hundred meters of each other. Two of the exposures show the northerly of the two faults flattening into a bedding plane fault with depth. These structures are probably associated with the folding, and provide further evidence that the folding is active and involves the youngest preserved Pleistocene marine terrace deposits.

Terrace 1 is also backtilted in area 1. The surface slopes away from the ocean toward the backedge of the terrace. Near the Coast Guard Reservation in section 3, south of Point Arena, the courses of two small streams have been deflected due to backtilting of terrace I. Instead of flowing more or less perpendicularly to the shoreline angle as expected for a non-deformed terrace, they flow parallel to the shoreline angle for parts of their lengths. Even though the observable eastward dip of the terrace surface in sections 2 & 3, just east of the Coast Guard station, has probably been enhanced by erosion due to the small stream running parallel to the shoreline angle, the course of the stream is probably controlled by the tectonic backtilting of the terrace surface.

It appears that this lowest terrace surface may be folded over the same axis as the underlying Miocene bedrock. Jahns and Hamilton (1971) documented the stratigraphy exposed in a deep excavation on the power plant site in sections 10 & 11 north of Arena Cove (Plate 3, cross section line E-F; Plate

Figure 3-7. Photo mosaic and line drawing showing sea-cliff exposure of Miocene bedrock thrust over Pleistocene marine terrace deposits. Location of exposure indicated as P7 on Figure 3 and Plate 3.

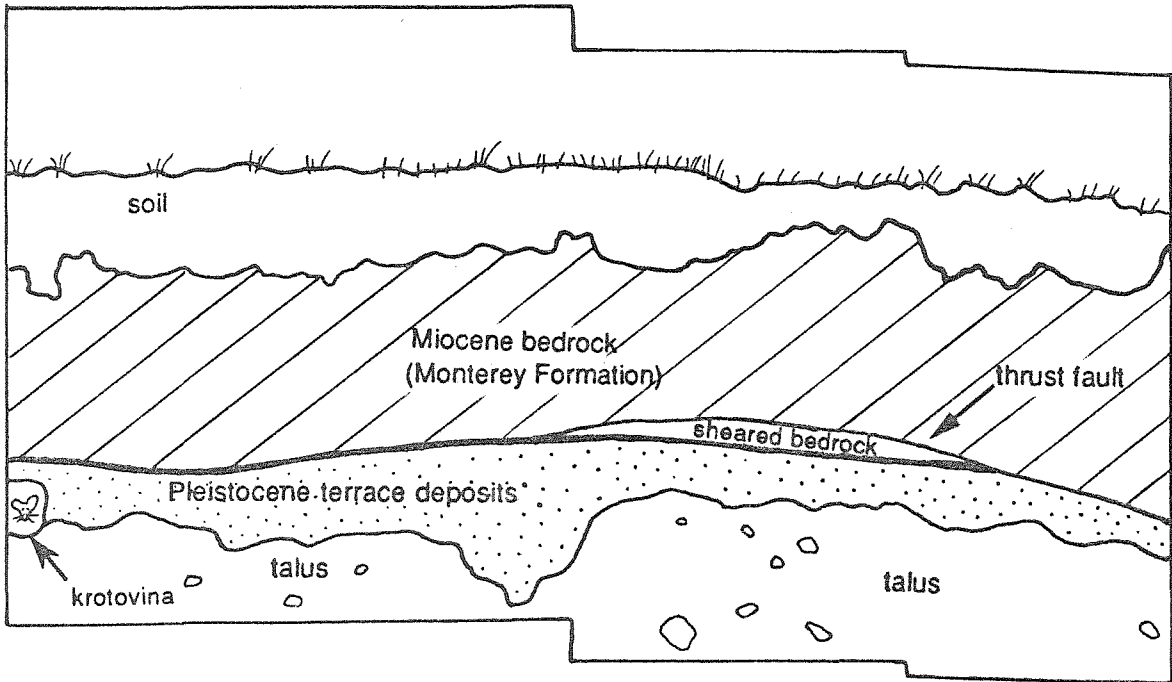
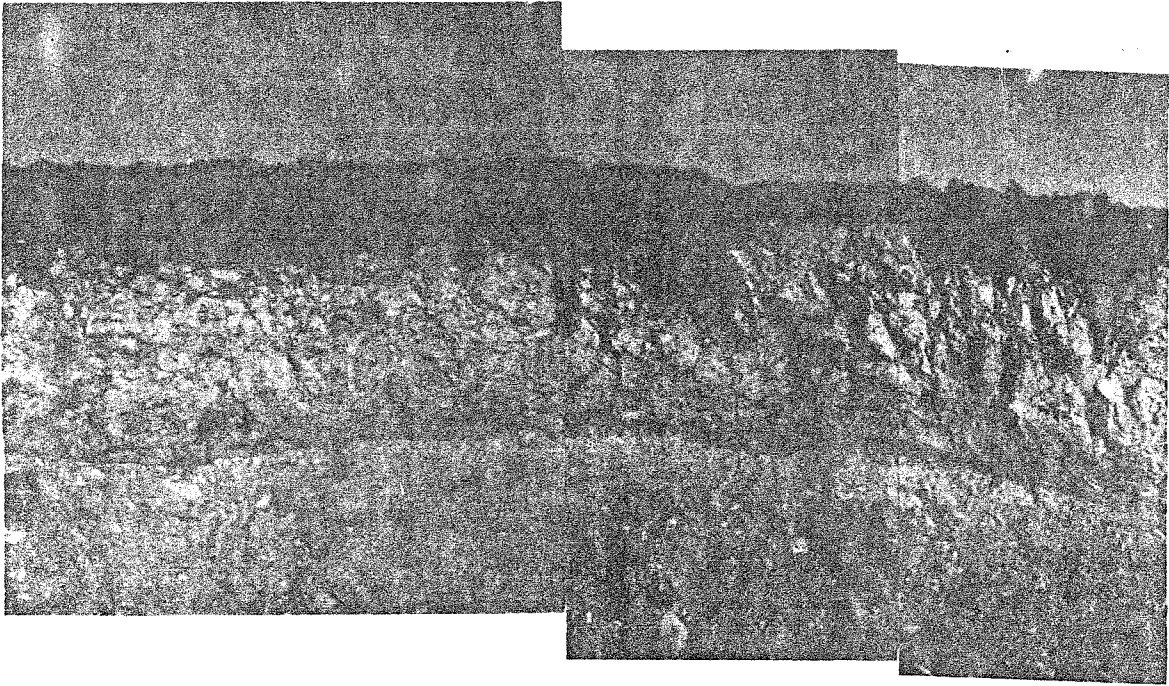


Figure 3-7

4). Their trench log very clearly shows an anticlinal axis in the bedrock running nearly perpendicularly to their trench. The carefully surveyed terrace surface also shows a change in dip directly over the anticlinal axis: west of the axis it dips seaward and east of the axis it dips nearly a degree toward the shoreline angle. The bedrock platform itself is very irregular so it is not as good a datum as the surface of the deposits, but the platform is also lower near the shoreline angle, as would be expected if the terrace is being folded as suggested.

The terrace III surface is also backtilted in area 1. This is clearly expressed just south of the town of Point Arena (sections 13 & 19, Plate 3) where terrace III slopes to the northeast, away from the coastline (Figure 3-8). This may account for the line of springs, small ponds and marshy areas present along the base of the backedge of this terrace. At this locality, the bedrock platform tilts landward, and groundwater is forced to flow in relatively permeable terrace deposits toward the shoreline angle. Where the groundwater encounters the ancient seacliff, the impermeable bedrock acts as a groundwater barrier, so the water rises to the surface. Terrace III is also backtilted north of Point Arena Creek. In this area there is another small pond that is probably due to the backtilting of the terrace and ponding of water against faulted bedrock.

These structures indicate a component of shortening

Figure 3-8. Photograph of terrace III looking southeast approximately parallel to the backedge of the terrace. Terrace surface slopes away from the modern beach toward its shoreline angle. Photograph is taken from locality marked P8 on Figure 3-6 and Plate 3.

← backedge of terrace ————— ocean →

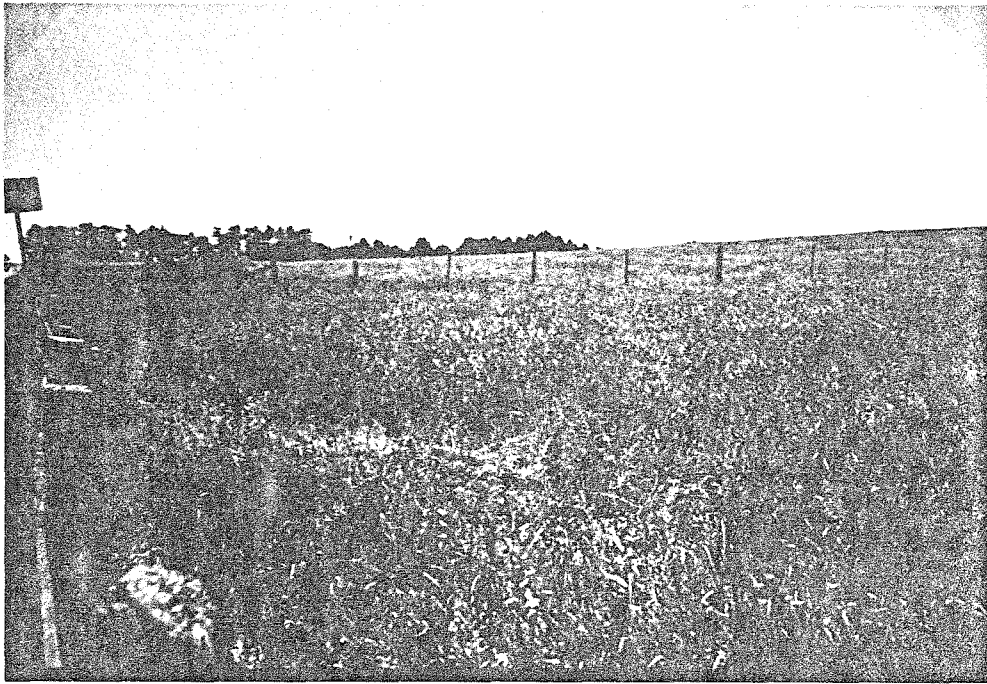


Figure 3-8

perpendicular to the San Andreas in this area. There are also compressional features in areas 2 and 3. Fault-perpendicular shortening is not unique to this region of California (see, for example, Zoback et al., 1987).

The Hathaway Creek fault, mapped by Jahns and Hamilton (1971) and by Boyle (1967) as a bedrock structure, has been active in Quaternary time as well, with northeast-side-down motion. Geomorphic evidence for the Quaternary activity of this fault includes the wide, marshy valley of Hathaway Creek as well as the lower elevation of terrace III on the northeast side of the fault. An exposure of several minor faults associated with this fault zone shows offset of the bedrock - terrace deposits contact in a road cut on Highway 1 (T 12 N, R 17 W, section 2). The maps of both earlier workers (Jahns and Hamilton, 1971; Boyle, 1967) indicate that the bedrock offset is up to the northeast, so this fault has apparently been reactivated in Quaternary time with the opposite sense of motion.

The higher terraces in area 1 undoubtedly have been deformed as well, but their vegetative cover and more subdued morphology make the observation of deformation more difficult.

Area 2

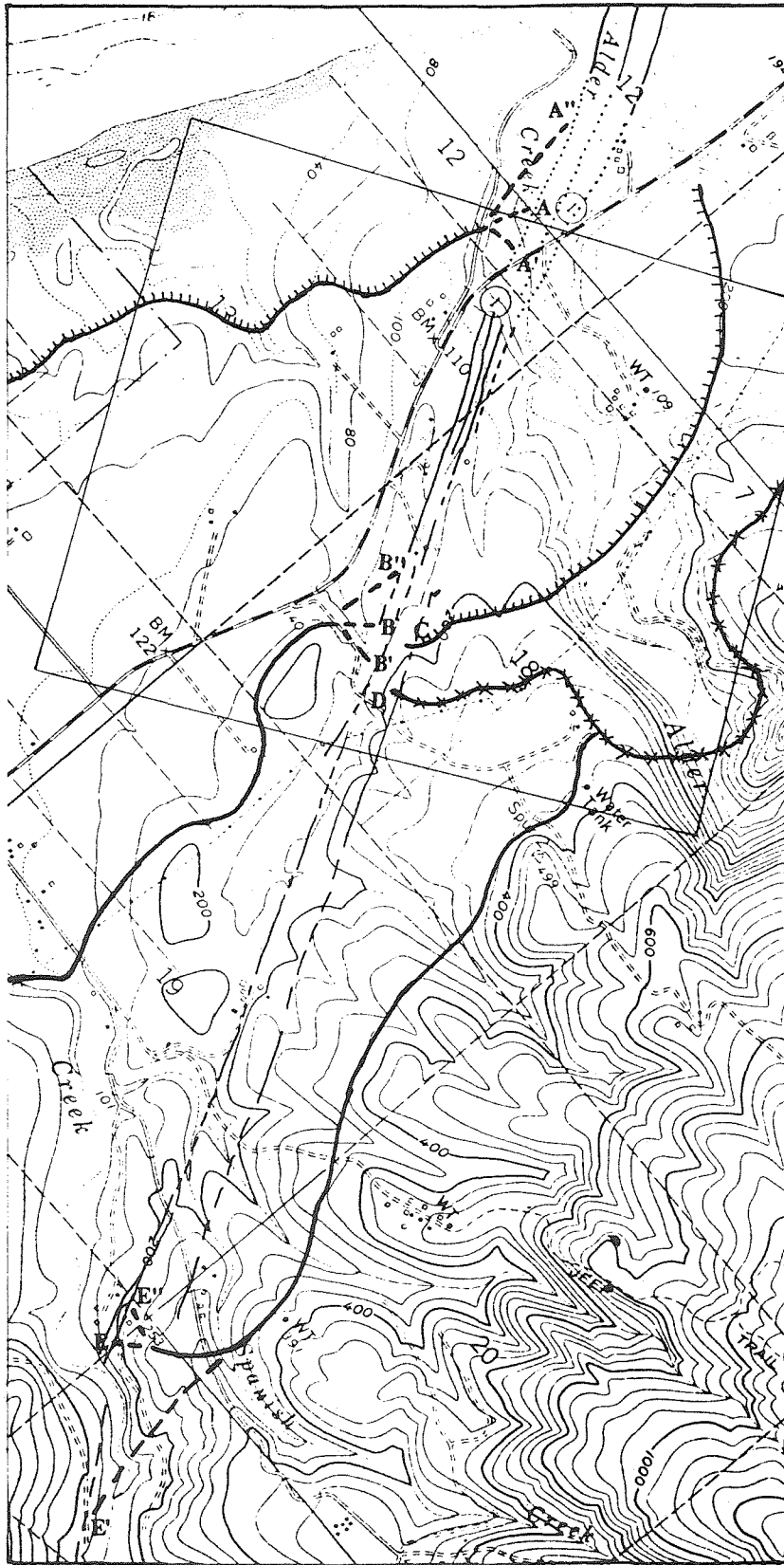
North of the Garcia River the geomorphic expression of the terraces differs dramatically from their geomorphic expression south of the river (Figure 3-6, Plate 3). Many

features in the region between the mouth of the Garcia River and the San Andreas fault indicate that this area is rising more slowly than adjacent regions I and II. These features include several lagoons and the accumulation of fluvial and wind-blown sediments, as well as lower relief and shallower incision of streams. There is one very obvious terrace surface, with a prominent backedge immediately east of Highway 1. West of this feature, south of Manchester, there is no topographic expression of a riser separating this terrace from a lower terrace. However, north of Manchester, a very subtle riser indicates the presence of a lower terrace. This feature is not seen south of Lagoon Creek because it is probably buried under the sand dunes there. This lower terrace is tentatively correlated with terrace I; the higher terrace is correlated with terrace III. Both of these terrace risers trend toward the San Andreas fault north of Manchester (Figure 3-9, A and B). The riser behind terrace III can be followed very clearly to within a few hundred meters of the fault zone (Figure 3-10). The riser behind terrace I is more difficult to follow for several reasons: as it approaches the fault zone it intersects several other faults, the terrace has been tilted (Figure 3-11), and a very thick section of terrace deposits obscures the morphologic expression of the terrace riser. However, a feature that probably represents the backedge of this lower terrace trends toward the San Andreas fault as shown in Figures 3-9, 3-10, 3-11, and Plate 3, and

intersects the valley of Alder Creek a few hundred meters away from the fault zone. Exposures along the beach to the south of the mouth of Alder Creek show the bedrock marine platform apparently dipping to the south and disappearing below the dunes north of Brush Creek. Exposures in the valley of Alder Creek west of Highway 1 also reveal the bedrock platform and, although outcrops are poor and sparse, it is clear that the bedrock does rise to near the surface just west of the highway. The coincidence of this and a slope on the surface suggests that this is the shoreline angle of the lower marine terrace.

North of the Garcia River, two reverse faults that are sub-parallel to the San Andreas form scarps on the terrace surfaces (Plate 3). The more southerly of these two is particularly well-expressed geomorphically. It forms a larger scarp on the higher, older terrace than on the younger terrace. This fault is well exposed in the sea cliff where it dips about 35° northeast. Other, smaller faults also cut the terrace deposits near the mouth of Alder Creek. Previous workers have postulated a Garcia River fault (Jahns and Hamilton, 1971) buried below the alluvial deposits of the Garcia. The dramatic change in terrace elevations and geomorphology across the Garcia does suggest the existence of such a structure. Because the dip of this structure is unknown, it is not certain whether it has a normal or reverse sense of motion.

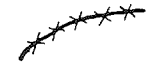
Figure 3-9. Map showing terrace risers and San Andreas fault zone. "A" indicates riser of terrace I in area 2, "B" indicates riser of terrace III; "C", "D", and "E" denote risers of terraces I, II, and III, respectively, in area 3. Correlation of terraces I and III are based on geomorphic position and are supported by preliminary data suggesting similarity of soil development. Offset of terrace riser I is 1.5 to 1.8 km; offset of terrace riser 2 is between 2.3 to 3.2 km. Region shown in Figure 3-10 is outlined by box.



PALEOSHORELINES:



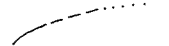
Terrace I



Terrace II



Terrace III



Fault Traces



SCALE: 1: 24,000

Figure 3-9

Figure 3-10. Aerial photo stereo pair showing risers of terraces I (C) & II (D) trending into the San Andreas fault zone near Point Arena. Photo of area indicated in Figure 3-9. Explanation of symbols same as for Figure 3-9; stream terraces of Alder Creek are outlined.

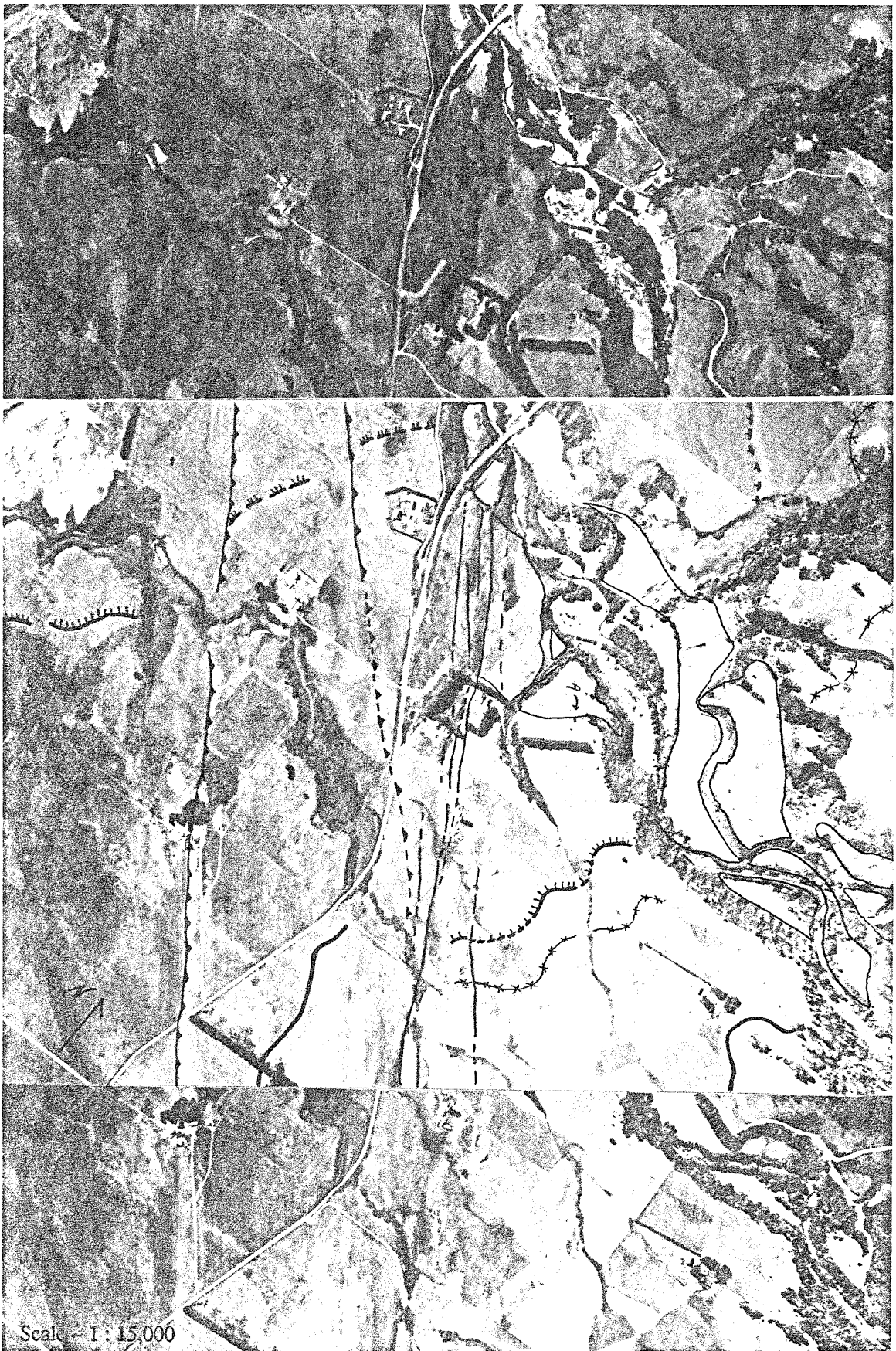


Figure 3-10

Figure 3-11. Photograph showing tilted terrace south of the mouth of Alder Creek. Terrace is faulted and tilted down to the southeast. Also indicated are terraces I-IV in area 3 and terraces I and III in area 2. The San Andreas fault zone is labeled. Photograph taken looking southeast from point labeled P11 in Figure 3-6 and Plate 3.

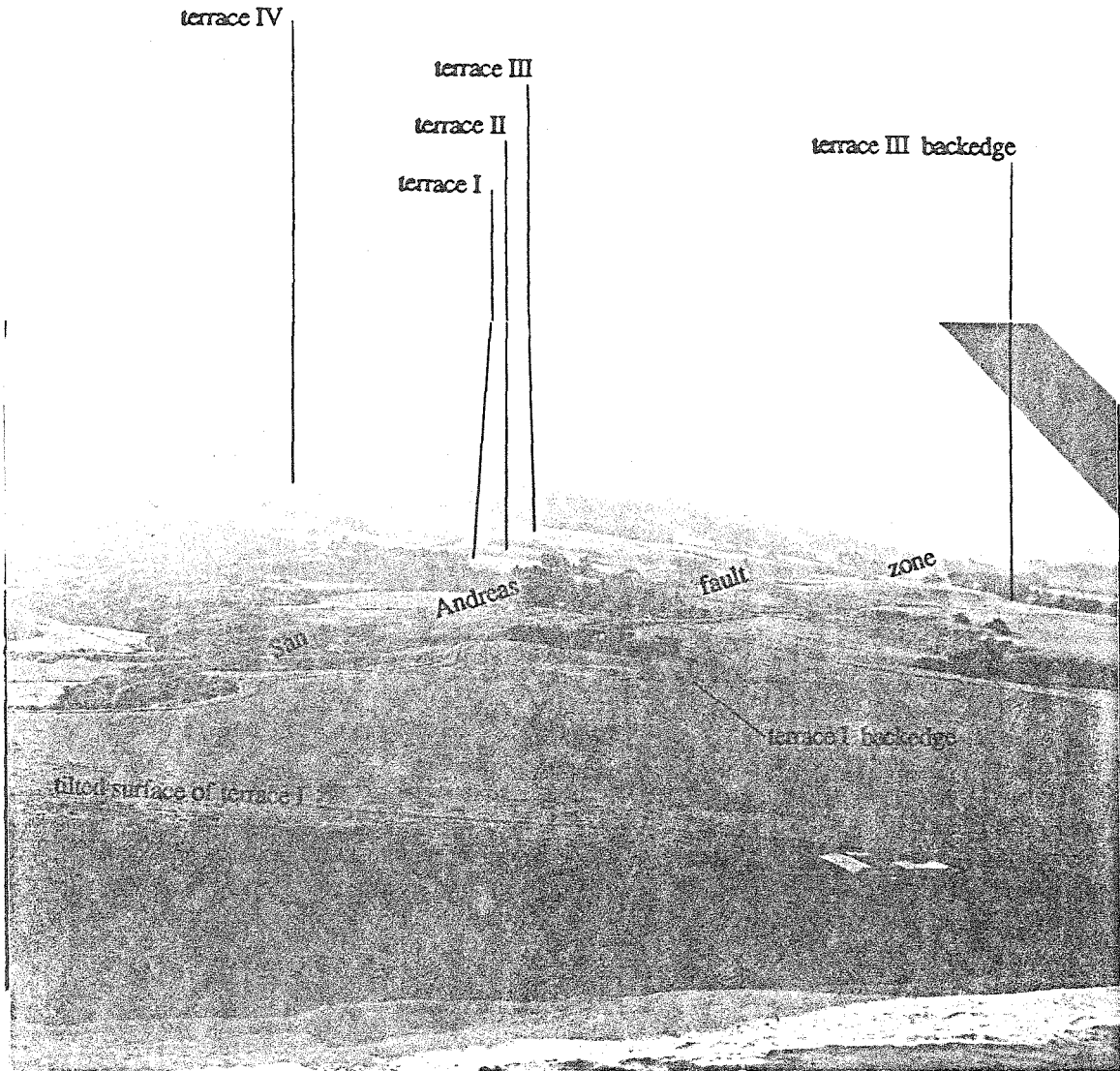


Figure 3-11

Reflection profiles show that in the offshore region north of Point Arena the San Andreas fault changes trend from about N30W to a trend of about N17W (Curry and Nason, 1967). One would expect this change in trend to be accompanied by extensional structures in the Point Arena area. This may be reflected in the relative subsidence of area II, suggesting the possibility that the postulated Garcia River fault may be a normal fault. However, this relative subsidence of area 2 could be due to folding and/or reverse faulting. The orientation of the postulated Garcia River fault in a nearly east-west direction lends support to the idea that it is a normal fault, but there is not enough evidence to make a very strong case for this.

Area 3

On the northeast side of the San Andreas fault zone at least six marine terrace levels exist (Plate 3). The lowest three terraces are of particular interest because their backedges trend very clearly into the San Andreas fault and are offset (Figures 3-9 through 3-12). The lowest of these is correlated with terrace I, the second with terrace II and the third with terrace III. The next two higher terraces are correlated with terraces IV and V and the highest terrace does

not have a correlative southwest of the fault. There are higher flat surfaces in the area that may represent still older marine terraces (for example, Bald Hill in section 4 T13N R16W, Plate 3).

In addition to the marine terraces, stream terraces of Alder Creek are shown on the map. The riser behind one of these very clearly trends into the San Andreas fault zone and has been offset (Figure 3-10). The offset equivalent of this feature may be represented by the thick sequence of terrace deposits overlying terrace 1 in the northwest portion of area 2.

The correlations suggested by mapping the terraces were tested by digging soil pits on representative surfaces assigned to terraces I and III in each of the three areas. Preliminary analysis of the soils data supports the correlations (Burke, personal communication, 1988) but further work must be done to confirm this.

Age estimates of the terraces

Few absolute dating methods are available for Pleistocene materials. The only materials found in association with the marine terraces that are suitable for age determination are solitary corals collected from the lowest terrace deposits near the Point Arena Lighthouse (Kennedy, 1978, 1981, and personal communication, 1986). A Uranium-series analysis of this material yielded an age of $76,000 \pm 4000$ ybp (Kennedy,

Figure 3-12. Photograph looking northeastward across the San Andreas fault zone at the backedges of terraces I and II in area 3 near their intersection with the fault zone. Photograph is taken at locality marked P12 on Figure 3-6 and Plate 3.

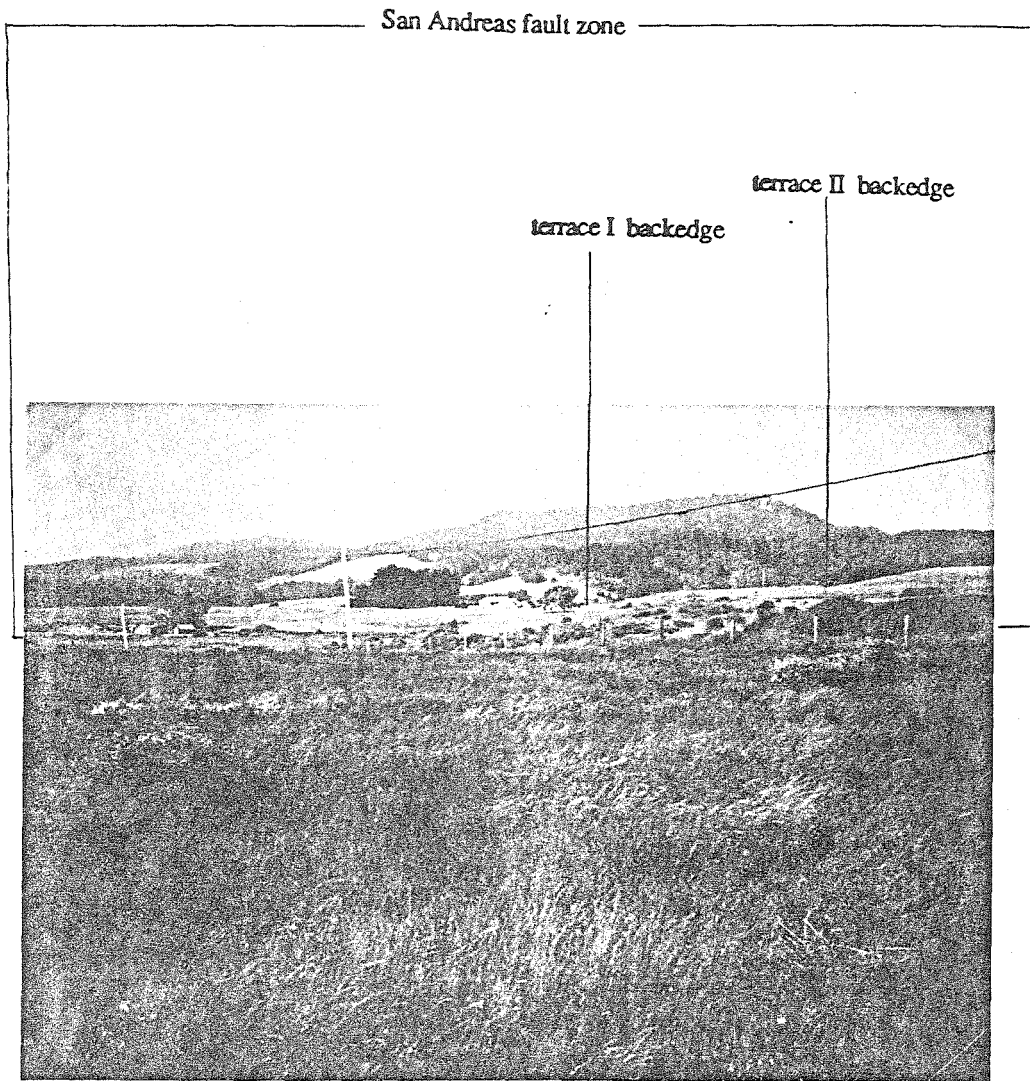


Figure 3-12

personal communication, 1988). Despite a thorough search for additional datable materials associated with the terraces, none was found.

It was necessary to use an alternative method to estimate the ages of the other terraces to calculate Pleistocene slip rates. I estimated the ages of the marine terraces by comparing the elevations of terraces within the three areas to the global high sea-level chronology of Bloom et al. (1974) and Chappell (1973), using the methods outlined by Bull (1985) and Lajoie (1986). These methods and the assumptions they rest on are outlined below.

A flight of marine terraces such as that preserved along the coast near Point Arena represents the interaction of Quaternary sea-level changes and tectonic uplift (e.g., Bull, 1985; Lajoie, 1986). Figure 3-13 shows a generalized marine terrace profile illustrating the terminology typically used in the discussion of terrace morphology. The wave-cut platform forming off the coast of California today dips gently seaward at angles between 0.3 and 1.0 degrees (Bradley and Griggs, 1976). Raised wave-cut platforms also must have dipped gently seaward at similar angles when they were formed. The intersection of the wave-cut platform and the sea cliff is known as the shoreline angle. This feature forms at an elevation that is approximately equal to that of the sea level at the time a terrace is cut. A thin veneer of marine terrace deposits typically covers the platform, and alluvial-colluvial

deposits typically overlies the marine deposits and bury the shoreline angles of uplifted terraces. The landward edge of a terrace surface is defined by a break-in-slope between an uplifted terrace and its relict sea cliff. This is higher in elevation than the shoreline angle of the terrace.

A bedrock wave-cut platform is formed during a high stand of sea level. Marine terraces can be preserved if the local uplift rate is high enough to bring the platform to an elevation above subsequent high sea-level stands (see, for example, Broecker et al., 1968, Mesolella et al., 1969, Bloom et al., 1974; Chappell, 1983). The current elevation of the shoreline angle is a function of both the elevation of sea level at the time of terrace formation and the amount of regional tectonic uplift. A rising coastline will preserve a flight of marine terraces that records past high sea-level stands if the rate of coastal retreat is not so high that the terraces are destroyed by erosion. The relationships between sea-level high stands, emergent marine terraces, and coastal uplift rate is best summarized by a figure from Lajoie (1986) which is reproduced here as Figure 3-14.

A flight of very well-studied marine terraces occurs on the rapidly uplifting Huon Peninsula of New Guinea (Bloom, et al., 1974; Chappell, 1983). These terraces have been dated by ²³⁴U/²³⁰Th methods on coral. The terrace ages and surveyed elevations of the shoreline angles of the terraces have allowed estimation of the times and elevations of sea-level

Figure 3-13. Generalized profile with definitions of terminology used to describe clastic marine terraces.

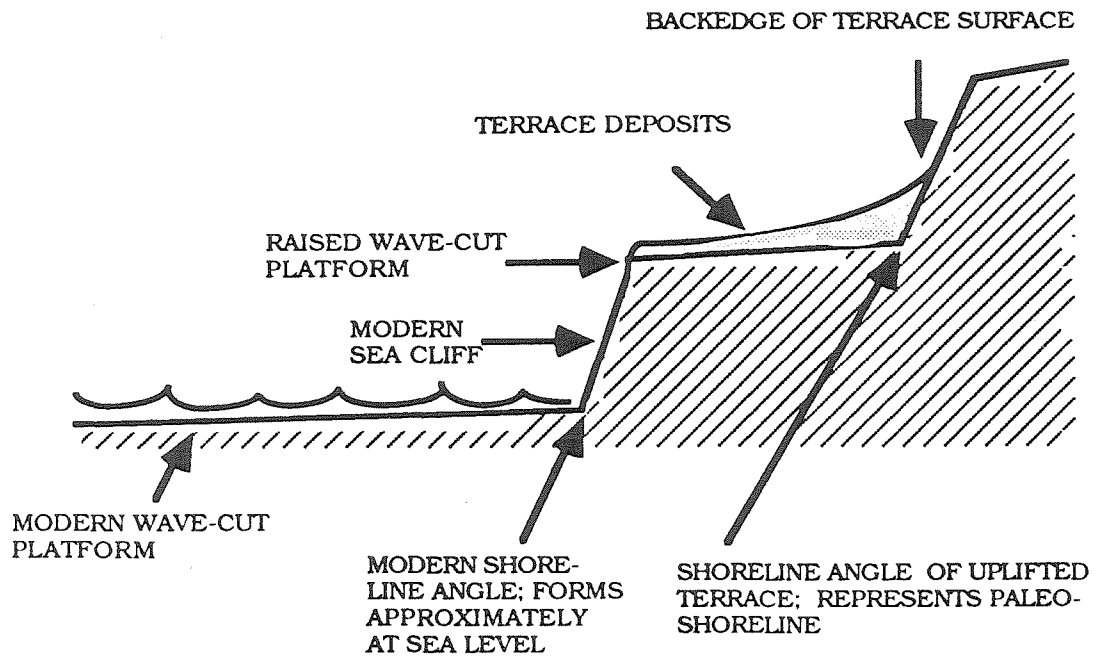


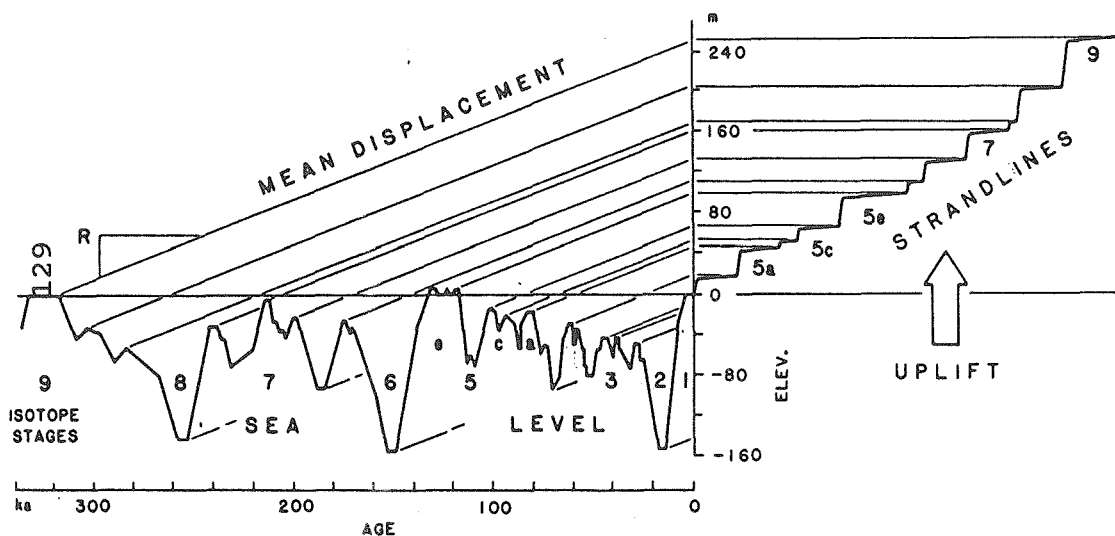
Figure 3-13

high stands for the last several hundred thousand years (e.g., Bull, 1984) (Figure 3-15).

The fact that terraces cut on the coast of New Guinea have been correlated with flights of dated terraces in different parts of the world confirms the hypothesis that these terraces were formed during times of global high sea-level stands (e.g., Chappell and Shackelton, 1987). Some workers have suggested that age estimates for undated flights of terraces can be made using data from the New Guinea terraces and the altitudinal spacing of an undated flight of terraces (Bull, 1985; Lajoie, 1986). This method of correlation assumes constant uplift rate and minimal relative differences in geoid height between New Guinea and other coastlines over the past several hundred thousand years.

If each of the five terrace levels recognized near Point Arena was formed during one of the global high sea-level stands that occurred during the Pleistocene epoch, and if the local uplift rate has been constant for the past several hundred thousand years, then the altitudinal spacing of the flight of terraces can be used to estimate their ages (Bull and Cooper, 1986, Bull, 1985). Since dateable material has only been found on one of the terraces near Point Arena (as discussed above) ages of the other terraces have been estimated using the methods proposed by Bull (1985) and Lajoie (1986). These methods have been used farther north along the California coast to estimate the ages of terraces in Humboldt

Figure 3-14. Figure from Lajoie (1986) summarizing relationships between global sea-level high stands and altitudinal spacing of marine terraces on a rising coastline.



Pleistocene sea-level fluctuations and origin of emergent Pleistocene strandlines. Emergent strandlines simultaneously record tectonic uplift and major sea-level highstands. The rising coastline is a moving strip chart on which sea-level highstands are recorded sequentially as strandlines whose ages increase with elevation. The slope (R) of the diagonal line connecting each highstand to the elevation of its strandline is the average uplift rate. If the uplift rate was constant, the uplift lines for all strandlines are parallel. Strandlines formed during lowstands are usually destroyed by subsequent

sea-level fluctuations and rarely appear in the emergent geologic record. Strandlines younger than 60 ka appear above sea level only where the uplift rate is greater than 1 m/ka. The sea-level fluctuation curve was derived from a sequence of U-series dated coral-reef strandlines on the Huon Peninsula, Papua New Guinea (Figure 6.2B) by subtracting tectonic uplift from the relative strandline record (Figure 6.5A). Sea-level curve modified from Chappell (1983); oxygen-isotope stages (1-9) from deep-sea cores (Shackleton and Opdyke, 1973).

Figure 3-15. Table of high sea-level elevations and ages compiled by Bull (1984) from Bloom et al. (1974) and Chappell (1983).

NUMBER	AGE, ka	ALTITUDE FORMED, meters
2A	30	-42
3A	40	-37
3B	46	-37
3C	57	-29
3D	64	-26
4A	76	-46
5A	83	-13
5B	94	-20
5C	103	-10
5D	120	+6
5E	133	+5
6A	176	-21
6B	202	-17
7A	214	-3
7B	242	-28
8A	286	-46
8B	305	-27
9A	320	+4
9B	336	+4

Figure 3-15

County (Carver et al., 1986).

Ideally, precise measurements of the current elevations of all shoreline angles in the undated flight of terraces should be known to attempt age estimates using this method, and the flight of terraces should have a large number of individual terraces. Because exposures of shoreline angles are very rare near Point Arena, this study uses estimates of the shoreline angle elevations made from topographic maps and field mapping. And, only a few terraces are preserved in the area, so there are fewer terraces to work with than is desirable for this method to be employed. However, even with these less than ideal conditions, use of this method in the Point Arena area yields age estimates for the terraces that are consistent between the three areas. These estimates imply a constant slip rate across the San Andreas fault and constant uplift rates within each area. No other possible correlation scheme gives consistent results (Appendix A).

Beginning with the single terrace that has been radiometrically dated (terrace I in area 1, see previous discussion), age assignments were made for the lowest five terraces in each area as follows. Assuming that terrace I was cut during one of the global high sea-level stands determined from the New Guinea terraces (Figure 3-15), the $76,000 \pm 4000$ year U-series date indicates that this terrace was cut during either the 76 Ka sea-level highstand or the 83 Ka highstand. Since the 76 Ka terrace was cut when sea level was 46 m below

modern sea level (Figure 3-15) for the shoreline angle to be at its current elevation of about 27 m the uplift rate would have to be nearly one mm/yr (73 meters in 76,000 years) - an unusually high rate for the California coast (Wehmiller et al., 1977). Also, at this uplift rate the predicted elevations of other terraces do not match the estimated elevations of the observed terraces in the area (Figure 3-16). However, if this terrace was cut during the 83 Ka high stand of sea level then the total uplift is about 40 meters (because the 83 ka highstand was at an elevation of about -13 meters, (Figure 3-15)), giving an uplift rate of 0.49 mm/yr. At this uplift rate, the predicted elevations of older terraces matches the estimated terrace elevations in the area reasonably well (Figure 3-16). All terraces younger than 83,000 years are predicted to be below modern sea level, except the 64 Ka terrace, which should be within a few meters of modern sea level. It is possible that this terrace is represented by the bedrock platform that is near sea level along many parts of the coast south of Point Arena, around modern sea stacks, and along the modern shore (Figure 3-17).

If terrace I is 83,000 years old, then ages can be estimated for the four higher terrace levels in this area using the uplift rate of .49 mm/yr and correlation with known ages and elevations of global high sea level stands (Bull, 1984, 1988; Lajoie, 1987). Estimated shoreline angle elevations of the five terraces are listed in Figure 3-16

Figure 3-16. A. Table showing predicted terrace elevations at an uplift rate of 1 mm/yr. B. Table showing predicted terrace elevations at 0.49 mm/yr and estimated shoreline angle elevations of terraces I-IV in area 1. Asterisk (*) denotes terraces not expected to be preserved with these uplift rates because they are lower than succeeding sea-level high stands. Terraces expected to be preserved that are not present or are unrecognized near Point Arena are indicated in italic print. Terraces correlated with terraces mapped near Point Arena are indicated in boldface. C. Inferred uplift-rate plot for area 1 shows that estimated shoreline-angle elevations and age assignments are consistent with a constant uplift rate of 0.49 mm/yr.

A.

Age (New Guinea terraces),	Predicted elevations, 1 mm/yr, m
30	-12
40	3
46	28
57	28
64	38
76	30
83	70
94	74
103	93
120	126
133	138
176	155
202	185
214	211
242	214
286	240
305	278
320	324
336	340

B.

Age (New Guinea terraces), Ka	Predicted elevations, .49 mm/yr, (meters)	Terraces of Area 1	Estimated shoreline angle elevations, Area 1, (meters)
30	-27		
40	-17		
46	-14		
57	-1		
64	5		
76	9		
83	27	I	24-28
94	26		
103	41	II	40-50
120	65		
133	70	III	65-75
176	65		
202	82		
214	102	IV	95-110
242	91		
286	94		
305	122		
320	161	V	145-160
336	169		

C.

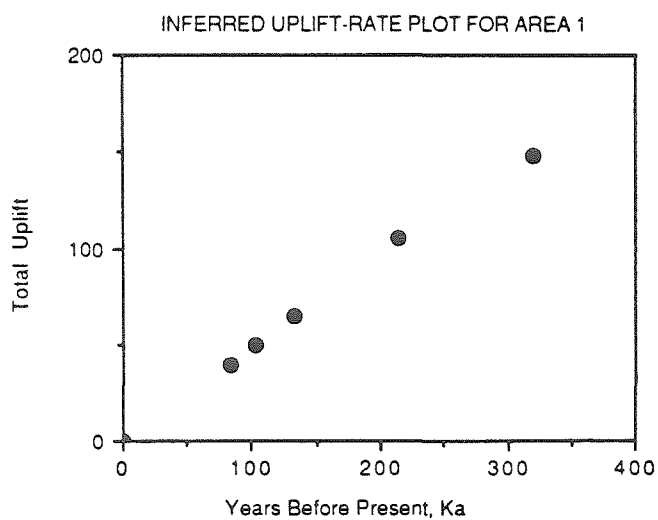


Figure 3-16

along with the predicted elevations of terraces cut during global high sea-level stands given the uplift rate of .49 mm/yr. The elevations are estimated from topographic maps and field observations. Terrace level II most likely corresponds to the 103 Ka high stand, terrace III with the 133 Ka high stand, terrace IV with 214 Ka high stand and level V with the 320 Ka high stand. These correlations imply that four terrace levels are missing or not recognized in the area: 120 Ka, 202 Ka, 305 Ka, and 336 Ka.

In area 2, between the Garcia River and the San Andreas fault, the uplift rate is lower than in the surrounding areas. The backedge of the surface of terrace III is at an elevation of about 49 m. No exposures of the shoreline angle are present. However, projection of seismic refraction profiles in this area allows estimation of the elevation of the buried shoreline angle of the bedrock platform. This value, reported by Valavanis (1983), is 125 to 130 feet, or about 39 m. If this terrace was cut at 5 m above present sea level 133,000 years ago, then the uplift rate in area 2 is about 0.25 mm/yr. At this uplift rate, the 83 Ka terrace is predicted to be at about 7.7 m (25 feet). The surface elevation of the backedge of the lowest terrace in area 2 varies from about 30 feet (9 m) south of Brush Creek to about 70 feet (21 m) near Manchester campground. Two of Valavanis' refraction profiles cross the backedge of terrace I (though he interpreted this feature to be the modern sea cliff rather than the back edge

of terrace I) and show the bedrock shoreline angle to be at 25 and 28 feet (7.6 and 8.5 m) respectively, matching the predicted value well. Just south of Alder Creek, on the upthrown side of two reverse faults, the surface elevation of the backedge is nearly 100 feet (30 m); in this area another of Valavanis' profiles shows the bedrock shoreline angle at about 40 feet (12 m). This is higher than, but generally consistent with, exposures in Alder Creek.

In area 3, northeast of the San Andreas fault, several marine terrace risers intersect the San Andreas fault (Figures 3-9 through 3-12). Six terraces are present in this area (Plate 3). Estimated shoreline angle elevations of these terraces are listed in Figure 3-18. If the ages of the lowest five terraces are the same as the ages assigned to the five terraces in area 1, then constructing an inferred plot of uplift rate yields a consistent uplift rate of about 0.75 mm/yr (Figure 3-18). The relatively high uplift rate is reflected in the topography of the area which is much higher than that of the adjacent Gualala block. No other feasible age assignments for these terraces are consistent with a constant uplift rate in this area (Appendix A). These age estimates imply that six terraces are missing or unrecognized in the area: 120, 176, 202, 286, 305, and 336 Ka. In addition, the highest recognized terrace, terrace VI, at about 1000 feet, is older than the 336 Ka terrace in New Guinea; at the

Figure 3-17. Photograph showing possible 64 Ka terrace near Point Arena. View is northwest from P17, located on Figure 3-6 and Plate 3.

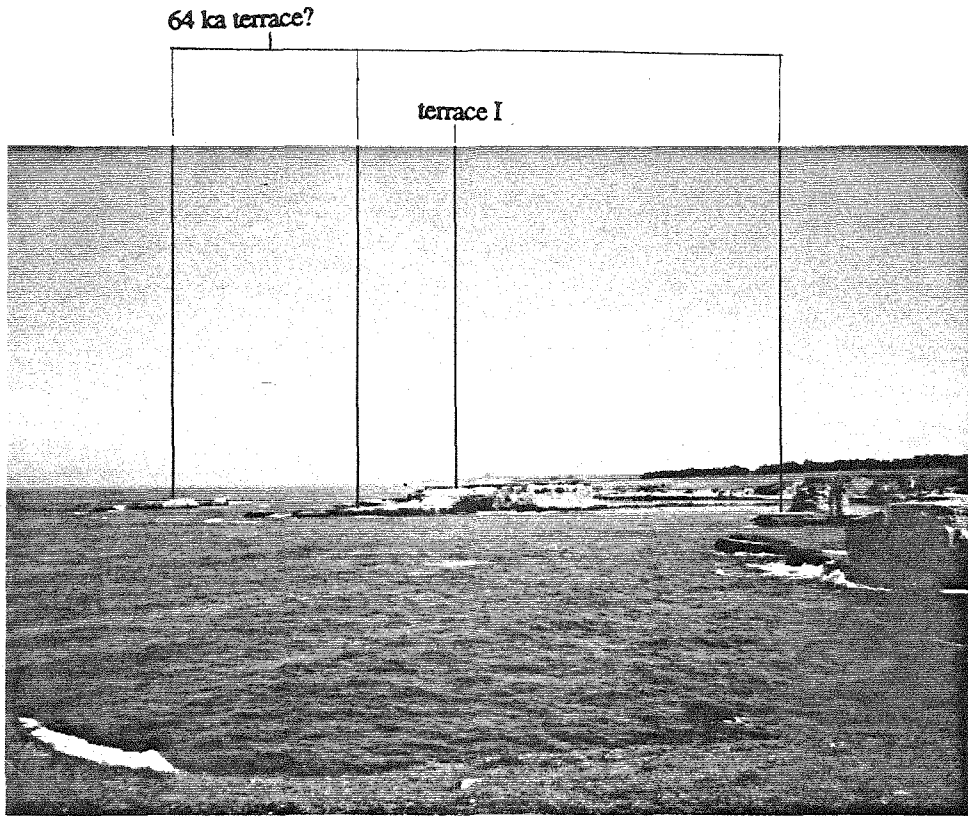


Figure 3-17

uplift rate of 0.75 mm/yr, this terrace would be about 400-420 Ka.

Offset Across the San Andreas Fault.

If the assigned terrace ages are correct, then the lowest terrace in area 2 correlates to the lowest terrace in area 3 and formed 83,000 years bp. The shoreline angle of this terrace crossed the San Andreas fault at the time of terrace formation. If the shoreline cut straight across the fault like the modern shoreline in most of the places that it crosses the San Andreas, then projecting the trend of the shoreline angle to the fault on either side allows an estimate of the amount of offset since the time of formation of the terrace. In area 3 the shoreline angle of the lowest terrace approaches the fault zone so closely that its point of intersection with the fault is constrained to within a few tens of meters (C on Figure 3-9). In area 2, however, the shoreline angle of the lowest terrace intersects the valley of Alder Creek before it reaches the fault zone, so its projection to the fault is uncertain within about 500 meters (A, A', A" in Figure 3-9). This uncertainty also reflects the fact that the fault in this region is buried below recent deposits of Alder Creek, so its exact location is unknown. Three possible points of intersection are indicated on Figure 3-9: the best guess (A) and likely limits (A', A'') on either side. The distances between these and C are 1.5, 1.35, and 1.8 km, respectively.

Figure 3-18. A. Table of predicted elevations of terraces at an uplift rate of 0.75 mm/yr and the estimated elevations of the shoreline angles of terraces I-IV in area 3. Asterisk (*) denotes terraces not expected to be preserved at this uplift rate due to reoccupation by succeeding high stands. *Italic print* denotes terraces that should be preserved but are not recognized in area 3. Terraces correlated with terraces mapped near Point Arena are indicated in **boldface**. B. Inferred uplift-rate plot for area 3 shows that the assigned ages and estimated elevations of the lowest five terraces are consistent with a constant uplift rate of 0.75 mm/yr. No other possible age assignments give a constant uplift rate (see Appendix A).

A

Age (New Guinea terraces), Ka	Predicted elevations, .75 mm/yr (meters)	Terraces of Area 3	Estimated shoreline angle elevations, Area 3, (meters)
30	-64		
40	-7		
46	-2		
57	14		
64	22		
76	11		
83	49	I	45-55
94	*50		
103	67	II	65-75
120	96		
133	105	III	95-110
176	111		
202	135		
214	157	IV	150-160
242	*153		
286	169		
305	202		
320	244	V	240-255
336	256		
?	?	VI	300-315

B.

Uplift rate: .75mm/yr

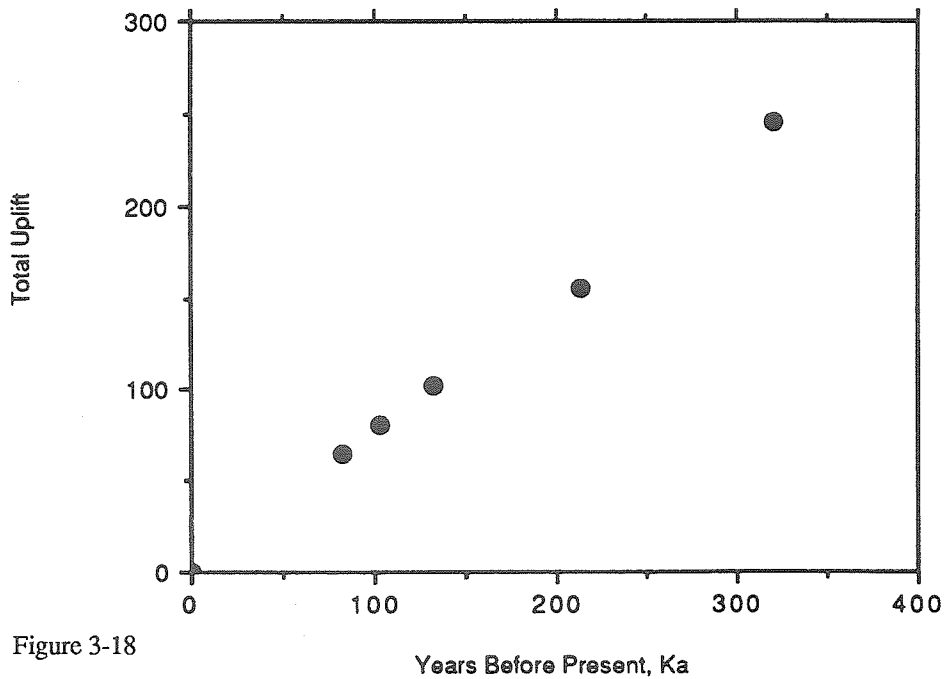


Figure 3-18

Years Before Present, Ka

This much offset in 83,000 years implies a slip rate of between about 16 and 22 mm/yr, with the best estimate at about 18 mm/yr.

Terrace II northeast of the fault does not appear to have a correlative on the southwest side of the fault in area 2. Probably this is because it was destroyed by the formation of terrace I in the area. Hence the next older offset shoreline angle that has a measurable offset is that of terrace III, which is estimated to be 133,000 years old. Again several possible projections of the shoreline angle into the fault zone are shown in Figure 3-9: the most likely, projected straight along the trend of the shoreline angle as it approaches the fault (E), and reasonable limits on either side (E', E''). These projections imply the most likely offset (E to B) is about 2.5 km. Reasonable bounding limits are 3.2 km and 2.3 km. This suggests a slip rate of between about 17 and 24 mm/yr, with the best estimate at about 19 mm/yr. That the two slip rates derived from the offsets of the shoreline angles of these two terraces are so similar lends support to the age assignments, because no other correlation would also imply consistent slip rates across the San Andreas.

Stream terraces of Alder Creek

In addition to the risers of marine terraces I, II, and III, another feature in area 3 clearly trends into and is offset across the San Andreas fault. This is the riser of a

stream terrace above Alder Creek (A on Figure 3-10). No obvious correlative of this feature is seen across the fault zone. However, it is possible that the thick sequence of fluvial sediments that covers terrace I south of Alder Creek in area 2 is related to the fluvial sediments of this stream terrace. Charcoal collected from near the top of the fluvial sediments exposed in the south wall of the Alder Creek stream gorge yielded an AMS radiocarbon age of $33,900 \pm 1300$ years bp (Plate 3). The age of the incision that formed the riser is greater than the age of the sediments deposited on the terrace below the riser, but less than the age of the surface above the riser; therefore the age of this riser is between about 34,000 and 83,000 (the estimated age of marine terrace I) years bp. Since it is younger than marine terrace I, it should be offset a smaller distance. This means its correlative should be found southeast of the modern Alder Creek mouth and today's shoreline. The only obvious candidate is the backedge of marine terrace I. It is reasonable that Alder Creek would have flowed along this feature at some time after the 83,000 ka sea-level high stand. If it is the case that this feature is correlative with the stream terrace riser, then the offset of the riser is about 820 meters. This much offset in 34 to 83 thousand years implies a slip rate between 10 and 24 mm/yr, in the same range as the slip rates determined from the offset marine terraces. Also, if this hypothesis is correct, it suggests that the backedge of marine

terrace I may have retreated due to stream erosion, making the measured offset smaller, and the calculated slip rate lower than it really is.

The modern gorge of Alder Creek also appears to be offset across the San Andreas fault. This offset is on the order of 650 to 900 meters. The age of the sediments near the top of the stream terrace into which the gorge is cut is greater than the age of the gorge, but should be only slightly older. Therefore, the gorge was cut soon after 34,000 years bp. The offset of 650 to 900 meters in 34,000 years implies a slip rate of 19 to 26 mm/yr, also in the same range as suggested by the arguments involving the marine terraces.

DISCUSSION

The best estimate for the average slip rate across the San Andreas fault near Point Arena since late Pleistocene time is about 18-19 mm/yr. This slip rate, if correct, has several implications. Since it is consistent with the maximum average late Holocene slip rate of 24 mm/yr near Point Arena determined nearby (see Chapter 2), it appears that no major change in slip rate has occurred between the last few thousand and the last few hundred thousand years. This slip rate is somewhat higher than the approximately 12 mm/yr rate determined by Hall (1984) for the last 1200 years south of San Francisco. Several factors could be responsible for this difference. First, the San Gregorio fault apparently joins the

San Andreas fault near Bolinas, between the two study sites, so rates of slip on the fault north of the junction may be greater than rates south of the junction, in a similar fashion as proposed for the San Jacinto - San Andreas system in southern California (Prentice, et al., 1985). Furthermore, Hall's slip rate is a minimum, so it does not necessarily indicate a different rate than the rate suggested by this study. Hall's slip rate is based on the amount of offset that has occurred on a small stream since the stream was captured and abandoned its old valley. The time of abandonment of the old valley is determined from the radiocarbon date of a sample collected near the top of the alluvium in the abandoned channel. The radiocarbon date represents a maximum age for the time of abandonment, and therefore the slip rate is a minimum, "because detrital charcoal is always older than the layer containing it, because the charcoal was collected at least six inches below the surface and because some time may have elapsed between the last deposition and offset" (Hall, 1984, p. 294). The amount of displacement is 44 feet (13.4 m), a well-constrained value, assuming the channel initially was cut straight across the fault. If the channel was captured in a geometry that caused the channel to initially flow to the southeast along the fault before entering the main valley, the amount of displacement measured would be a minimum, another factor in considering this slip rate a minimum.

My slip rate of about 19 mm/yr, although higher than that

suggested for the fault south of San Francisco, is still much lower than proposed Pacific - North American plate motion. The RM2 model of Minster and Jordan (1978) suggests 53-59 mm/yr; the more recent NUVEL-1 model of DeMets et al. (1987) suggests a lower rate of relative motion, 46-51 mm/yr. Even so, the rate of slip on the San Andreas along the creeping segment and farther south (about 32 mm/yr) is much greater than the slip rate proposed in this study. This implies that some percentage of the plate motion is being accommodated on other structures. It is estimated that about 10 mm/yr is taken up by extension in the Basin and Range, but this still leaves a considerable amount of slip that is not accounted for on the northern San Andreas. Clearly some of this is being taken up on other faults and folds near the San Andreas as described above, but other fault zones are probably also involved in accommodating the entire plate motion. In northern California at the latitude of Point Arena, the Maacama fault, about 50 km east of Point Arena, is taking up an unknown percentage of this missing slip. Other unstudied faults, both on and off shore, may also be important structures. The understanding of these structures is important both in terms of assessing their potential seismic hazard and in understanding how slip is distributed across the modern Pacific-North America plate boundary.

REFERENCES

- Bloom, A.L., Broecker, W.S., Chappell, J., Matthews, R.K., and Mesolella, K.J., 1974, Quaternary sea-level fluctuations on a tectonic coast: new $^{230}\text{Th}/^{234}\text{U}$ dates from the Huon Peninsula, New Guinea: *Quaternary Res.*, v. 4, pp. 185-205.
- Borchardt, G., Lienkamper, J.J., and Schwartz, D.P., 1987, Holocene slip rate of the Hayward fault at Fremont, California: *EOS, Trans. Am. Geophys. Union*, v. 68, n. 44, p. 1506.
- Boyle, M.W., 1967, The stratigraphy, sedimentation, and structure of an area near Point Arena, California: unpublished M.S. thesis, Univ. of Calif., Berkeley.
- Bradley, W.C., and Griggs, G.B., 1976, Form, genesis, and deformation of central California wave-cut platforms: *Geol. Soc. Am. Bull.*, v. 87, pp. 433-449.
- Broecker, W.S., Thurber, D.L., Goddard, J., Ku, T.-L., Matthews, R.K., and Mesollela, K.J., 1968, Milankovitch hypothesis supported by precise dating of coral reefs and deep-sea sediments: *Science*, v. 159, pp. 297-300.
- Bull, W.L., 1985, Correlation of flights of global marine

terraces: Tectonic Geomorphology, M. Morisawa and J. Hack, eds., Binghamton Symposia in Geomorphology, International Series, 15, pp. 129-152.

Bull, W.L., and Cooper, A.F., 1986, Uplifted marine terraces along the Alpine fault, New Zealand: *Science*, v. 234, pp. 1225-1228.

Burford, R.O., and Harsh, P., 1980, Slip on the San Andreas fault in central California from alignment array surveys: *Bull. Seis. Soc. Am.*, v. 70, n. 4, pp. 1233-1261.

Carver, G.A., Burke, R.M., and Kelsey, H.M., 1986, Quaternary deformation in the region of the Mendocino triple junction: Final Report to the National Earthquake Hazard Reduction Program of the U.S. Geological Survey, Contract no. 14-08-001-22009.

Chappell, J., 1983, A revised sea-level record for the last 300,000 years on Papua New Guinea: *Search*, v. 14, pp.99-101.

Chappell, J. and Shackelton, N.J., 1986, Oxygen isotopes and sea level: *Nature*, v. 324, pp. 137-140.

Curray, J.R., and Nason, R.D., 1967, San Andreas fault north of Point Arena, California: *Geol. Soc. Am. Bull.*, v. 78,

pp. 413-418.

DeMets, C., Gordon, R.G., Stein, S., Argus, D.F., 1987, A revised estimate of Pacific-North America motion and implications for western North America plate boundary zone tectonics: *Geophys. Res. Letters*, v. 14, n. 9, pp. 911-914.

Fox, K.F., 1983, Tectonic setting of Late Miocene, Pliocene, and Pleistocene rocks in part of the Coast Ranges north of San Francisco, California: U.S.G.S. Prof. Pap. 1239.

Hall, N.T., 1984, Holocene history of the San Andreas fault between Crystal Springs Reservoir and San Andreas Dam, San Mateo County, California; *Bull. Seis. Soc. Am.*, v. 74, n. 1, pp 281-299.

Herd, D.G., 1978, Intracontinental plate boundary east of Cape Mendocino, California: *Geology*, v. 6, pp. 721-725.

Jahns, R.H., and Hamilton, D.H., 1971, Geology of the Mendocino Power Plant, in: Mendocino Power Plant Preliminary Safety Analysis Report: submitted to the U.S. Atomic Energy Commission by Pac. Gas & Elec. Co., v. 1, appendix 2.5.

Kelsey, H.M., and Cashman, S.M., 1983, Wrench faulting in northern California and its tectonic implications:

Tectonics, v. 2, n. 6, pp. 565-576.

Kennedy, G.L., 1978, Pleistocene paleoecology, zoogeography and geochronology of marine invertebrate faunas of the Pacific Northwest coast (San Francisco Bay to Puget Sound): Ph.D. thesis, Dept. Geol., Univ. Calif., Davis, 824 pp.

Kennedy, G.L., 1981, Pleistocene marine invertebrates from the Mendocino coast, northern California: Western Society of Malacologists, Annual Report, v. 13, pp. 13-14.

Lajoie, K.R., 1986, Coastal tectonics, in: Active Tectonics, National Academy Press.

Lisowski, M., and Prescott, W.H., 1981, Short range distance measurements along the San Andreas fault in Central California, Bull. Seis. Soc. Am., v. 71, n. 5, pp. 1607-1624.

Mesolella, K.J., Matthews, R.K., Broecker, W.S., and Thurber, D.L., 1969, The astronomical theory of climatic change: Barbados data: J. of Geology, v. 77, pp. 250-274.

Minster, J.B., and Jordan, T.H., 1978, Present-day plate motions: J. Geophys. Res., v. 83, n. B11, pp. 5331-5354.

Nason, R.D., 1971, Investigation of fault creep slippage in northern and central California: Ph.D. thesis, Univ. Calif. San Diego.

Prentice, C.S., Weldon, R.J., and Sieh, K.E., 1985, Distribution of slip between the San Andreas and San Jacinto faults, southern California: Geol. Soc. Am., Abstracts with Programs, v. 18, n. 2, p. 172.

Prescott, W.H., Lisowski, M., and Savage, J.C., 1981, Geodetic measurement of crustal deformation on the San Andreas, Hayward, and Calaveras faults near San Francisco, California: J.G.R., v.86, pp. 10853-10869.

Prescott, W.H., and Yu, S.-B., 1986, Geodetic measurement of horizontal deformation in the northern San Francisco Bay region, California: J.G.R., v.91, n. B7, pp. 7475-7484.

Sarna-Wojcicki, A.M., Meyer, C.E., and Slate, J.L., 1986, Displacement of a ca. 6 Ma tuff across the San Andreas fault system, northern California: EOS v. 67, n. 44, p. 1224.

Savage, J.C., and Burford, R.O., 1973, Geodetic determination of relative plate motion in central California: J. Geophys. Res., v. 78, n. 5, pp. 832-845.

Valavanis, D.S., 1983, Abrasion platform morphology of the lowest marine terrace, Arena Cove to Alder Creek, Mendocino County, California: unpublished M.A. thesis, Department of Geography, California State University, Hayward.

Wagner, D.L., and Bortugno, E.J., 1982, Geologic map of the Santa Rosa Quadrangle: Regional Geologic Map Series, Calif. Div. Mines of Geology.

Weber, Gerald B. and Lajoie. K. R., 1977, Late Pleistocene and Holocene tectonics of the San Gregorio fault zone between Moss Beach and Point Ano Nuevo, San Mateo County, California, GSA Abstracts with Programs, 9(4), p. 524.

Wehmiller, J.F., Lajoie, K.R., Kvenvolden, K.A., Peterson, E., Belknap, D.F., Kennedy, G.L., Addicott, W.O., Vedder, J.G., and Wright, R.W., 1977, Correlation and chronology of Pacific coast marine terrace deposits of continental United States by fossil amino acid stereochemistry - technique evaluation, relative ages, kinetic model ages, and geologic implications: U.S. Geol. Survey Open File Report 77-680.

Zoback, M.D., Zoback, M.L., Mount, V.S., Suppe, J., Eaton, J.P., Healy, J.H., Oppenheimer, D., Reasenber, P., Jones, L., Raleigh, C.B., Wong, I.G., Scotti, O., and Wentworth,

C., 1987, New evidence on the state of stress of the San Andreas fault system: *Science*, v. 238, pp. 1105-1111.

CHAPTER 4: THE OHLSON RANCH FORMATION, GEOMORPHOLOGY OF THE GUALALA AND GARCIA RIVERS, AND A TENTATIVE PLIOCENE SLIP RATE ACROSS THE NORTHERN SAN ANDREAS FAULT

ABSTRACT

Correlation of the Pliocene Ohlson Ranch Formation in northwestern Sonoma County with deposits 50 km to the northwest, near Point Arena, provides piercing points to use in calculation of a Pliocene slip rate for the northern San Andreas fault. Similarities in lithology, molluscan fauna, and foraminiferal fauna between the two areas supports the correlation of the deposits. A fission-track age of 3.3 ± 0.8 Ma on zircons collected from a tuff within the Ohlson Ranch Formation is in agreement with the Pliocene age determined previously from the molluscan fauna. The geomorphology of the region, especially of the two major river drainages, supports the proposed 50 km offset. If valid, this correlation implies a Pliocene slip rate of at least 12-20 mm/yr for the northern San Andreas fault. This rate is similar to the late Pleistocene and Holocene slip rates proposed in Chapters Two and Three, thus, the rate of slip appears not to have varied by more than a factor of two over the past several million years. This rate also implies that much of the Pacific-North American plate motion at this latitude must be accommodated on other structures.

INTRODUCTION

There is a discrepancy between the 12 mm/yr Holocene slip rate determined for the northern San Andreas fault determined by Hall (1984), and the 37 mm/yr late Miocene rate suggested by Sarna-Wojcicki, et al. (1986) (see Chapter 1, pp. 11-16, Chapter 2, pp. 28-33 and Chapter 3, pp. 89-91). If both of these rates are correct, then the San Andreas is moving at a rate three times faster north of San Francisco than south of San Francisco, or the slip rate of the northern San Andreas fault has slowed down.

To better understand the behavior of the fault over time, I attempted to determine the longer term slip rate for the northern San Andreas fault. A Pliocene unit, the Ohlson Ranch Formation, occurs northeast of and adjacent to the San Andreas fault in northwestern Sonoma County, northeast of Fort Ross (Figure 4-1). A search for the offset equivalent of this unit on the Gualala block, and constraints on the age of the unit led to the calculation of a tentative Pliocene slip rate for the northern San Andreas fault.

OHLSON RANCH FORMATION

Introduction

The Ohlson Ranch Formation, as defined and mapped by Higgins (1960), caps the flat to gently rolling ridge crests

Figure 4-1: Map showing the distribution of the Ohlson Ranch Formation, a quiet-water, marine unit, deposited in a small Pliocene embayment. Map modified from Higgins (1960).

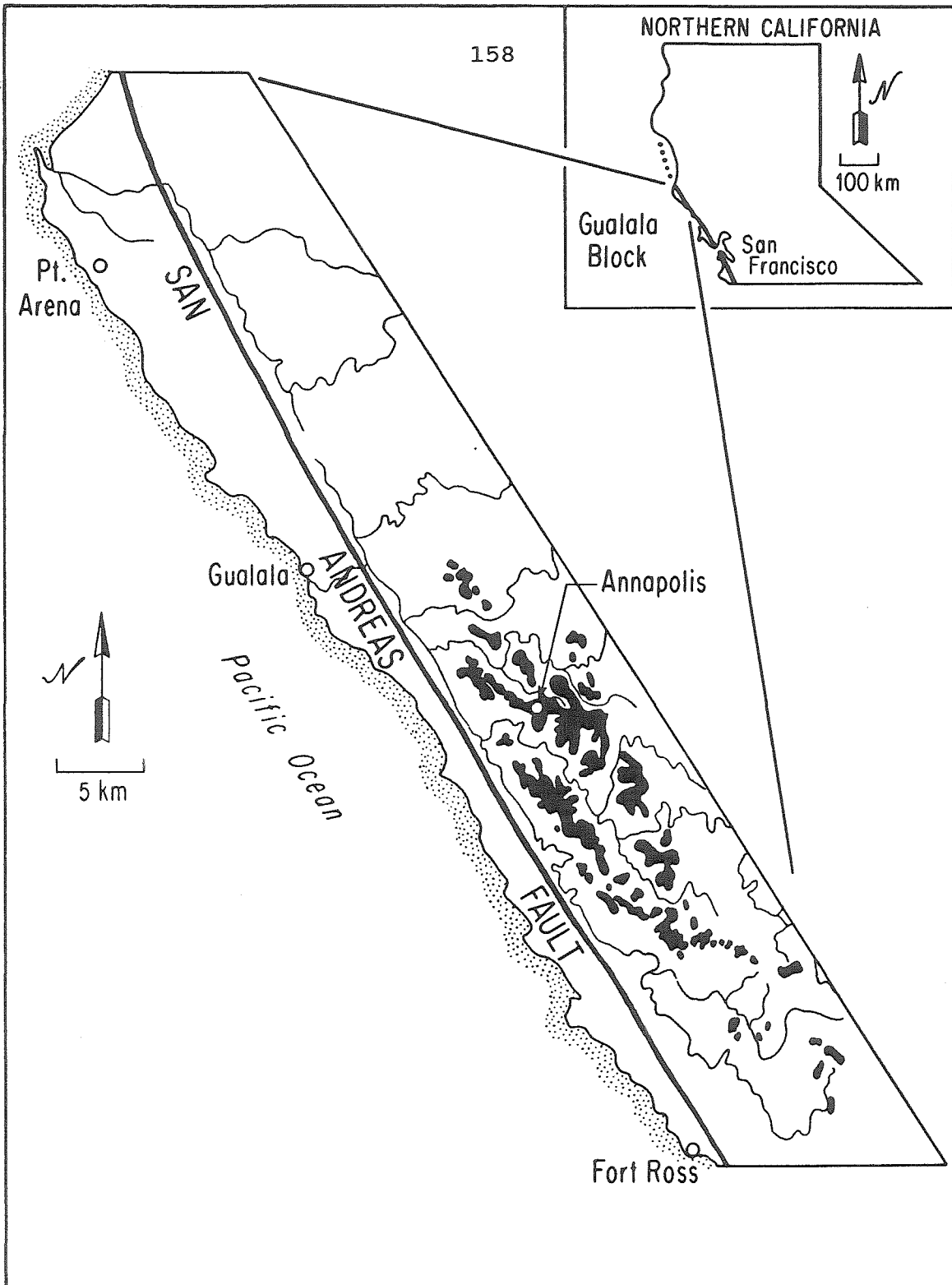


Figure 4-1

near and southeast of Annapolis on the east side of the San Andreas fault adjacent to the Gualala block (Figure 4-1). This unit consists of siltstone, sandstone and conglomerate and is generally poorly exposed. Two occurrences of volcanic ash beds were reported by Higgins (1960). The Ohlson Ranch Formation contains marine macro and microfossils and is typically associated with relict sea stacks composed of the underlying Franciscan sandstone and glaucophane schist. These rocks are commonly riddled with mollusk borings (Figure 4-2), that indicate deposition of the Ohlson Ranch Formation close to a rocky marine seacoast.

Age and Depositional Environment

The Ohlson Ranch Formation was assigned a Pliocene age on the basis of the molluscan fauna collected by Higgins (Peck, 1960). Peck identified 2 faunal assemblages: one characteristic of the middle Pliocene (which includes Patinopectin purisimaensis, P. cf coosensis, and Colus recurvus), the second characteristic of the upper Pliocene (containing Chlamys egregius and Terebratalia arnoldi etchegoini). Foraminifera separated from 3 samples of the Ohlson Ranch Formation (Table 1) belong to a post-Miocene fauna, but because all the species are still living, these do not enable more definitive assignment of age. Ingle (written communication, 1988) believes that the character of the assemblage suggests a mid- to late- Pliocene age.

Figure 4-2: Photograph of a typical Franciscan knob surrounded by the Ohlson Ranch Formation. These rocks typically display mollusk borings, several of which are indicated on the photo.

mollusk borings

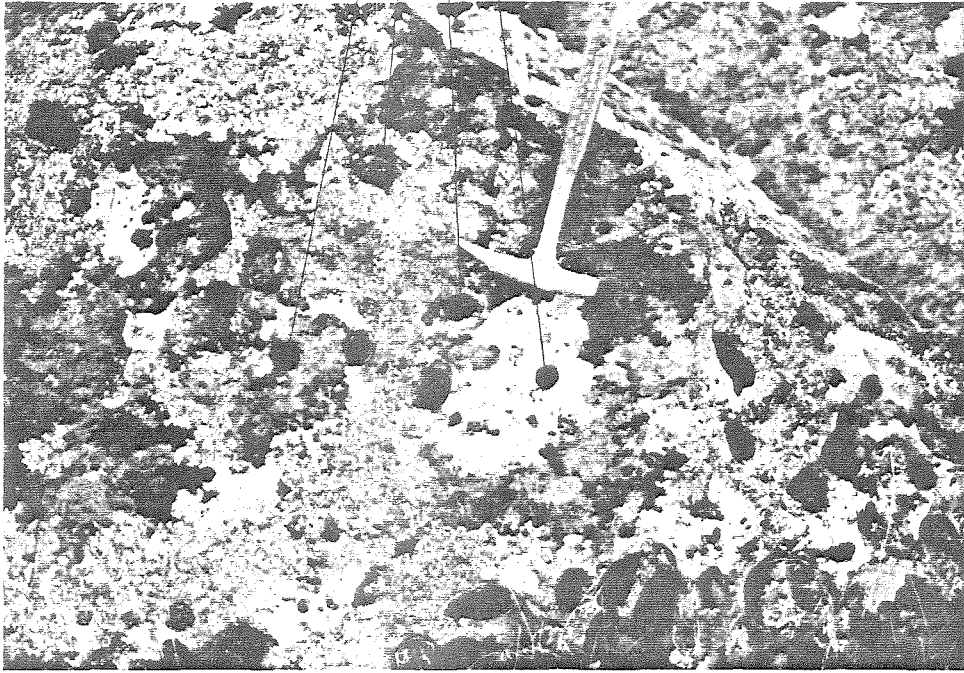


Figure 4-2

Table 1: list of foraminifera recovered from the Ohlson Ranch Formation identified by J.C. Ingle.

TABLE 4-1
FORAMINIFERA RECOVERED FROM THE OHLSON RANCH FORMATION
(Analyses by J.C. Ingle)

Sample 87-OR-51A

Bolivina vaughani Natland
Buccella frigida (Cushman)
Buccella sp.
Buccella tennerima (Bandy)
Buliminella elegantissima (d'Orbigny)
Cassidulina limbata Cushman & Hughes
Cassidulina sp.
Cassidulina tortuosa Cushman & Hughes
Cibicides fletcheri Galloway & Wissler
Cibicides lobatus (d'Orbigny)
Discorbis sp.
Elphidium cf. incertum Williamson
Elphidium clavatum Cushman emend. Loeblich & Tappan
Elphidium clavatum Cushman emend. Loeblich & Tappan
Elphidium granulosus (Galloway & Wissler)
Florilus (Nonionella) basispinata (Cushman & Moyer)
Florilus (Nonionella) miocenica stella (Cushman & Moyer)
Globigerina bulloides d'Orbigny
Globigerina quinqueloba Natland
Lagena Acuticosta Reuss
Nonion sp.
Planulina depressa (d'Orbigny)
Textularia sp.
Trifarina (Angulogerina) baggi (Galloway & Wissler)

(Table 4-1 cont'd)

Sample 87-OR-51B

<i>Bolivina vaughani</i> Natland
<i>Buccella frigida</i> (Cushman)
<i>Buccella</i> sp.
<i>Buccella tennerima</i> (Bandy)
<i>Buliminella elegantissima</i> (d'Orbigny)
<i>Cassidulina bradshawi</i> Uchio
<i>Cassidulina tortuosa</i> Cushman & Hughes
<i>Cibicides fletcheri</i> Galloway & Wissler
<i>Cibicides lobatus</i> (d'Orbigny)
<i>Discorbis</i> sp.
<i>Elphidium clavatum</i> Cushman emend. Loeblich & Tappan
<i>Fissurina lucida</i> (Williamson)
<i>Florilus</i> (<i>Nonionella</i>) <i>basispinata</i> (Cushman & Moyer)
<i>Florilus</i> (<i>Nonionella</i>) <i>miocenica stella</i> (Cushman & Moyer)
<i>Fursenkoina</i> (<i>Virgulina</i>) <i>bramletti</i> (Galloway & Moyer)
<i>Globigerina bulloides</i> d'Orbigny
<i>Lagena Acuticosta</i> Reuss
<i>Oolina catenulata</i> (Williamson)

Sample 87-OR-54

<i>Buccella frigida</i> (Cushman)
<i>Buliminella elegantissima</i> (d'Orbigny)
<i>Cassidulina</i> sp.
<i>Elphidium clavatum</i> Cushman emend. Loeblich & Tappan
<i>Elphidium incertum</i> Williamson
<i>Florilus</i> (<i>Nonionella</i>) <i>basispinata</i> (Cushman & Moyer)
<i>Globigerina bulloides</i> d'Orbigny
<i>Oolina catenulata</i> (Williamson)
<i>Trifarina</i> (<i>Angulogerina</i>) <i>baggi</i> (Galloway & Wissler)

In addition to the faunal evidence, zircons separated from one of the tuff beds in the formation yielded a fission track age of 3.3 ± 0.8 Ma (2 sigma error) (Naeser, written communication, 1988). The zircons submitted for analysis exhibited well-preserved crystal faces, and though the faces exhibited a pitted appearance, they did not appear to have suffered much abrasion. Therefore, these crystals were probably an original component of the tuff, not a detrital addition (L. T. Silver, personal communication, 1987).

The dominant lithology of the Ohlson Ranch Formation is fine- to very fine-grained, massive sandstone and silty sandstone. Together with the fossils preserved in the sediment, this indicates deposition in a quiet-water, marine environment, such as a small, protected bay or coastal inlet. The foraminiferal assemblage indicates an inner- to mid-shelf depositional environment (Ingle, written communication, 1988). The preservation of the volcanic ashes, which show little sign of reworking in thin section, also points to a quiet-water, bay environment.

There may be at least one unconformity within the Ohlson Ranch Formation (Higgins, 1960; Peck, 1960), though limited exposure and typical lack of bedding makes this difficult to confirm. The reason for suggesting such an unconformity is Peck's identification of the two different Pliocene faunal assemblages. The upper Pliocene assemblage is found only in

coarse sandstones, while the middle Pliocene assemblages are found only in fine-grained sandstones. One interpretation of this phenomenon, suggested by both Higgins and Peck, is that the coarse sandstones represent a later depositional phase implying an unconformity of unknown magnitude. Higgins cites field relations that support but do not prove the presence of a significant unconformity between the fine and coarse sandstones.

This paleontological data indicates a middle to upper Pliocene age for the Ohlson Ranch Formation. The fission-track age of the tuff (3.3 ± 0.8 Ma) is in agreement with this age determination. The Pliocene embayment that existed in this area must have receded sometime after 3.3 ± 0.8 Ma. The presence of upper Pliocene fossils suggests that it receded in late Pliocene time, closer to the younger limit of the fission-track age range.

Pliocene Surfaces and Paleoshoreline

As first noted by Higgins (1960), the ancient surfaces represented by the flat to gently rolling ridge crests in this area can be classified into three categories: those that are capped by the Ohlson Ranch sediments (which overlie planar and relatively unweathered Franciscan bedrock surfaces that are typically mollusk-bored and associated with relict sea stacks) and two types of bedrock surfaces. The first type of bedrock surface is relatively unweathered, may display mollusk borings

and sea stacks, and in some places is overlain by a thin veneer of rounded cobbles. Surfaces of this type were interpreted by Higgins as stripped surfaces: areas that were invaded by the Pliocene sea (which created the fresh bedrock surface) and were subsequently stripped of their Pliocene sedimentary cover. The other bedrock surfaces are quite different in character: they are never associated with sea stacks or mollusk borings, and the Franciscan is deeply weathered with a thick soil and colluvial cover. These surfaces were interpreted to represent areas that remained above sea level during the time of Ohlson Ranch deposition. Using these criteria, Higgins approximated the boundaries of the Ohlson Ranch basin.

As defined by Higgins, the southwestern edge of the Ohlson Ranch basin trends toward the San Andreas fault near the confluence of Sproule Creek and South Fork Gualala River (Figure 4-3). Although subsequent erosion has obliterated the exact location of the intersection of this shoreline and the fault zone, projection of the trend of the shoreline across the valley suggests that this intersection was located approximately as shown in Figure 4-3. This raises the question: where is the continuation of this shoreline west of the San Andreas fault?

Figure 4-3: Map showing the paleoshoreline of the Ohlson Ranch Formation (heavy dashed line) as determined by Higgins (1960). Dotted continuation of this line indicates projection of the shoreline to the San Andreas fault. Location of shoreline is based on the distribution of three types of ancient surfaces: those that are overlain by the Ohlson Ranch Formation, those that the Ohlson Ranch Formation has been stripped off of, and those that were never covered by the Pliocene sea and are therefore deeply weathered. Upper (?) Pliocene marine deposits near Point Arena are also shown, with postulated offset shoreline.

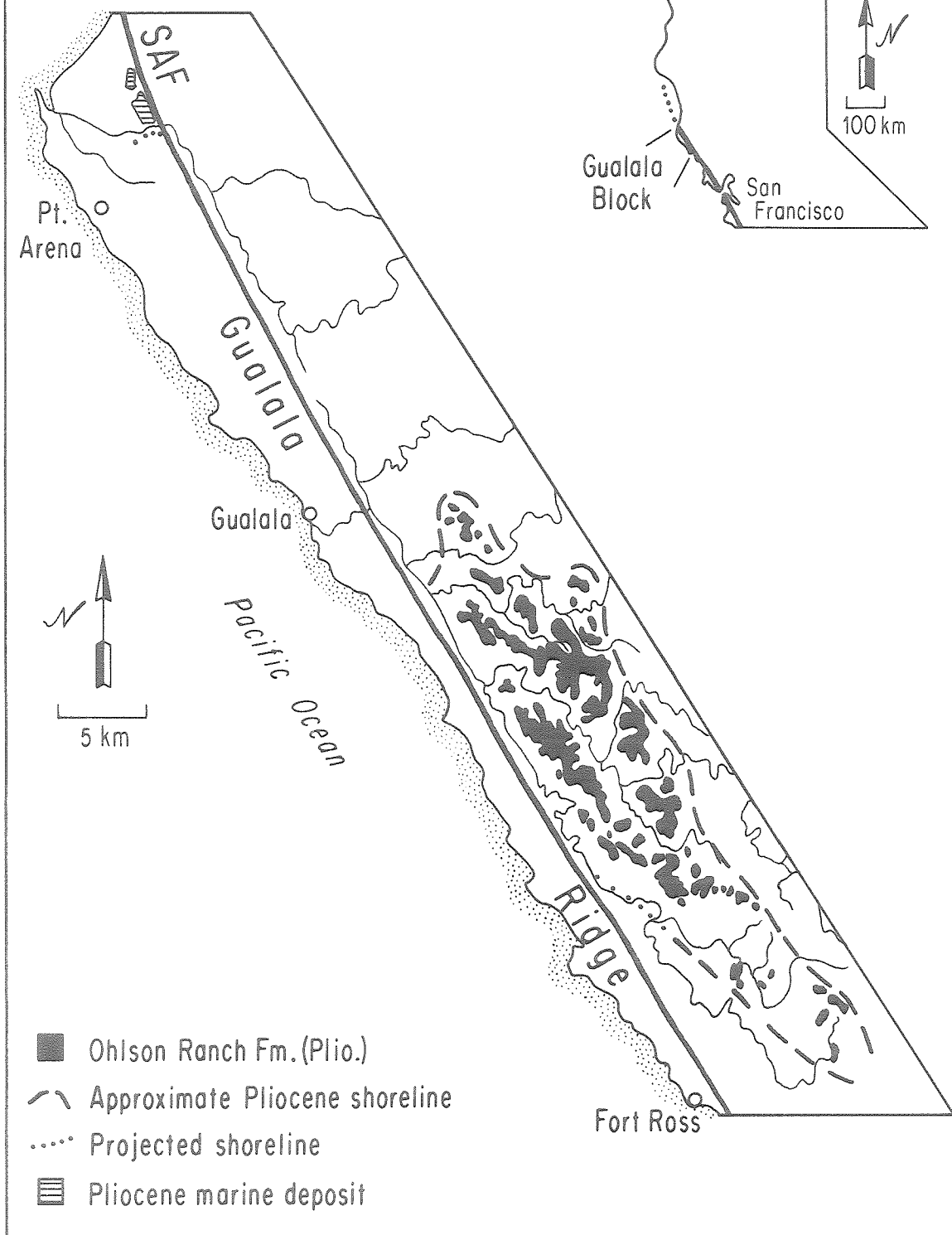


Figure 4-3

GUALALA BLOCKGualala Ridge and Pliocene Marine Deposits

A series of uplifted Pleistocene marine terraces steps up from the coast to the top of Gualala Ridge, the "backbone" of the Gualala block. The conspicuously flat to gently rolling nature of this ridge suggests that its summit could represent an ancient surface. However, where exposures exist, marine deposits are absent on these surfaces. Typically, they are underlain by weathered bedrock, much like the surfaces that lie southeast of the Ohlson Ranch shoreline, east of the fault. The only marine deposits identified along the summit of Gualala ridge are near Point Arena (Figure 4-3). Here, the ridge drops abruptly in elevation across the Garcia River. The surface is capped by fine to very fine-grained sandstone similar in appearance to that of the Ohlson Ranch Formation. These sediments contain both mollusks and foraminifera. The mollusks were tentatively identified as Upper (?) Pliocene (Durham and Peck, in Boyle, 1967). The foraminiferal assemblage (Table 2), while less diverse than that seen in the Ohlson Ranch Formation, is indicative of a similar depositional environment and age (Ingle, written communication, 1987, 1988). While neither the molluscan nor foraminiferal faunas proves a correlation between the beds at Point Arena and the

Table 2: List of foraminifera recovered from the Pliocene sediments near Point Arena, identified by J.C. Ingle.

TABLE 4-2

FORAMINIFERRA RECOVERED FROM PLIOCENE SANDSTONE NEAR POINT ARENA (SAMPLE 86-PAOR-1);

asterisk (*) indicates species is found in Ohlson Ranch Formation (Table 4-1).
(Analysis by J.C. Ingle) .

<i>Buccella tenerrima</i> (Bandy)	*
<i>Cibicides fletcheri</i> Galloway & Wissler	*
<i>Dyocibicides biserialis</i> Cushman & Valentine	
<i>Elphidium clavatum</i> Cushman emed. Loeblich & Tappan	*
<i>Elphidium hannai</i> (Cushman & Grant)	
<i>Elphidium</i> sp. (juvenile)	*
<i>Globigerina bulloides</i> d'Orbigny	*
<i>Oolina costata</i> (Williamson)	
<i>Pullenia</i> cf. <i>salisburyi</i> Stewart & Stewart	
<i>Trifarina angulosa</i> (Williamson)	

Ohlson Ranch Formation, they are both compatible with such a correlation.

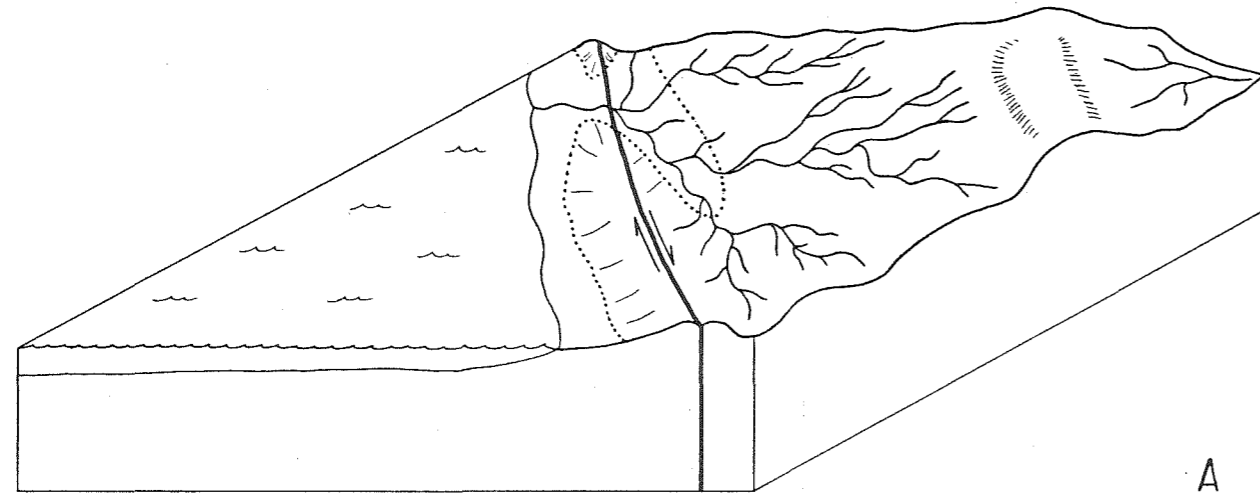
If this correlation is correct and if most of Gualala ridge was an area of subaerial exposure during the Pliocene, as suggested by the deeply weathered bedrock and lack of Pliocene sediments along its crest, then the southwestern shoreline of the Ohlson Ranch Formation may be offset across the San Andreas fault zone to the vicinity of Point Arena (Figure 4-3). This distance is approximately 50 km.

Evolution of Drainage Morphology

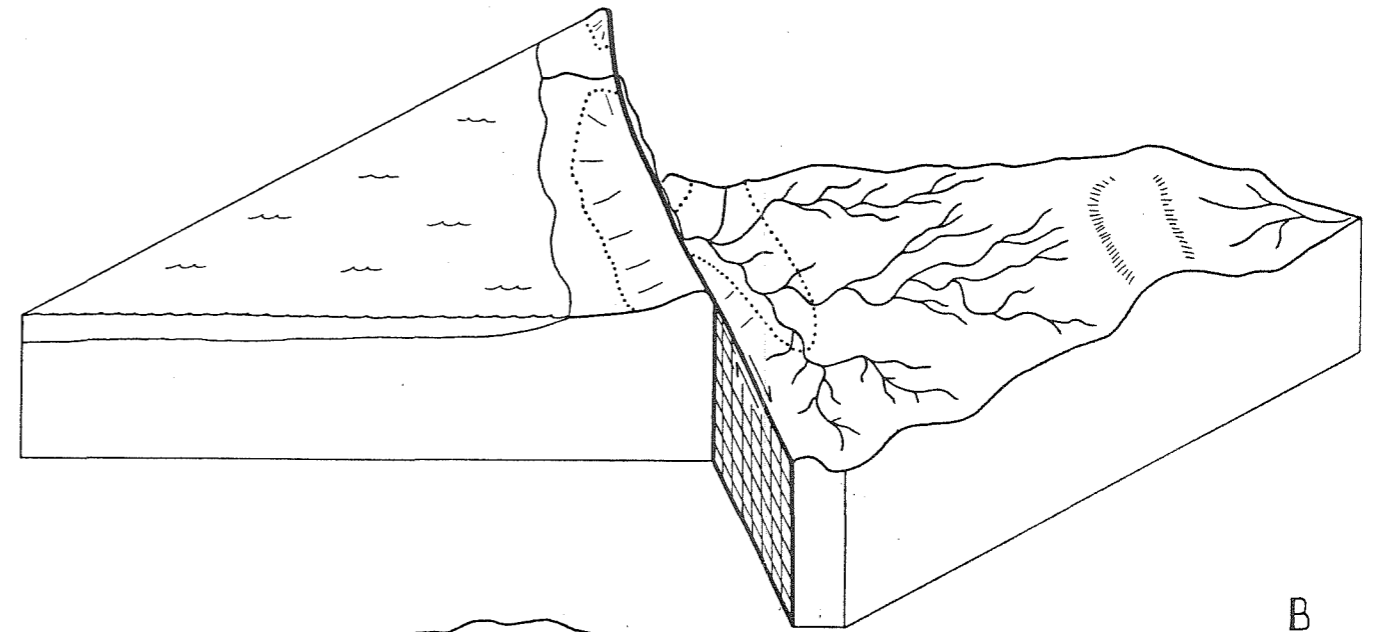
The similarities in lithology and in the molluscan and foraminiferal faunas between the Ohlson Ranch Formation and the deposits near Point Arena allow the proposed correlation, but do not prove it. Additional support for the correlation is found by considering the geomorphic evolution of the area.

Figure 4-4 is a series of block diagrams showing a likely scenario for the evolution of the Ohlson Ranch embayment after the retreat of the Pliocene sea. Sometime in the late Pliocene, the sea retreated from the Ohlson Ranch embayment. This newly emergent landscape was a low-lying flatland covered with Ohlson Ranch sediments. New drainages forming on this landscape would have flowed out to the ocean through the entrance to the former Ohlson Ranch bay, as depicted in Figure 4-4.A. This diagram shows the former shoreline of the Ohlson Ranch bay as a dotted line. As offset occurred on the San

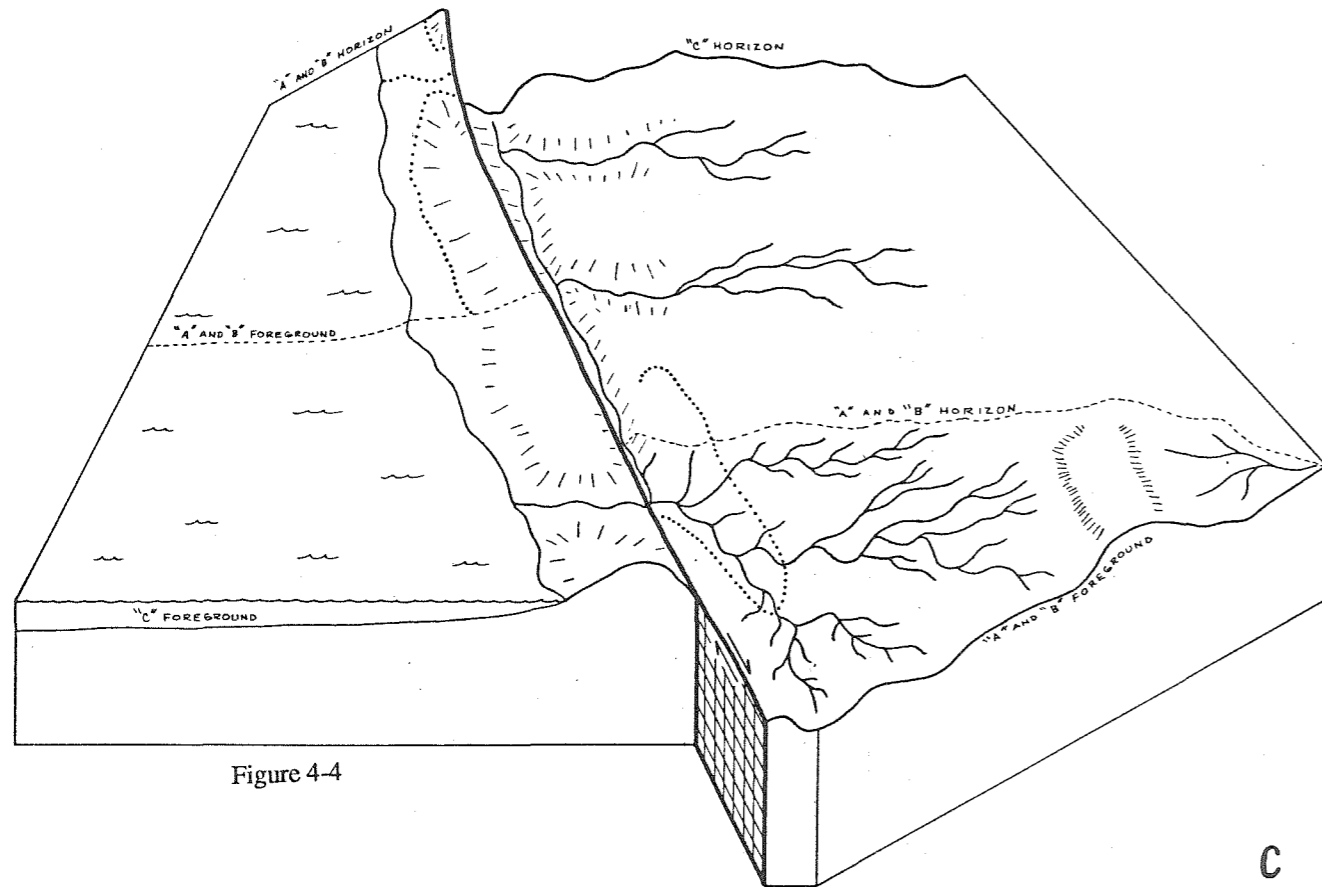
Figure 4-4: Series of block diagrams showing a scenario for the geomorphic evolution of the Ohlson Ranch embayment and the Gualala region. The dotted lines represent the Pliocene shoreline after retreat of the Pliocene sea, the heavy, solid line represents the San Andreas fault zone. Drawing A represents the region immediately after retreat of the sea: a low-lying flatland underlain by sediments of the Ohlson Ranch Formation. Drainages developing on this newly-emergent surface would have flowed out to the ocean through the abandoned entrance to the former Pliocene bay. Drawing B shows the effect of offset across the San Andreas fault: the stream system becomes progressively offset from its mouth. Drawing C shows capture of the drainage and abandonment of the original mouth due to further motion of the San Andreas fault. Drawing D shows the region after continued motion on the fault. The landscape of the Gualala region is very similar to that depicted in drawing D.



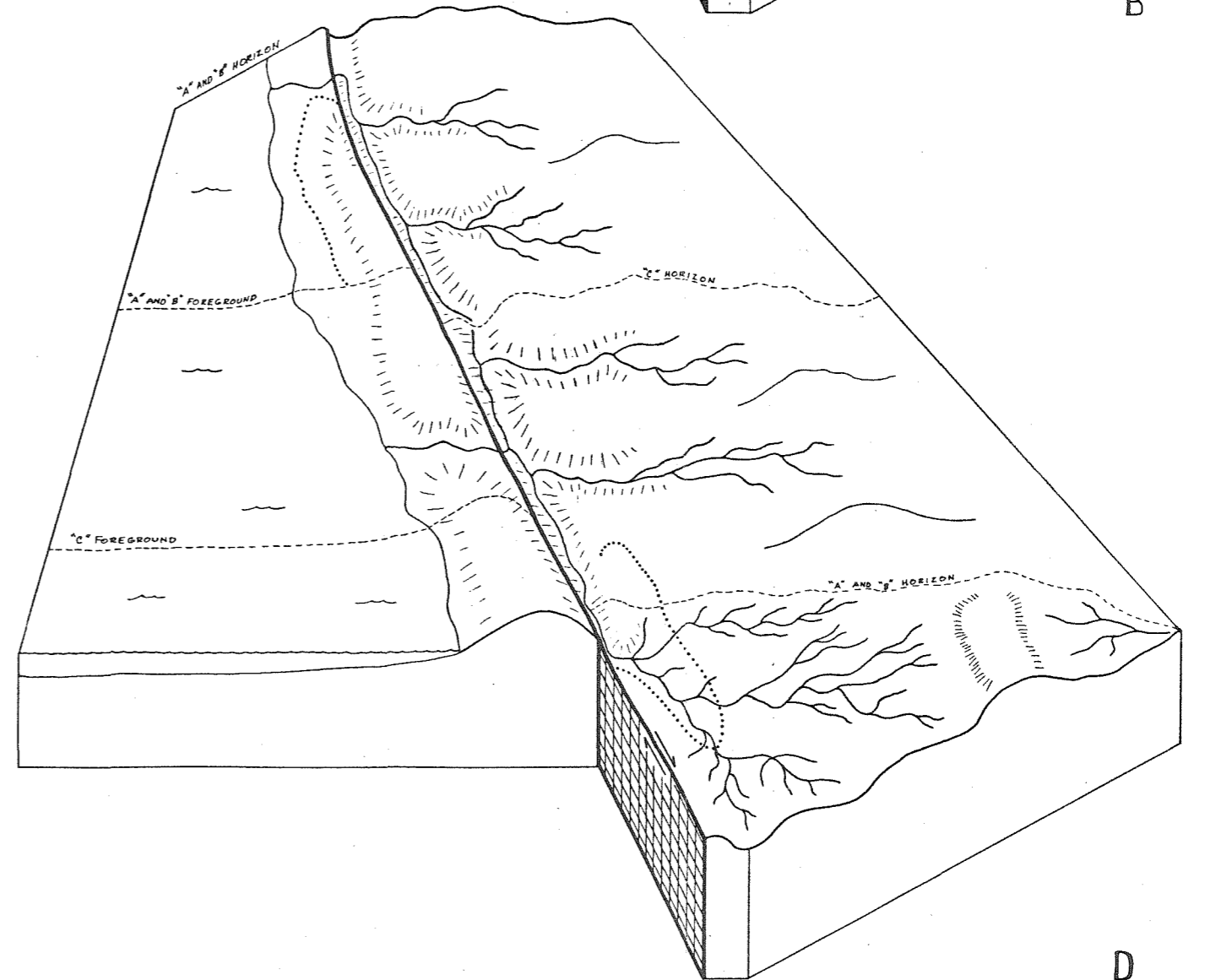
A



B



C



D

Figure 4-4

Andreas fault, this stream system would have been deflected in a right-lateral sense and continued to flow out through the entrance to the former Ohlson Ranch bay, as shown in Figure 4-4.B. At some time, the offset of the river mouth would have become so large that capture of the drainage occurred, as shown in Figure 4-4.C. Continued offset on the San Andreas fault would produce the landscape depicted in Figure 4-4.D. This is very similar to the current landscape of the Gualala region (Figure 4-5).

Several geomorphic features of the Gualala area lend support to the scenario outlined above. There are only 2 major rivers that provide drainage through the Gualala block from the region east of the San Andreas fault: the Gualala River, which enters the ocean near the town of Gualala, and the Garcia River, which flows into the ocean near Point Arena (Figure 4-5). Both rivers flow northwest along the San Andreas fault zone for tens of kilometers before reaching their mouths. It is the valleys occupied by these two rivers that form the very prominent "rift valley" that marks the San Andreas fault zone in this area (Figure 4-6).

Although the Gualala has a much larger drainage basin (Figure 4-5), the Garcia has just as broad a valley along the San Andreas fault zone, and its valley near Point Arena, near the river's mouth, is strikingly wide, given the amount

Figure 4-5: Map showing the drainage basins of the Gualala and Garcia rivers (heavy dashed line). The valley of the Garcia is just as wide as the Gualala valley, and the Garcia's mouth is much broader. This is surprising because the drainage area of the Gualala is much larger than that of the Garcia. However, this is expected if the Gualala originally flowed out through the current mouth of the Garcia. The morphology of the divide between the two drainages along the fault supports this idea, as does the presence of fluvial gravels (dotted region) perched on the divide, indicating that a river did indeed flow through the divide at one time. Diamonds show the distribution of mapped blueschist blocks in the Franciscan (from Wagner and Bortugno, 1982). Blueschist blocks have been found only in the Gualala drainage basin, and studies of the sediment currently carried in the streams (Wong and Klise, 1986) indicate that glaucophane is much more abundant in the Gualala sediments than in Garcia sediments. Preliminary study of sediments in the high fluvial terraces above the Garcia indicates that glaucophane is present in these sediments, supporting the idea that the Gualala River once flowed out through the mouth of the Garcia.

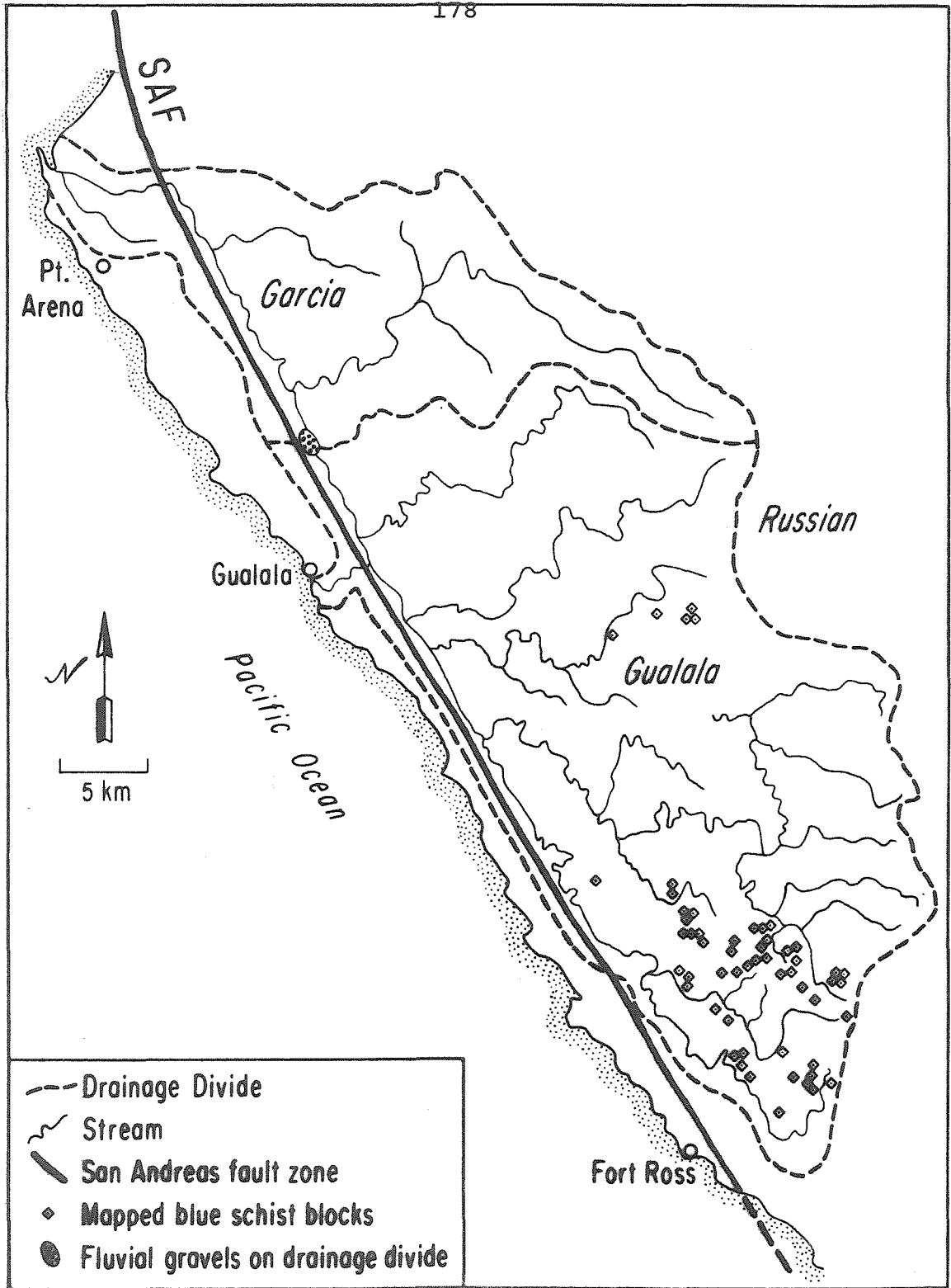


Figure 4-5

Figure 4-6: Photograph of raised relief map of the Gualala area showing the morphology of the "rift valley" of the San Andreas fault.

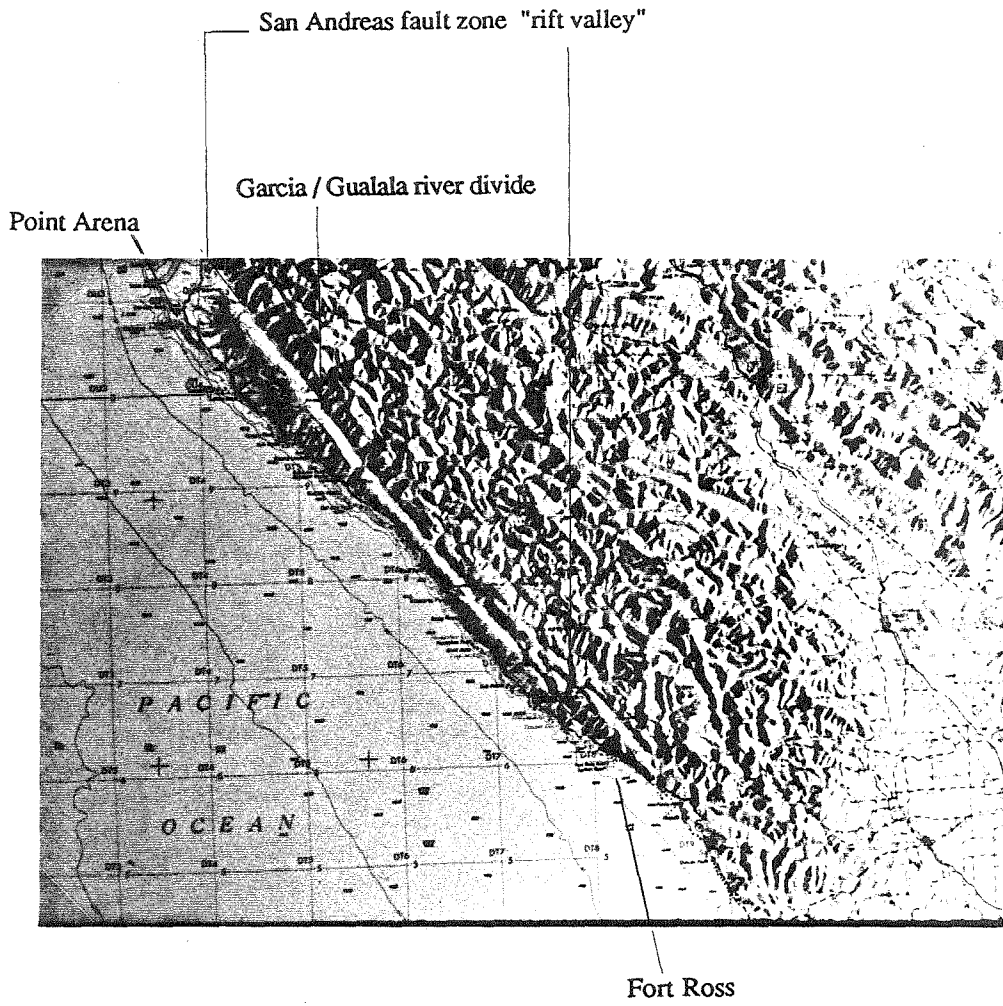


Figure 4-6

of flow it is currently accommodating. An hypothesis explaining these observations is that the flow through the current main valley and mouth of the Garcia was at one time much greater than it is now, and that some portion of the original drainage has been captured. The only likely candidate for such diversion is the current Gualala River: in other words, the stream system that now drains out of the mouth of the Gualala once flowed out of the mouth of the Garcia near Point Arena.

If this is correct, then the current divide between the two rivers along the San Andreas fault zone (Figure 4-5) must have had the Gualala river flowing through it in the past. There are three lines of evidence that this is the case. First, the morphology of the divide where it crosses the San Andreas is very unusual in that it lies in a low point (<480 ft) between Gualala ridge and the first ridge to the east of the San Andreas. It is significant that the divide is in a valley that is no higher than some of the river terraces found above both rivers. So the morphology of the divide supports the idea that the Gualala River once flowed through it. In addition, fluvial gravels present in the divide show that a river did once flow through the area (Figure 4-5). Finally, the compositions of the fluvial terrace gravels suggest that the Gualala River was that river. The Santa Rosa sheet of the state geologic map shows a difference in the rock type within the current watersheds of the Garcia and Gualala rivers:

whereas many blueschist blocks exist within the area currently drained by the Gualala, none are mapped within the current drainage of the Garcia (Figure 4-5). Although this may be an artifact of the degree of detail of the mapping done in the two areas, a preliminary study of the sediment carried by the modern rivers revealed glaucophane in the thin section of a sample taken near the mouth of the Gualala, and no glaucophane in the thin section of the sample taken near the mouth of the Garcia. A geochemical study of the modern sediment carried by northern California rivers shows a significant difference in the weight per cent of heavy minerals (including glaucophane) in samples from the Garcia and Gualala rivers: 0.8% for the Garcia and 5.3% for the Gualala, though some of the heavy mineral suite in the Garcia sediments is glaucophane (Wong and Klise, 1986). Thin sections of samples taken from river terraces above the modern Garcia do contain glaucophane. Although more work needs to be done to bolster these initial findings, these preliminary data support the hypothesis that the Gualala river at one time flowed out the mouth of the Garcia, depositing glaucophane on the terraces, and that, since its capture, little glaucophane (primarily that reworked from the terraces) has been deposited in the Garcia drainage.

Pliocene Slip Rate

If the original mouth of the Gualala river is now near

Point Arena, then it has most likely been offset from the point where the Gualala first encounters the San Andreas, essentially the same offset as proposed for the Ohlson Ranch shoreline (Figure 4-3). The ancestral Gualala river must have begun to form as the Pliocene sea retreated from the Ohlson Ranch embayment, forming a meandering channel across the nearly flat, newly emergent landscape. Continued uplift caused the meanders to become incised, while continued offset on the San Andreas separated the mouth from the headwaters. Eventually, much of the drainage was captured by the current mouth of the Gualala. The formation of the valley at the current mouth of the Gualala must have pre-dated the capture or the river would have continued flowing parallel to Gualala ridge. Reconstructing the Garcia mouth back to the Gualala also places the current mouth of the Gualala opposite the Russian River, suggesting that the valley currently occupied by the mouth of the Gualala was cut by the Russian River, abandoned, and reoccupied by the Gualala, all due to San Andreas offset since the retreat of the Pliocene sea. The best estimate for the time of abandonment of the Ohlson Ranch shoreline and the formation of the initial drainage is the fission track age of the volcanic ash collected from the Ohlson Ranch Formation: 3.3 ± 0.8 Ma. The ash is an unknown number of years older than the features described above, but seems to be near the top of the section. It, therefore, provides a maximum age approximation of the timing of retreat

of the Pliocene sea. This maximum may be close to the actual age of retreat.

The offset of 50 km in 3.3 ± 0.8 million years suggests a minimum average annual slip rate of 12-20 mm/yr since Pliocene time. If valid, this suggests that the slip rate of the northern San Andreas fault has not varied by more than, at most, a factor of two over the past few million years, and that these rates have been much lower than the total motion across the Pacific-North American plate boundary. This implies that much of the plate-boundary motion is accommodated on other structures at this latitude.

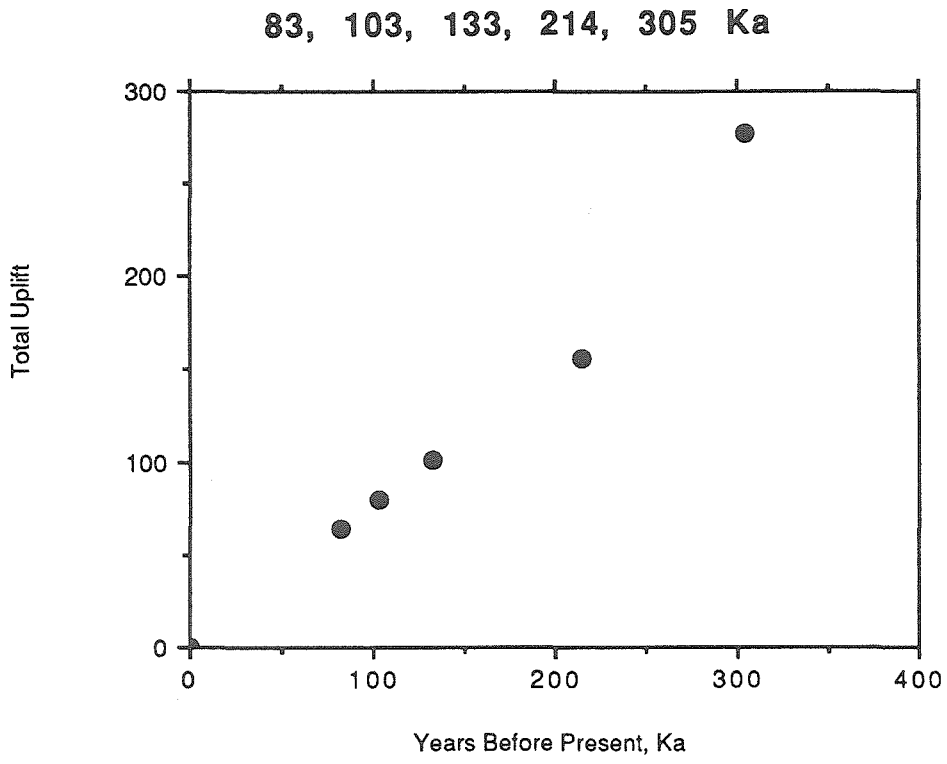
REFERENCES

- Boyle, M.W., 1967, Stratigraphy, sedimentation, and structure of an area near Point Arena, California: unpublished M.S. thesis, Univ. of Calif., Berkeley.
- Hall, 1984, Holocene history of the San Andreas fault between Crystal Springs Reservoir and San Andreas Dam, San Mateo County, California: B.S.S.A., v. 74, n. 1, pp. 281-299.
- Higgins, C.G., 1960, Ohlson Ranch Formation, Pliocene, Northwestern Sonoma County, California: Univ. Calif. Pubs. Geol. Sci., v. 36, n. 3, pp. 199-232.
- Peck, J.H., 1960, Paleontology and Correlation of the Ohlson Ranch Formation: Univ. Calif. Pubs. Geol. Sci., v. 36, n. 3, pp. 233-241.
- Sarna-Wojcicki, A.M., Meyer, C.E., and Slate, J.L., 1986, Displacement of a ca. 6 Ma tuff across the San Andreas fault system, northern California: EOS v. 67, n. 44, p. 1224.
- Wong, F.L., and Klise, D.H., 1986, Heavy mineral, clay mineral, and geochemical data of surface sediments from

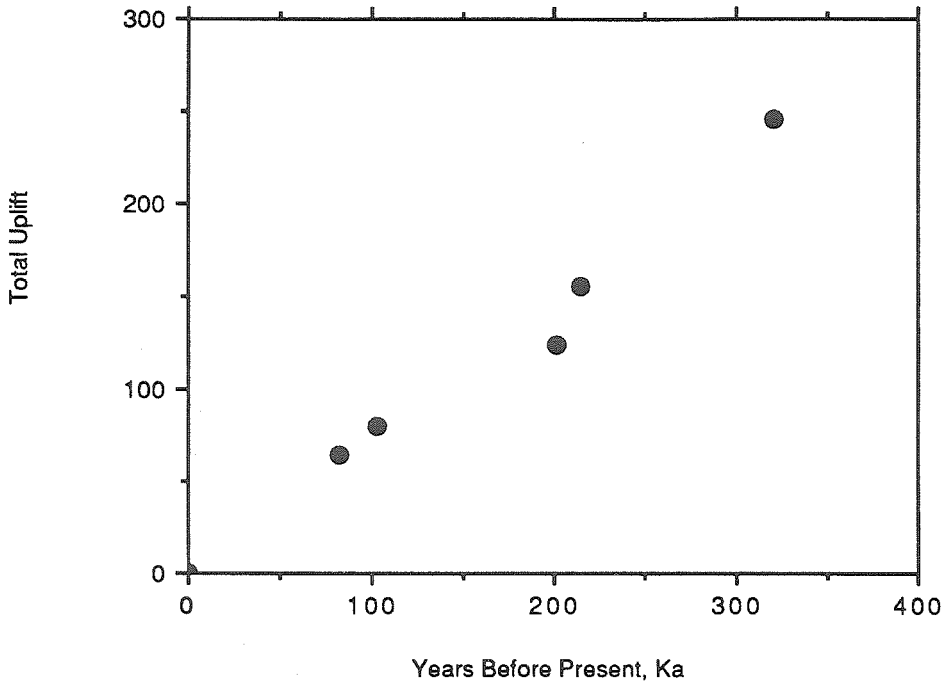
coastal northern California rivers: U.S. Geologic Survey
Open File Report 86-574.

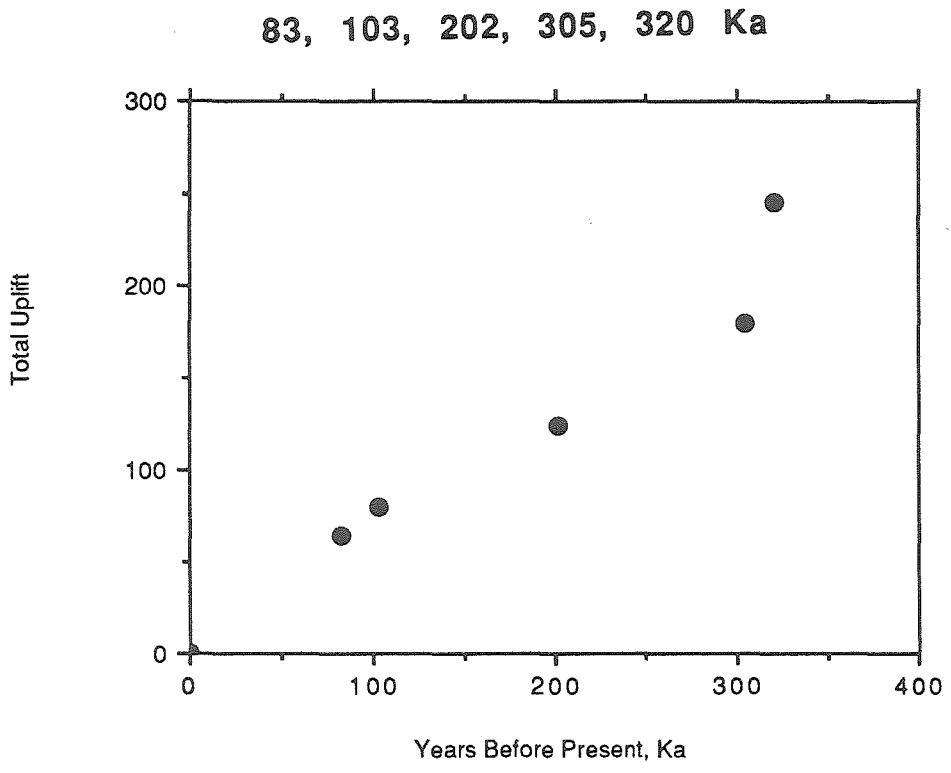
APPENDIX A: Age versus total uplift graphs for area 3.

The following graphs represent the age assignments attempted for the five lower terraces in area 3. The graphs are constructed using the estimated altitudes of the shoreline angles of each of the terraces, and the high sea-level-stand ages and elevations shown in 3-15. Total uplift is calculated for each age assignment by adding the absolute value of the elevation of sea level at the time of the assigned sea-level high stand to the estimated altitude of the shoreline angle. The only set of age assignments giving a constant uplift rate (straight line) is that shown in Figure 3-18. The following graphs show all other attempted age assignments, none of which are consistent with a constant uplift rate. The bold numbers above each graph are the ages assigned to terraces I-V for the case in consideration. All possible cases were considered.

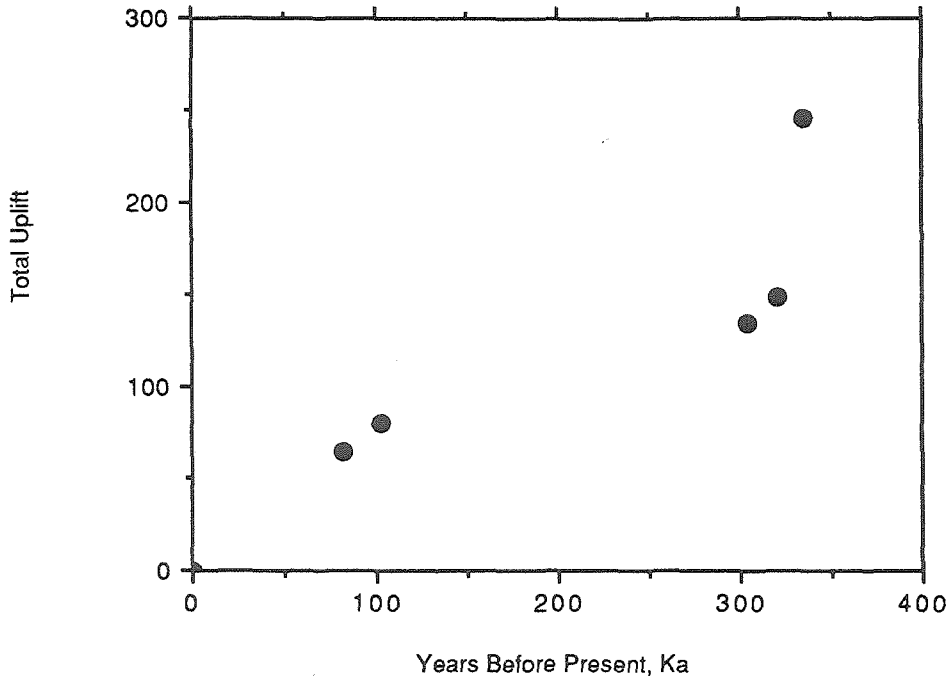


83, 103, 202, 214, 320 Ka

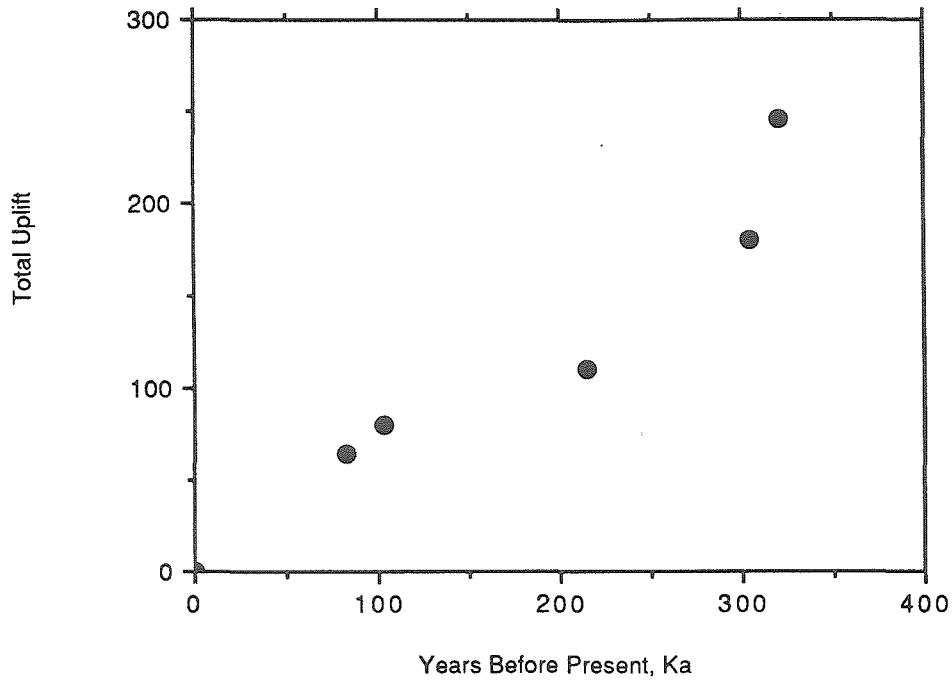


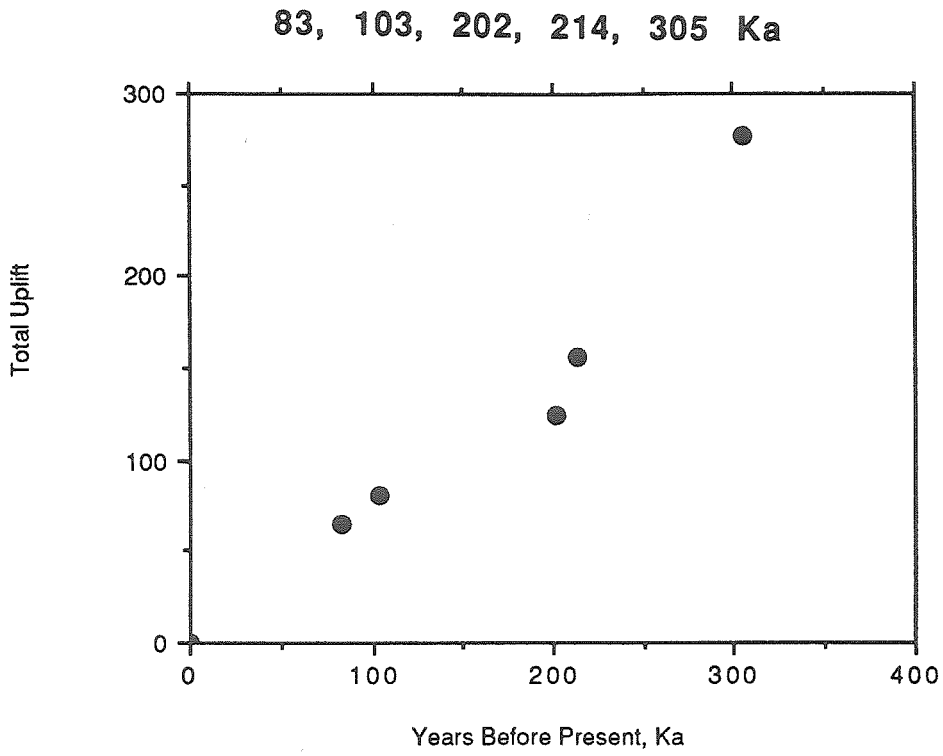


83, 103, 305, 320, 336 Ka

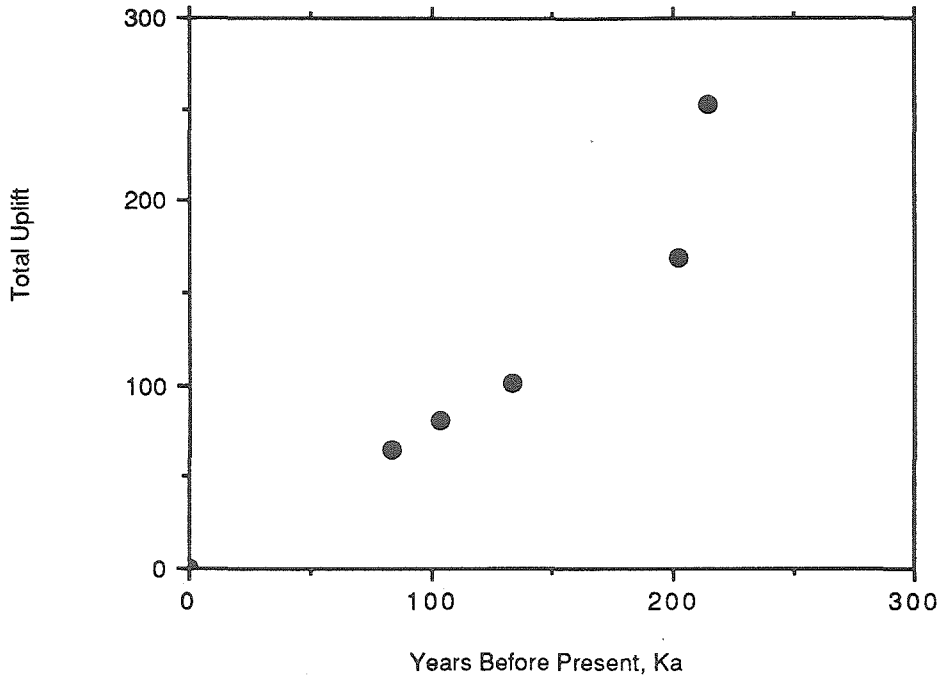


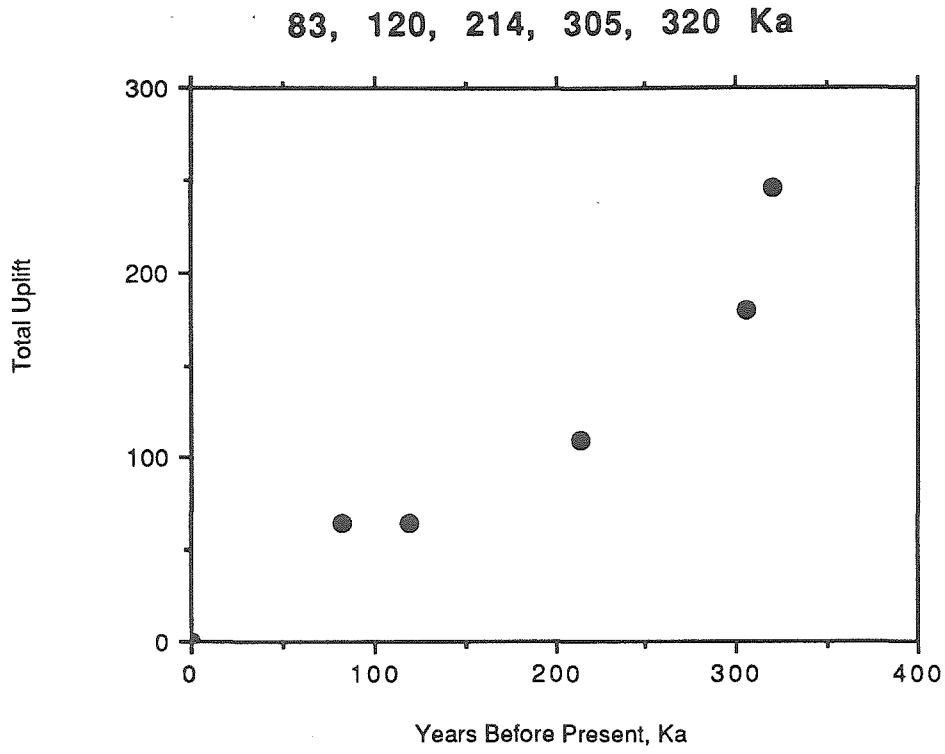
83, 103, 214, 305, 320 Ka

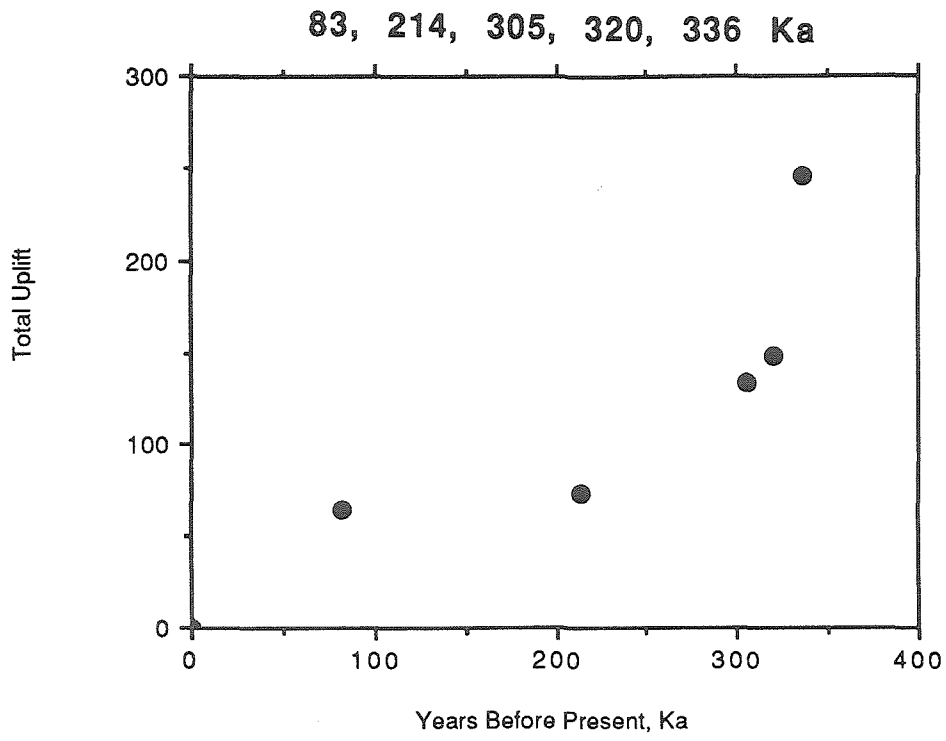


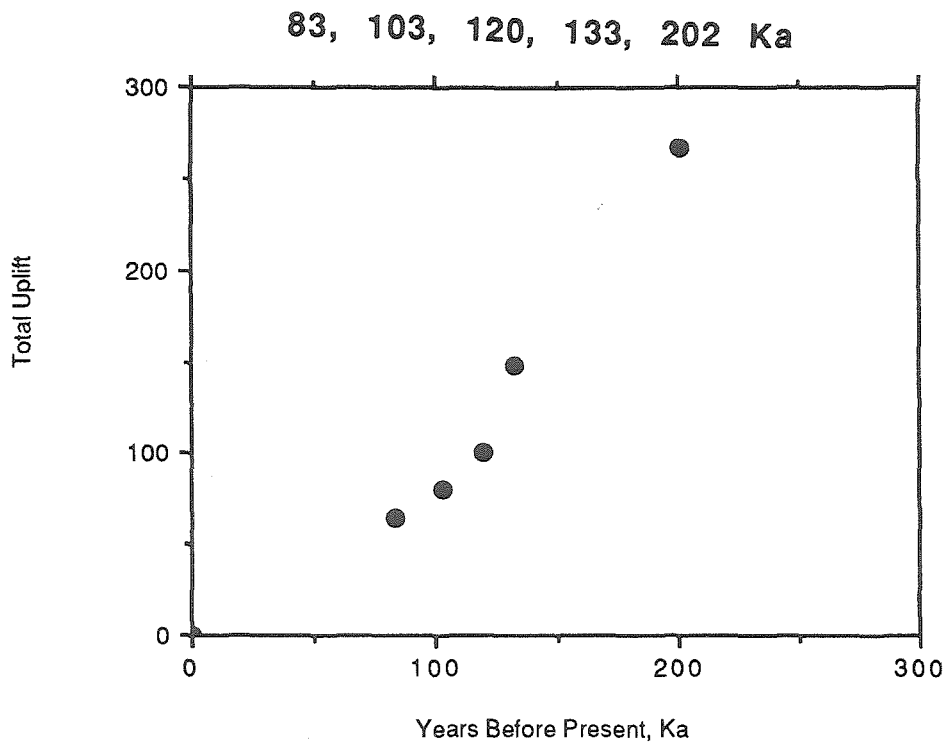


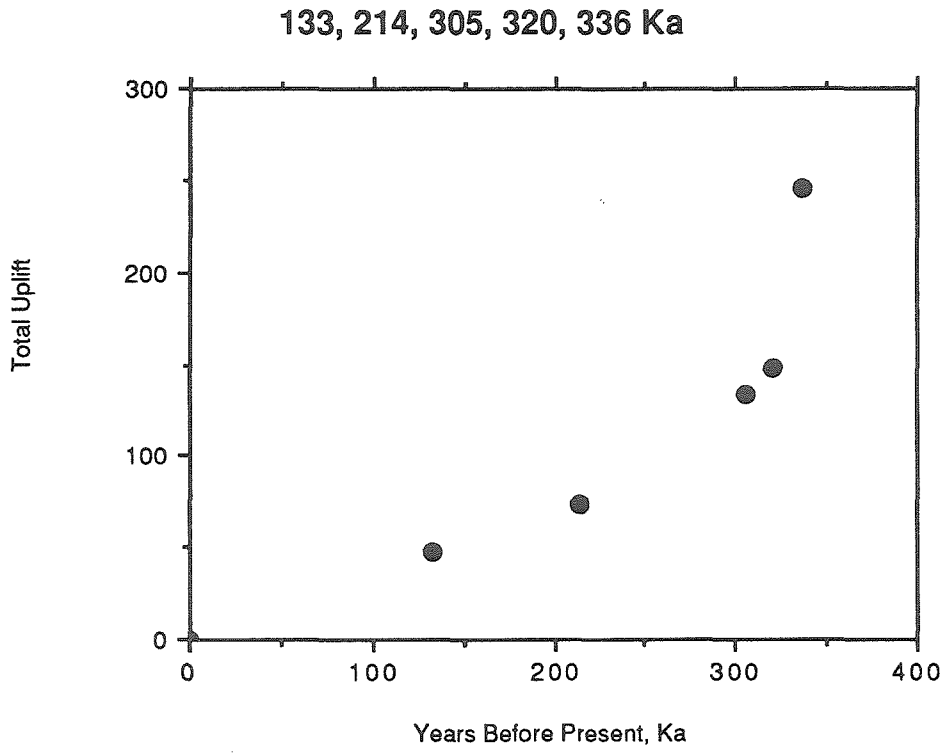
83, 103, 133, 202, 214 Ka



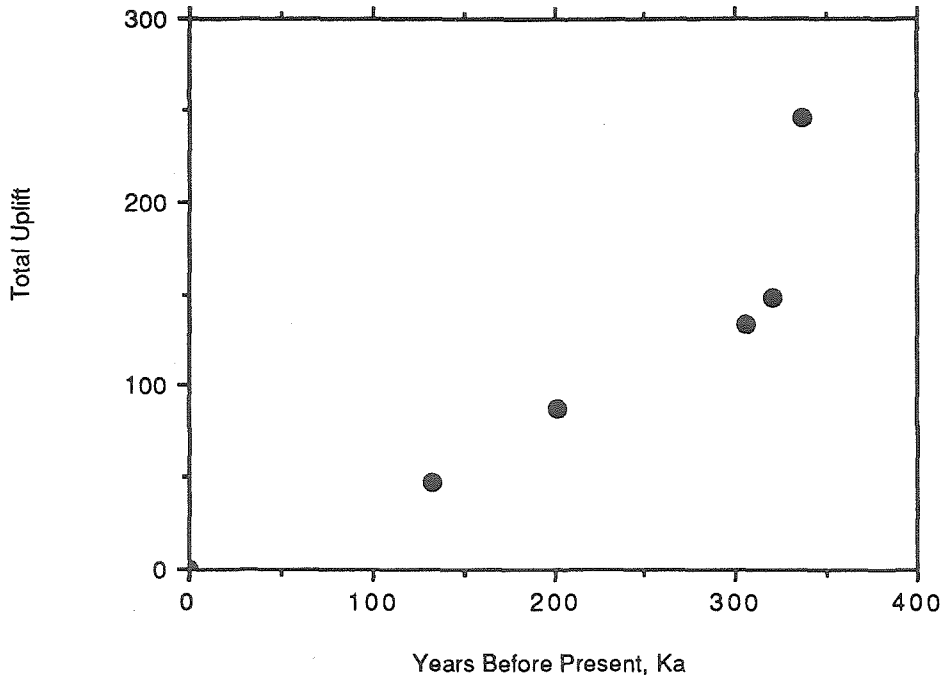


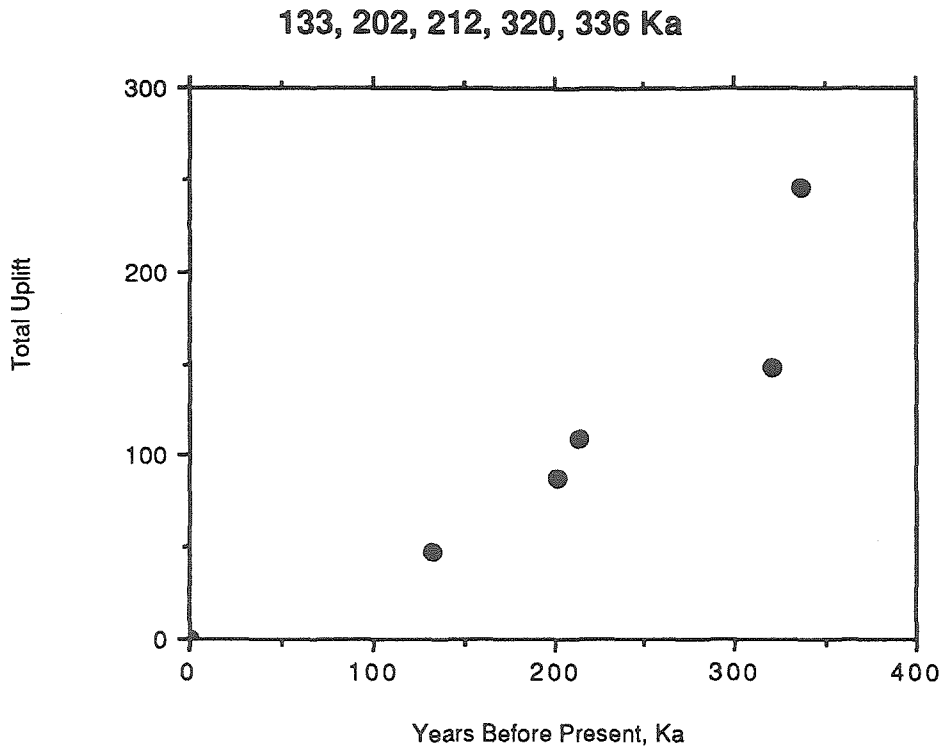




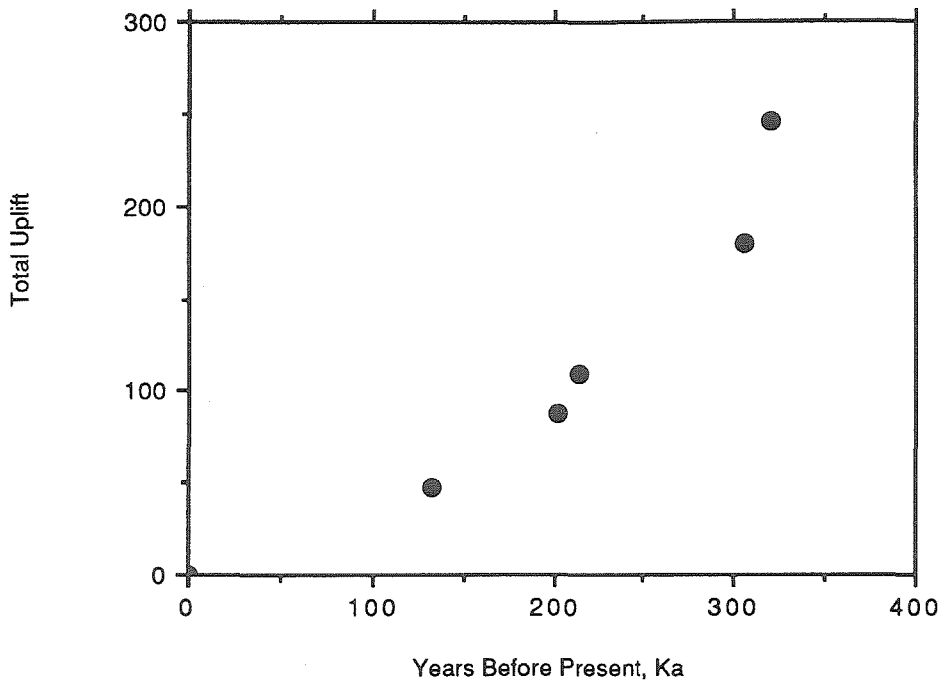


133, 202, 305, 320, 336 Ka

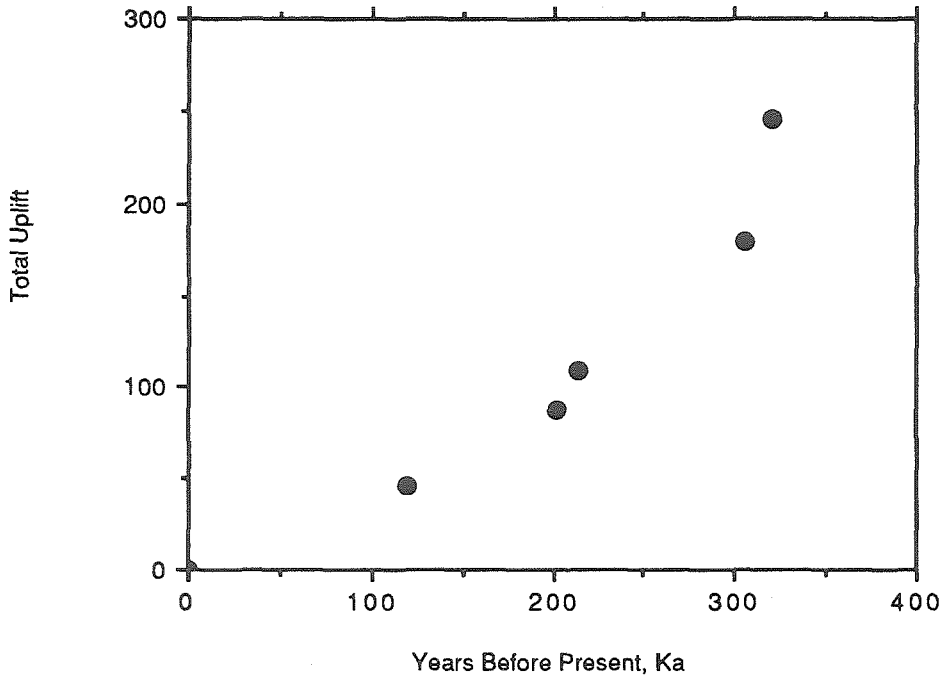




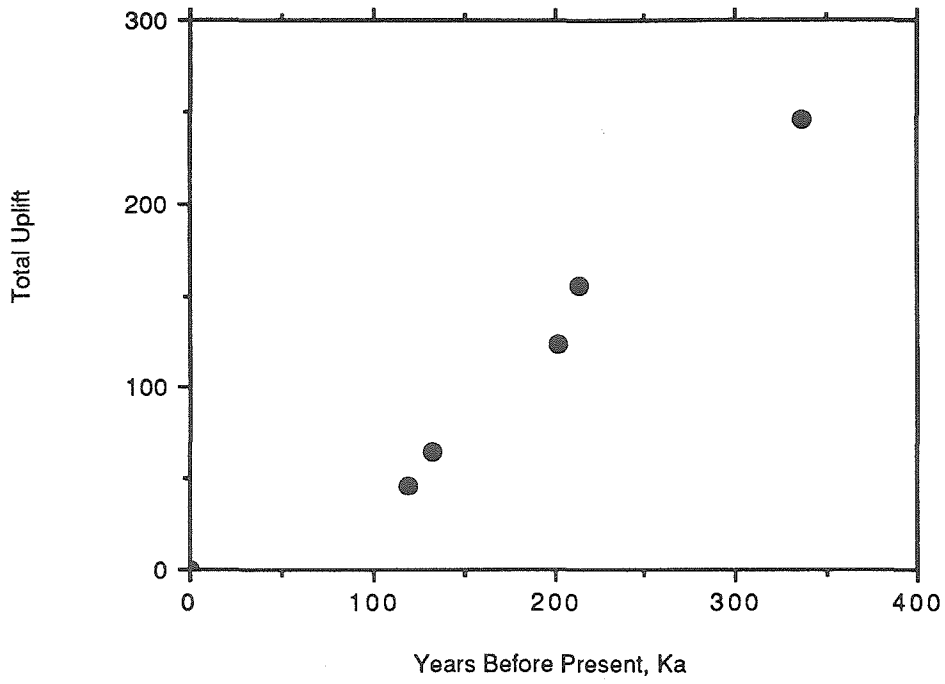
133, 202, 212, 305, 320 Ka



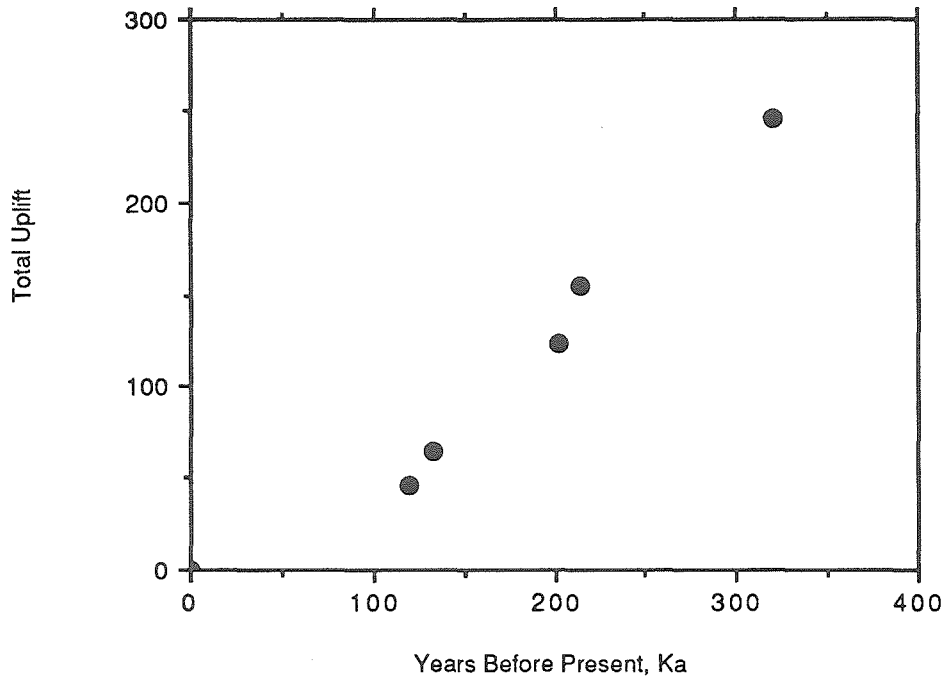
120, 202, 214, 305, 320, 336



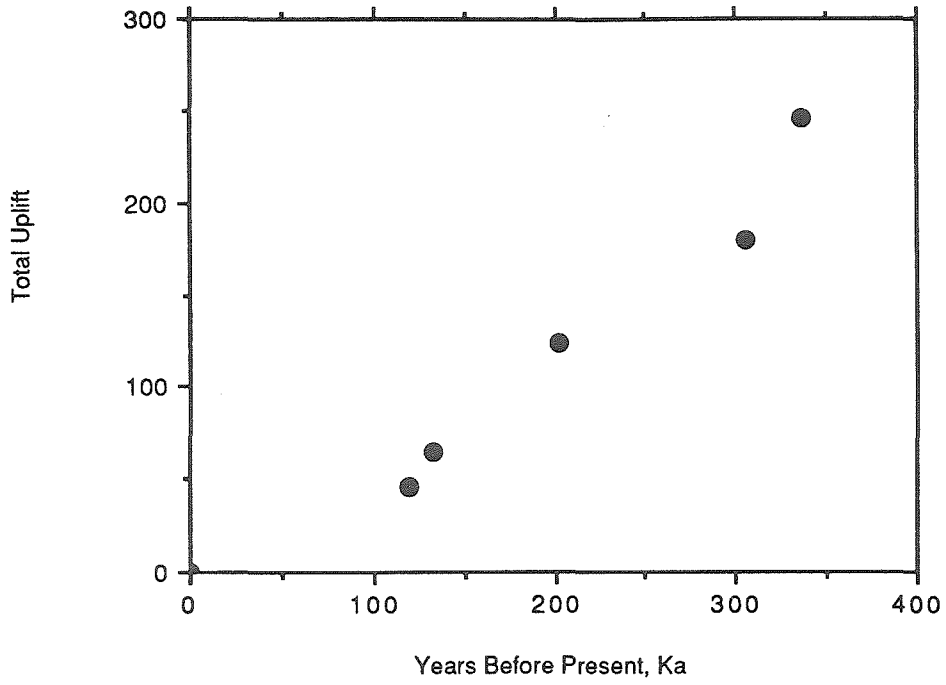
120, 133, 202, 214, 336 Ka



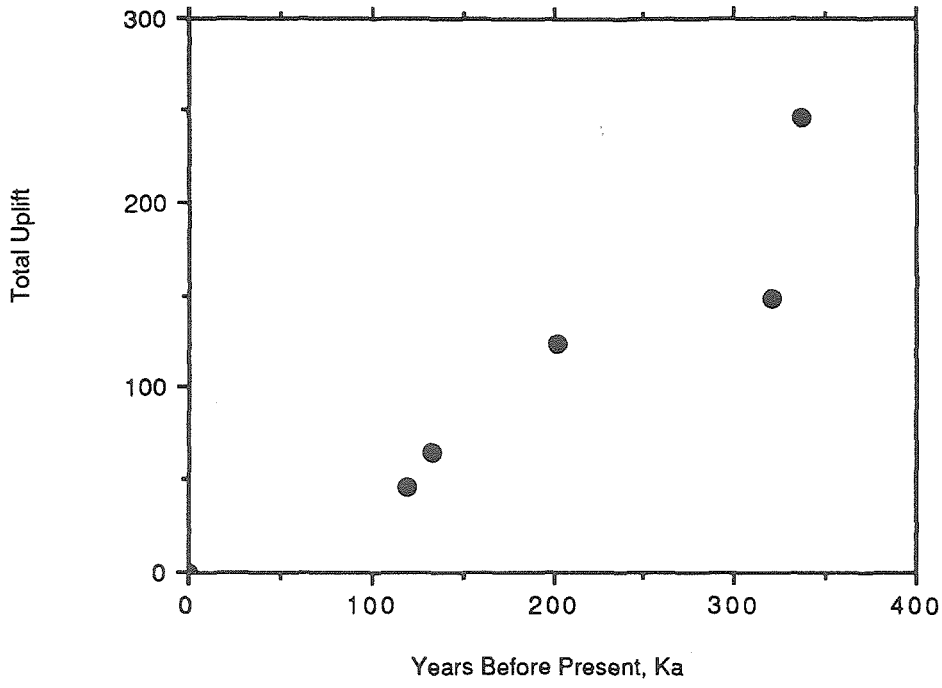
120, 133, 202, 214, 320 Ka

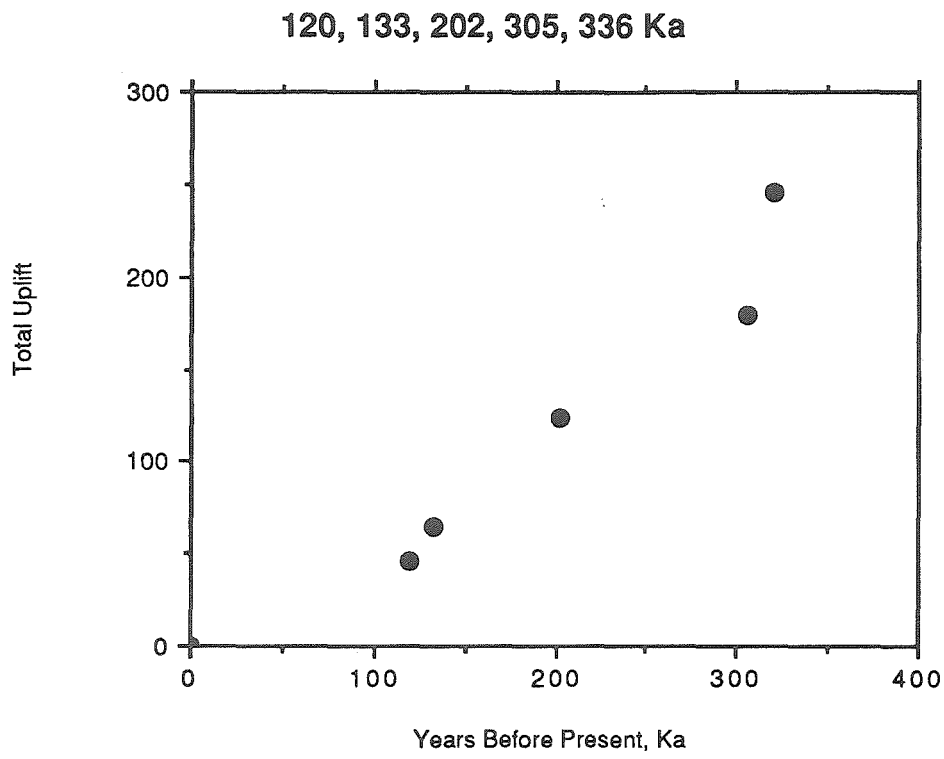


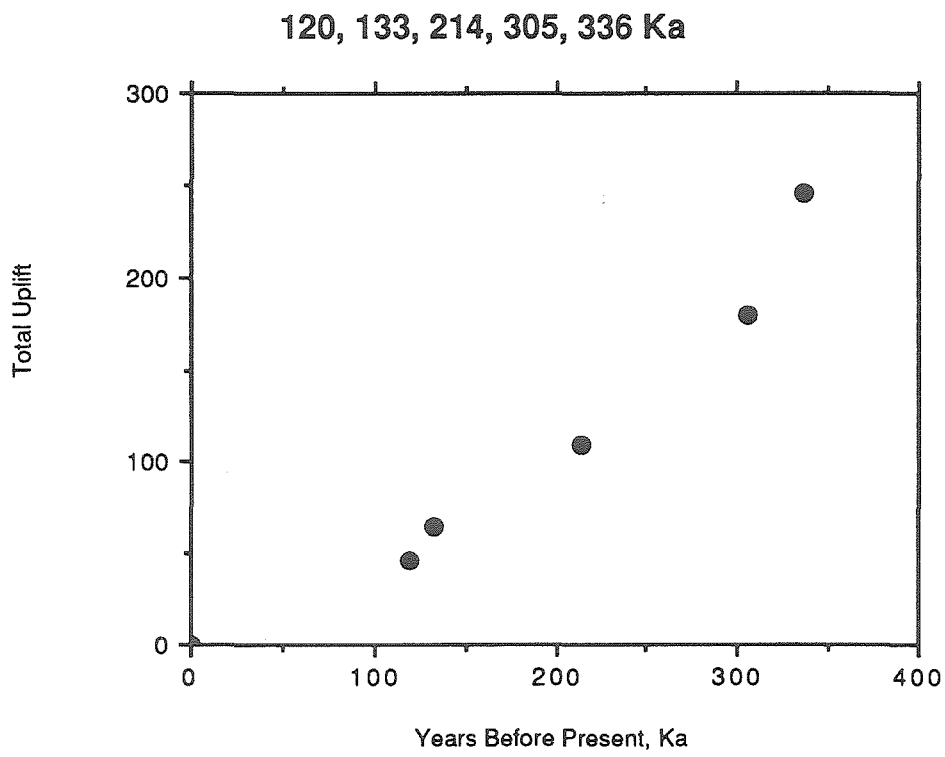
120, 133, 202, 305, 336 Ka



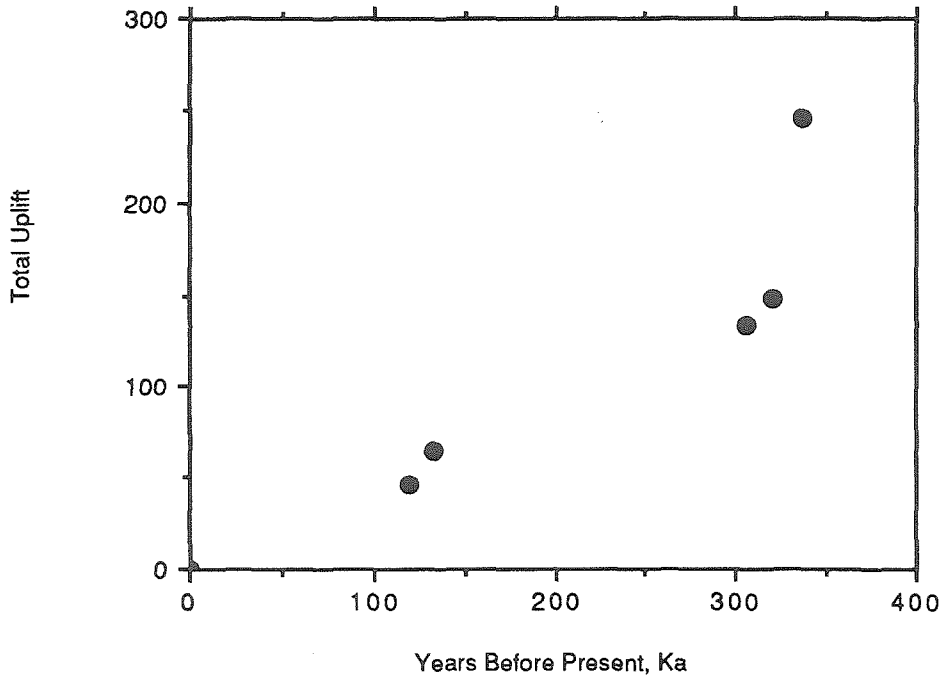
120, 133, 202, 320, 336 Ka

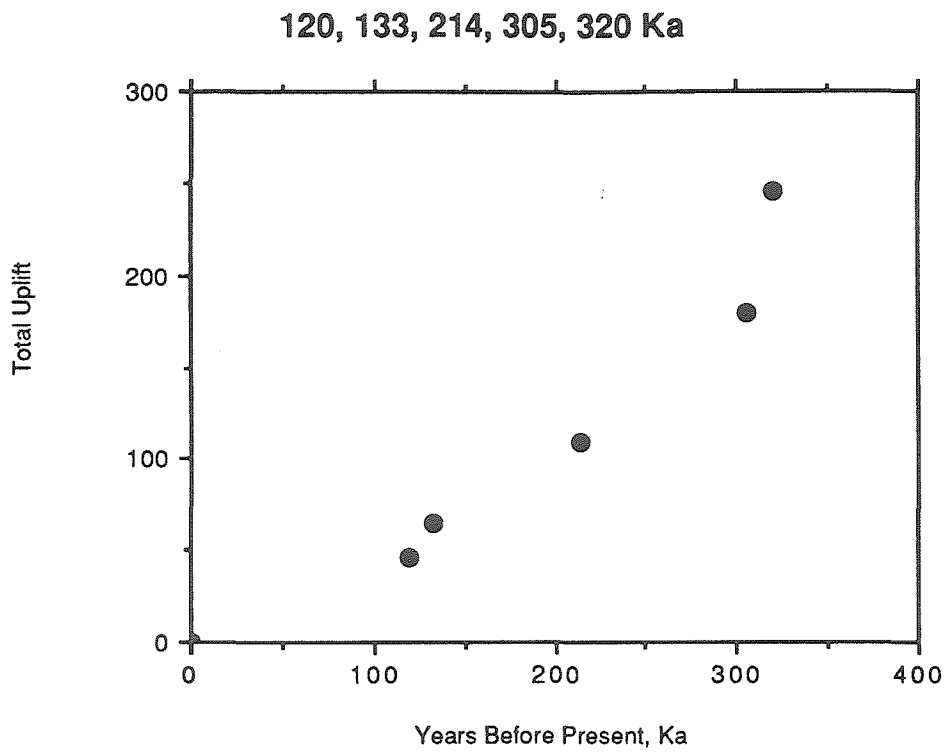


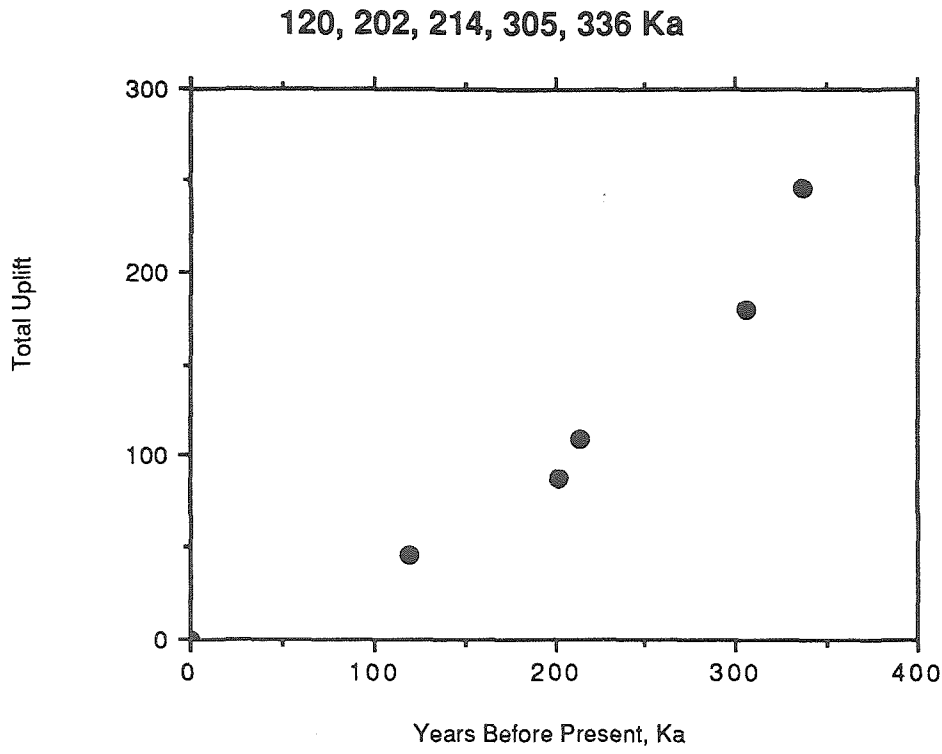


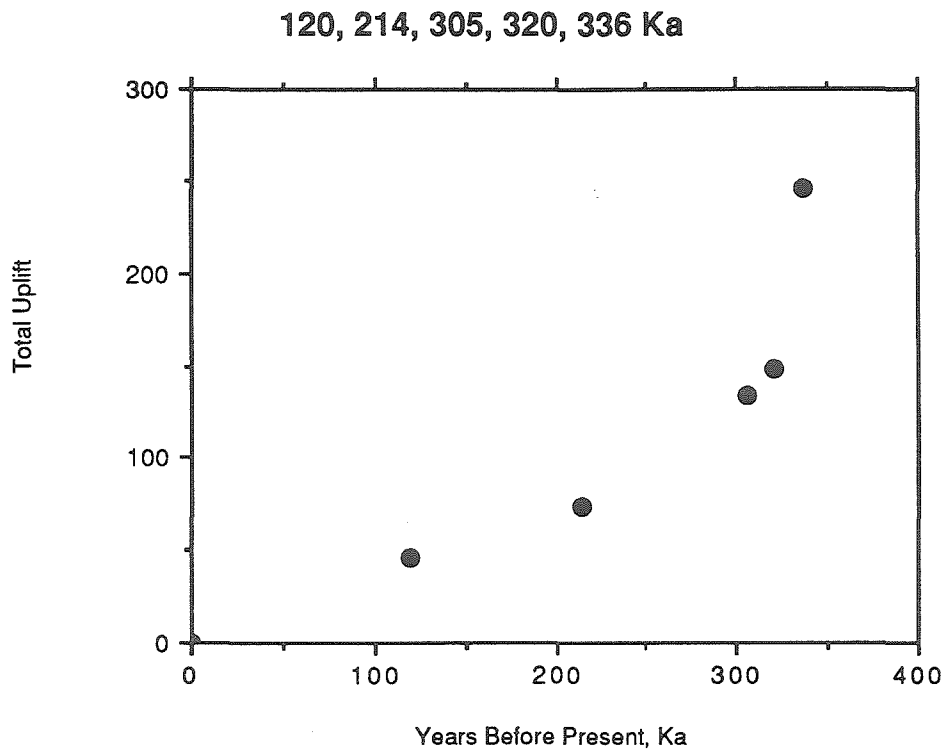


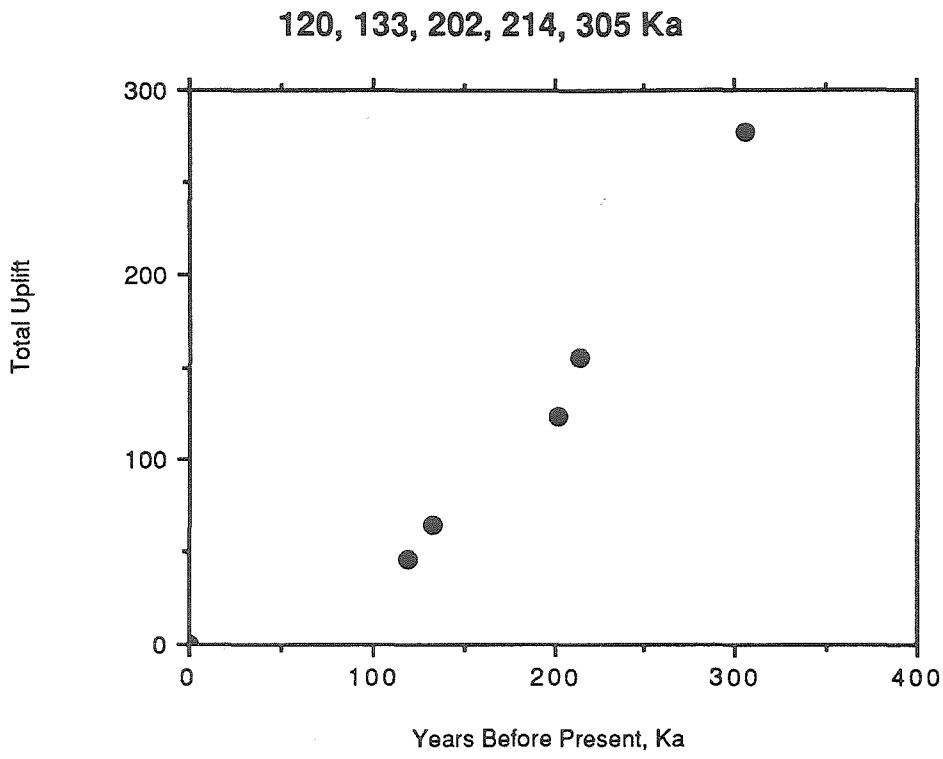
120, 133, 305, 320, 336 Ka

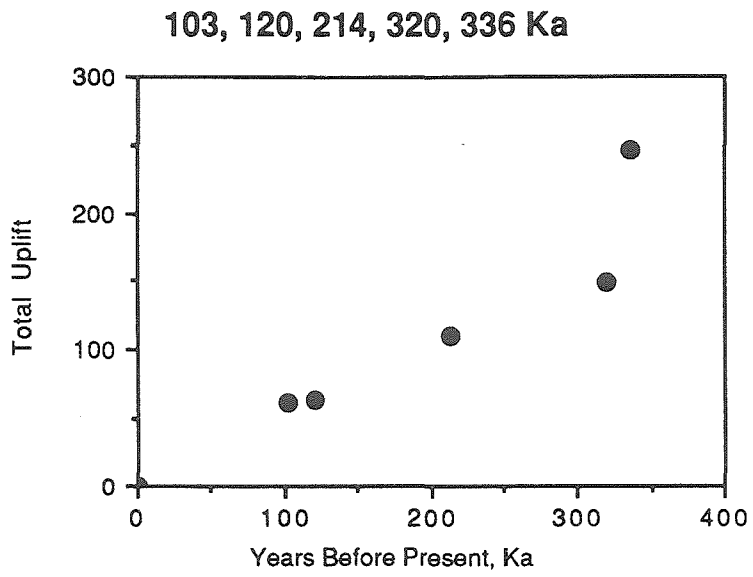


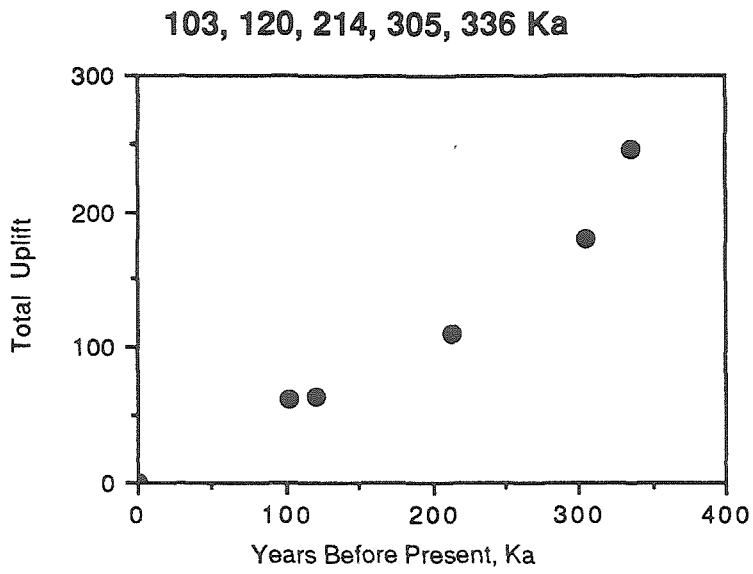


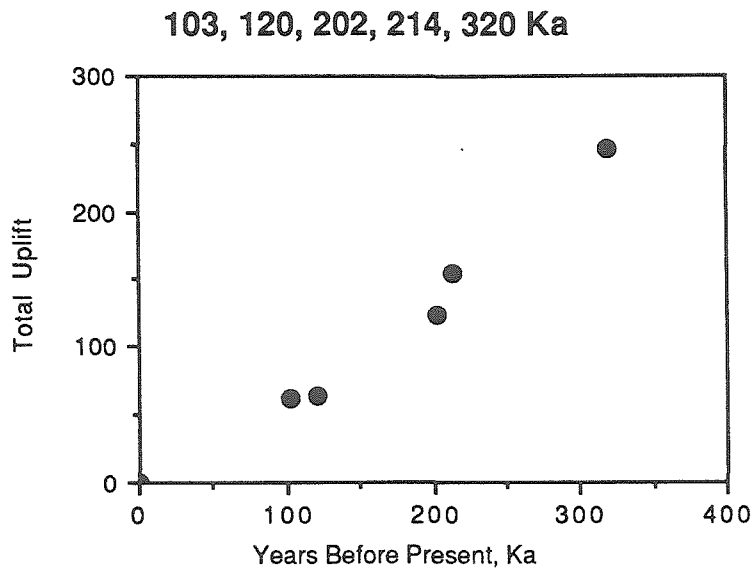


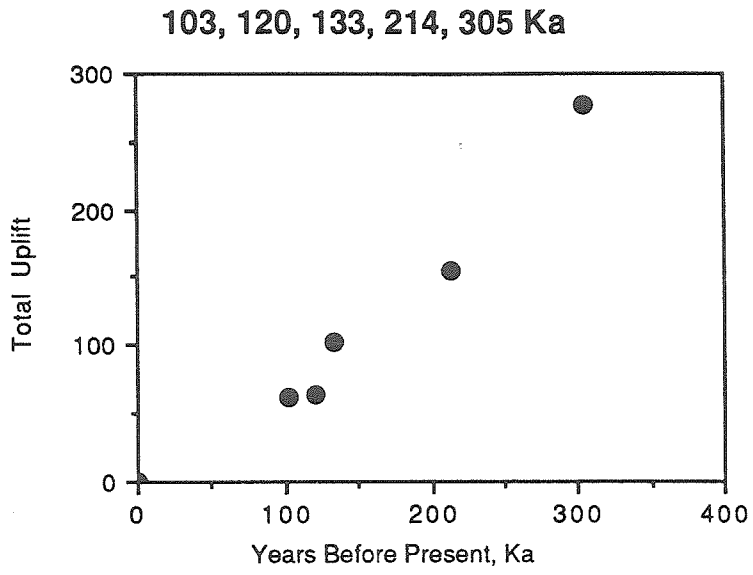


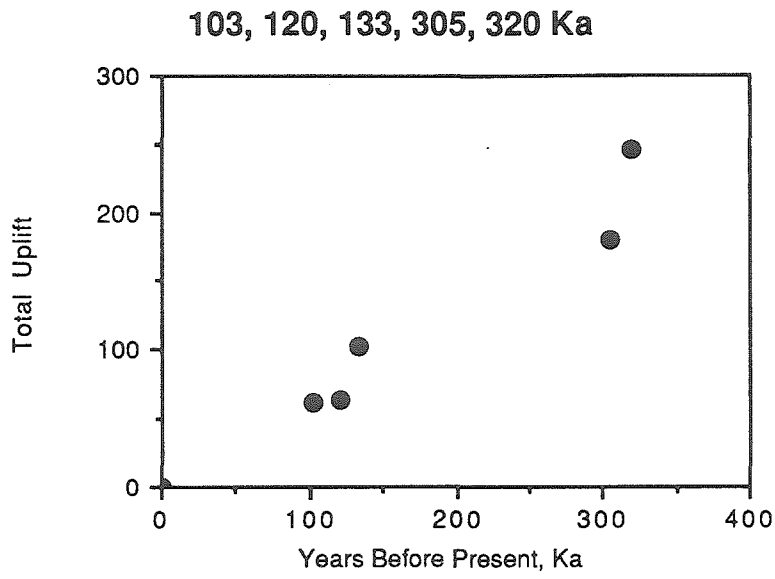




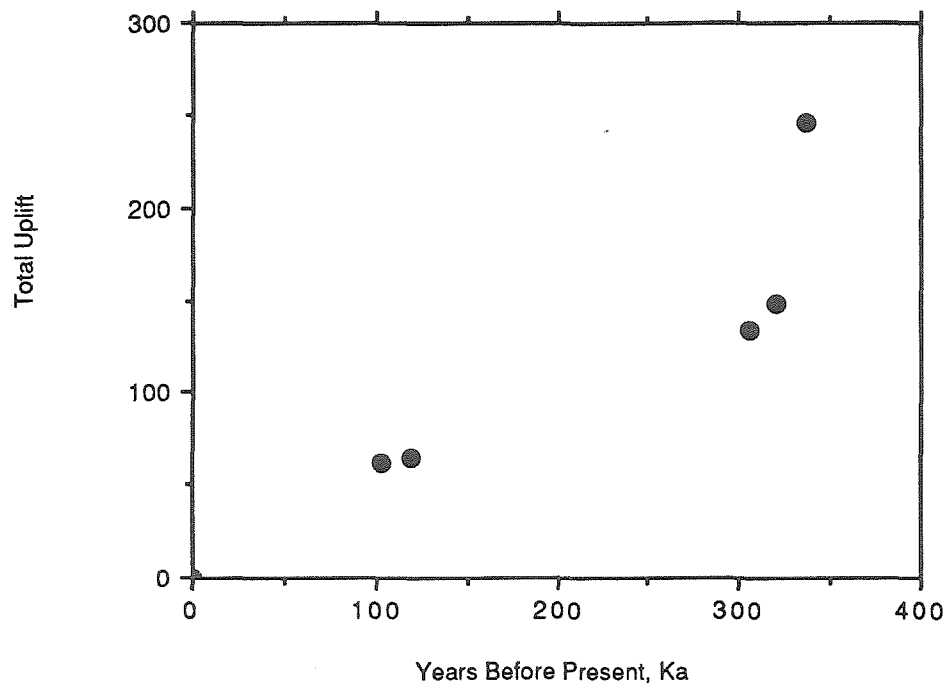




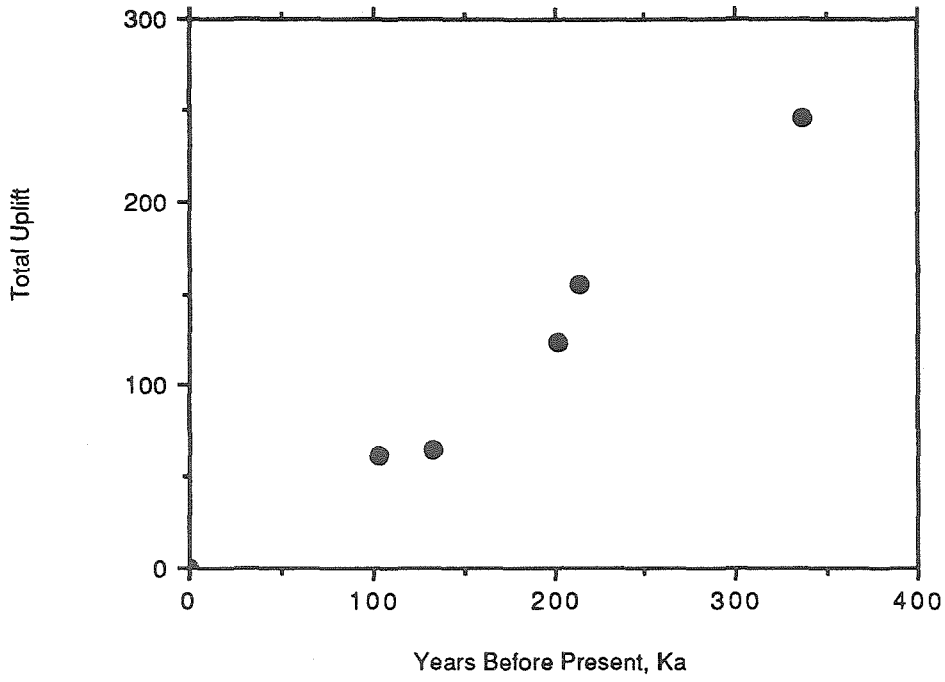




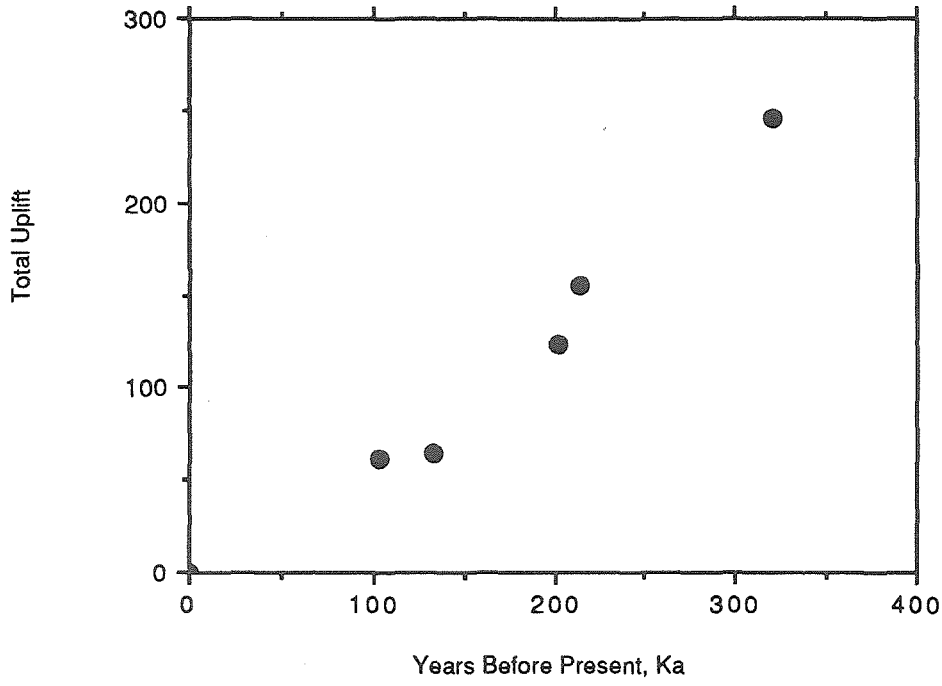
103, 120, 305, 320, 336 Ka

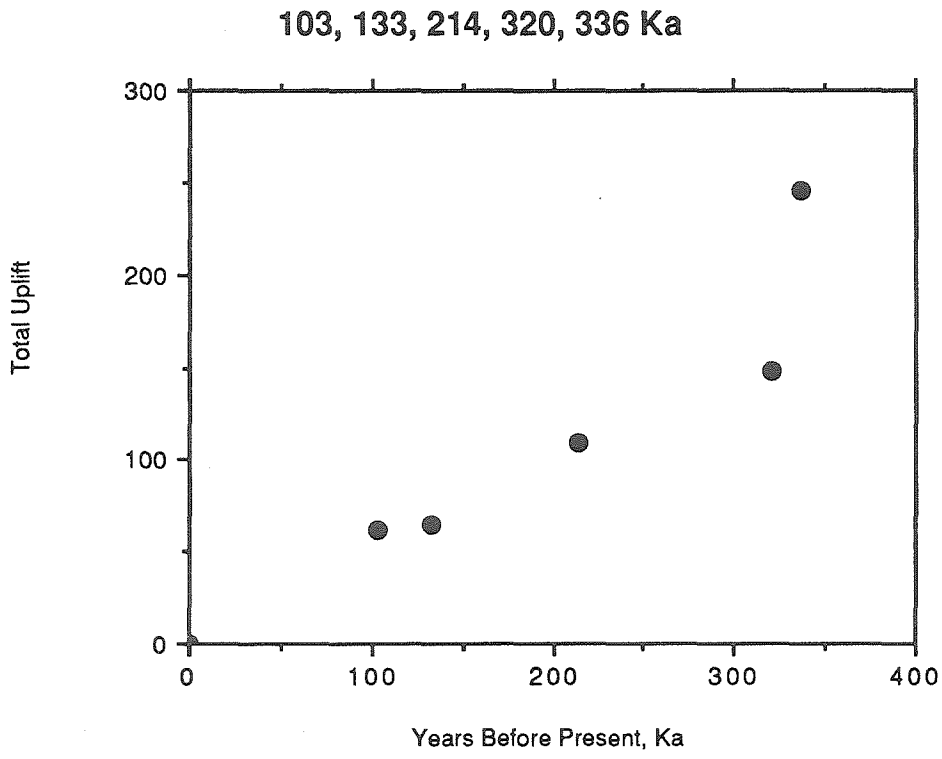


103, 133, 202, 214, 336 Ka

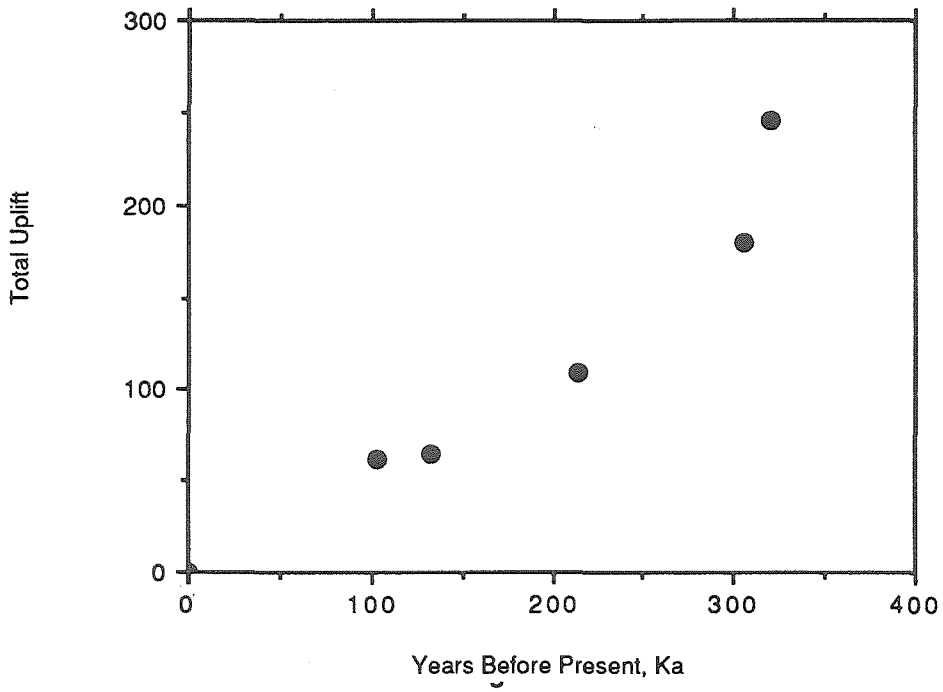


103, 133, 202, 214, 320 Ka

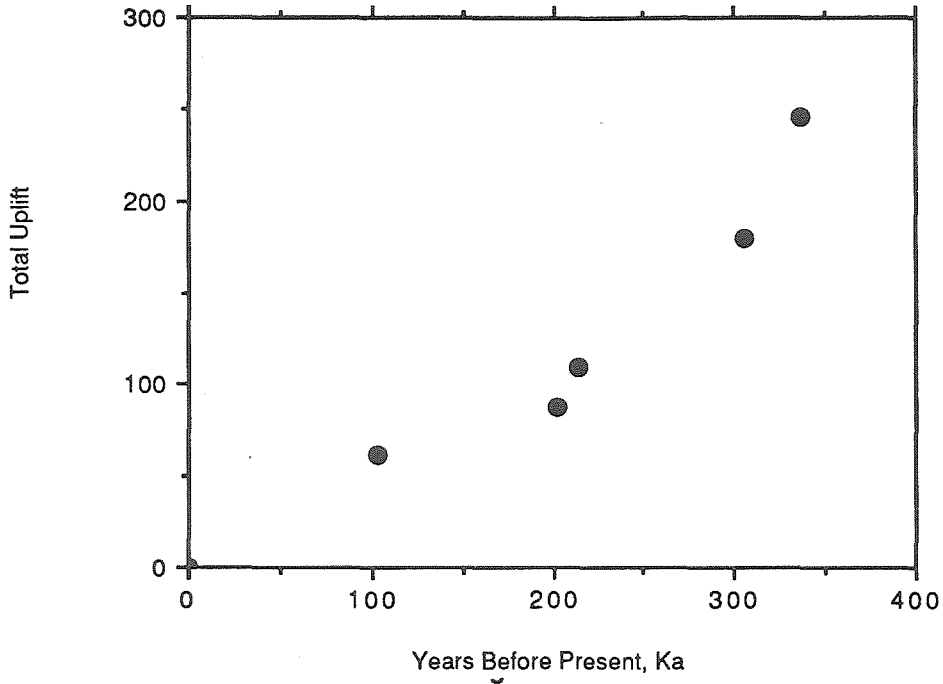


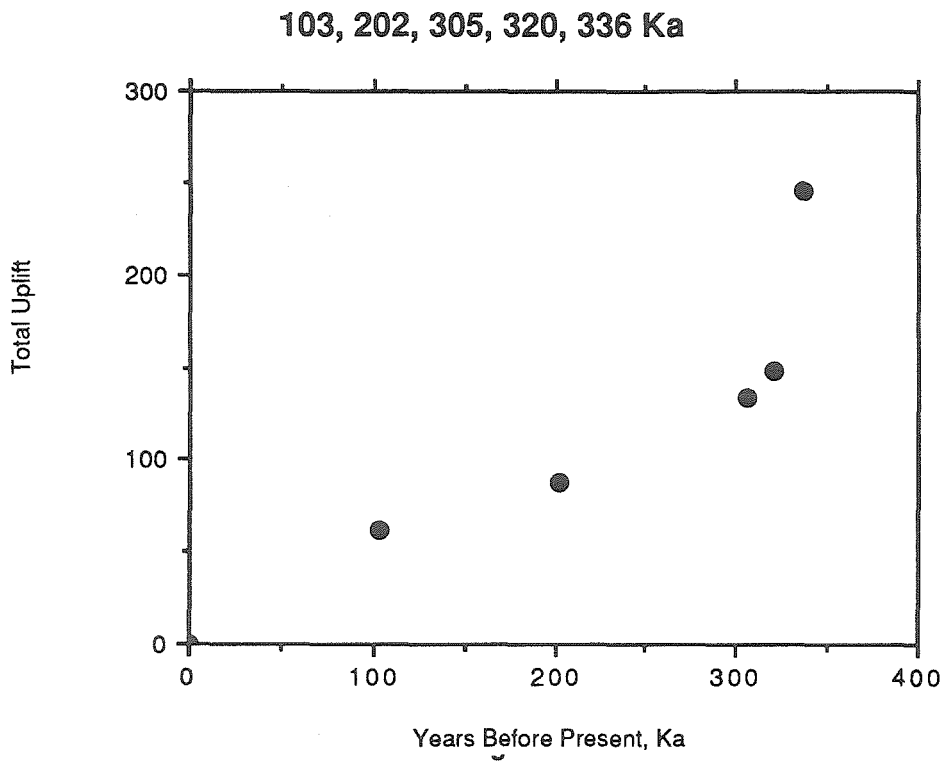


103, 133, 214, 305, 320 Ka

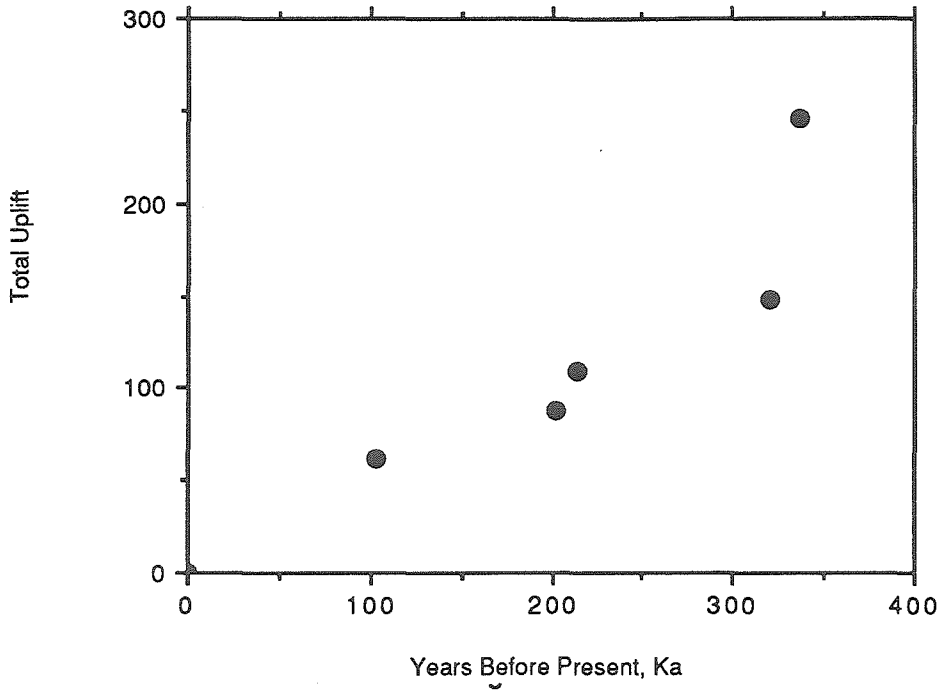


103, 202, 214, 305, 336 Ka

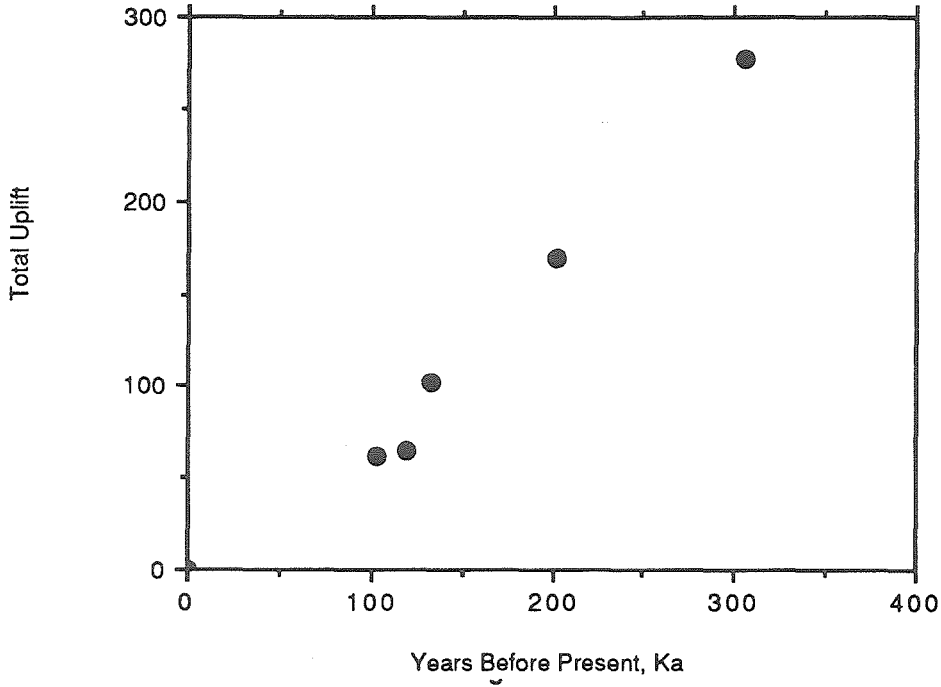


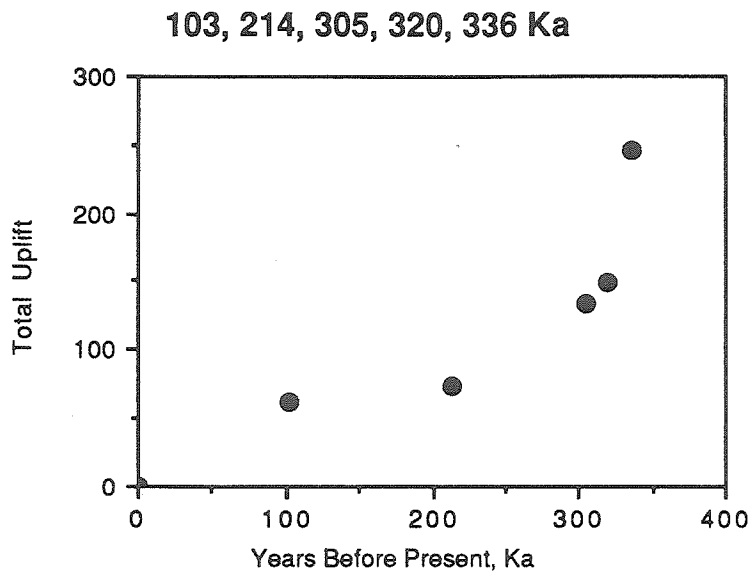


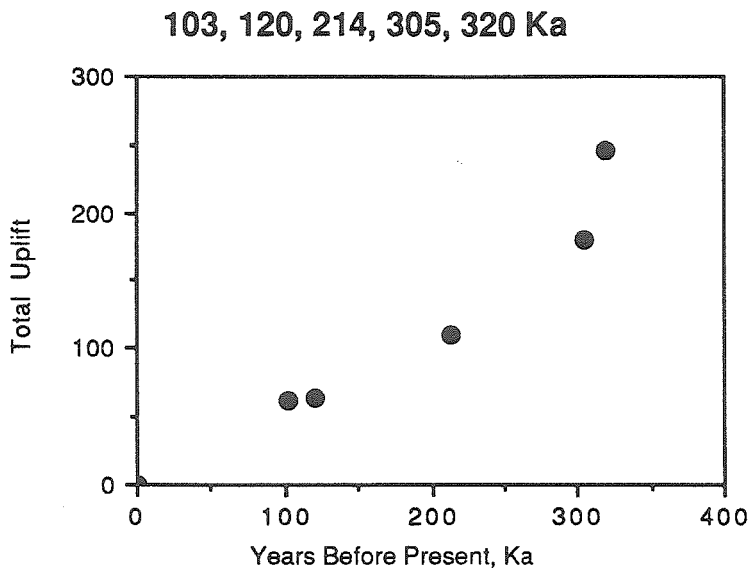
103, 202, 214, 320, 336 Ka

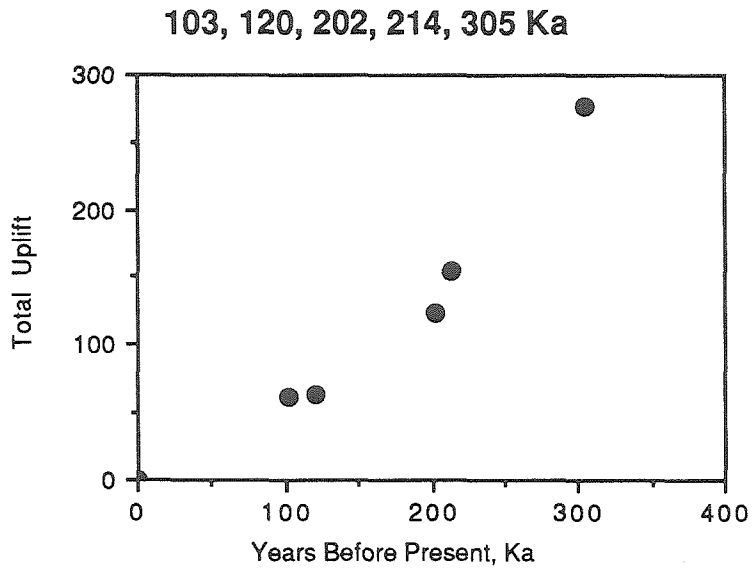


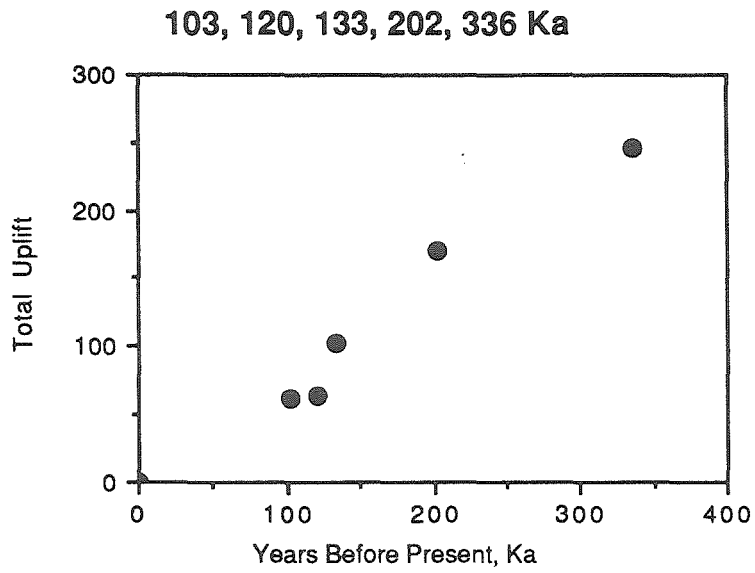
103, 120, 133, 202, 305 Ka

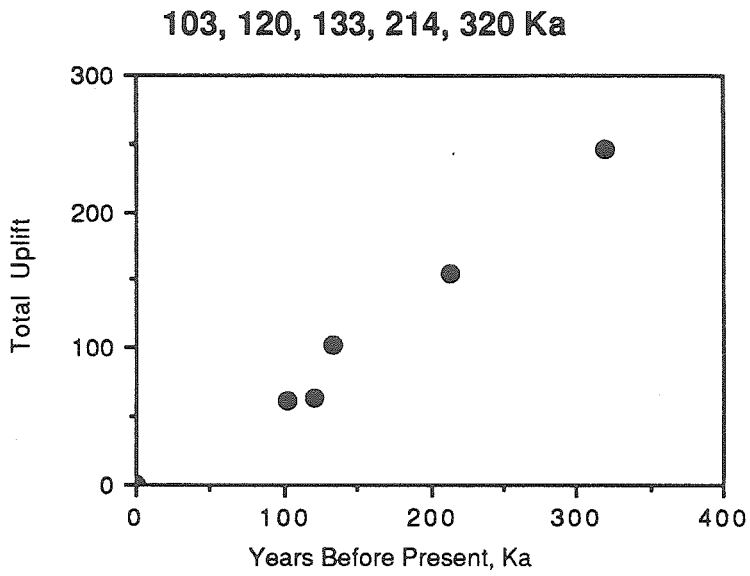


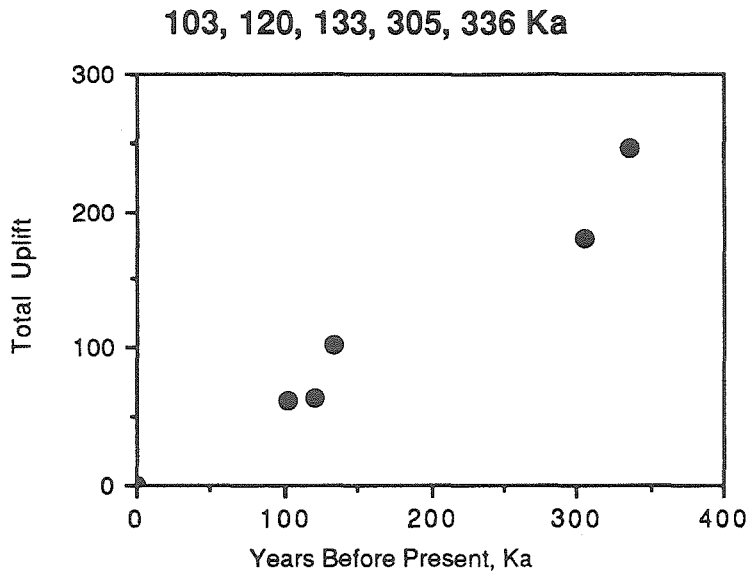


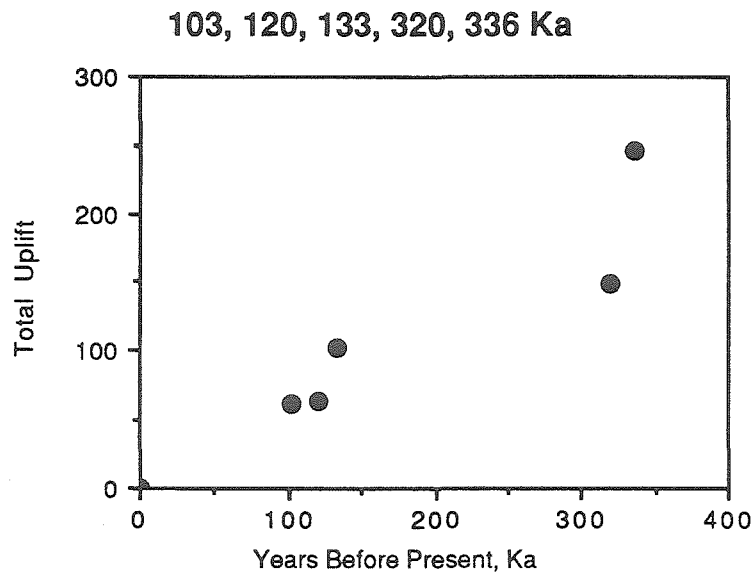


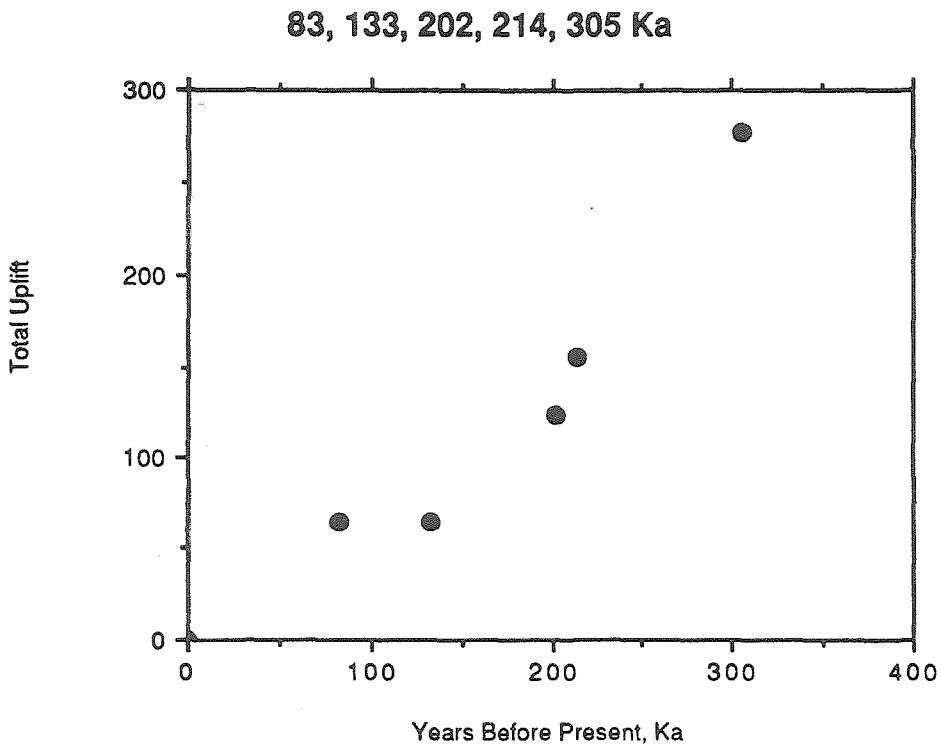


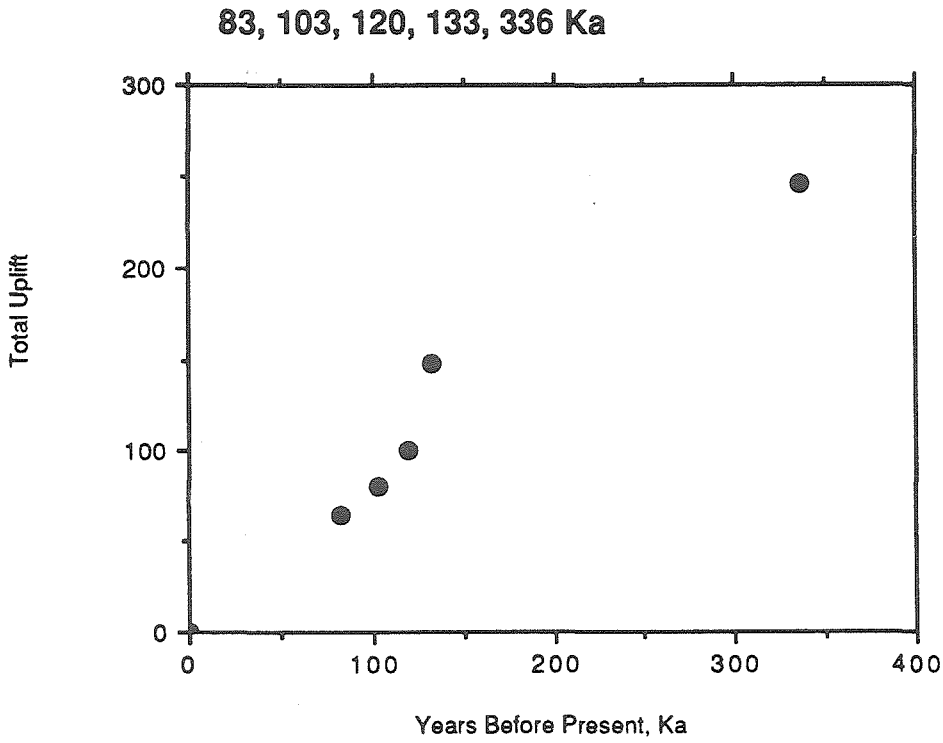


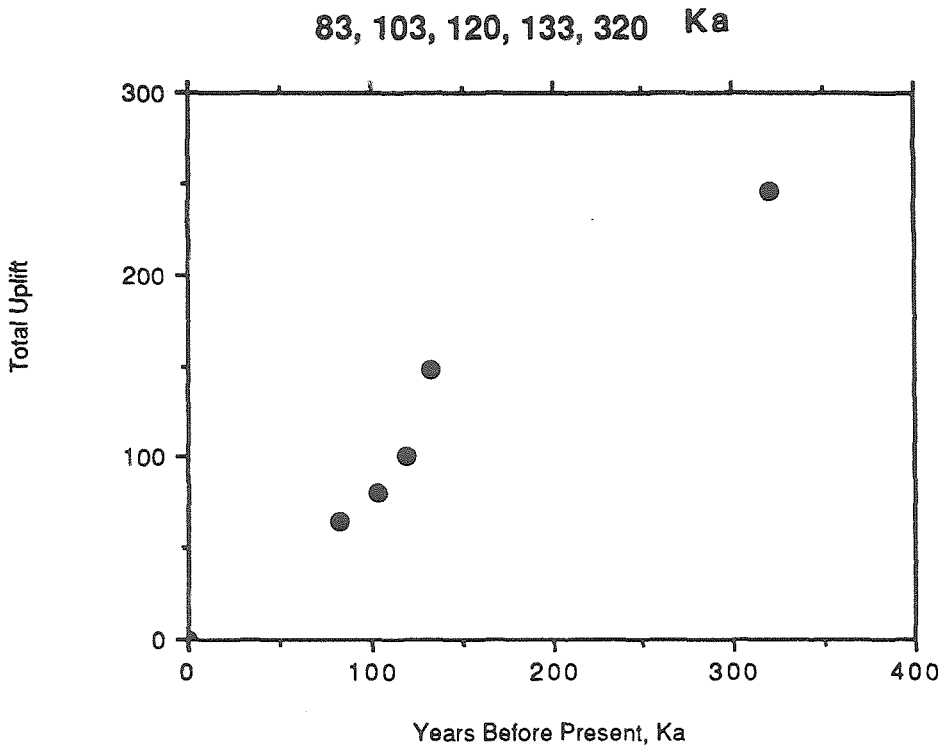


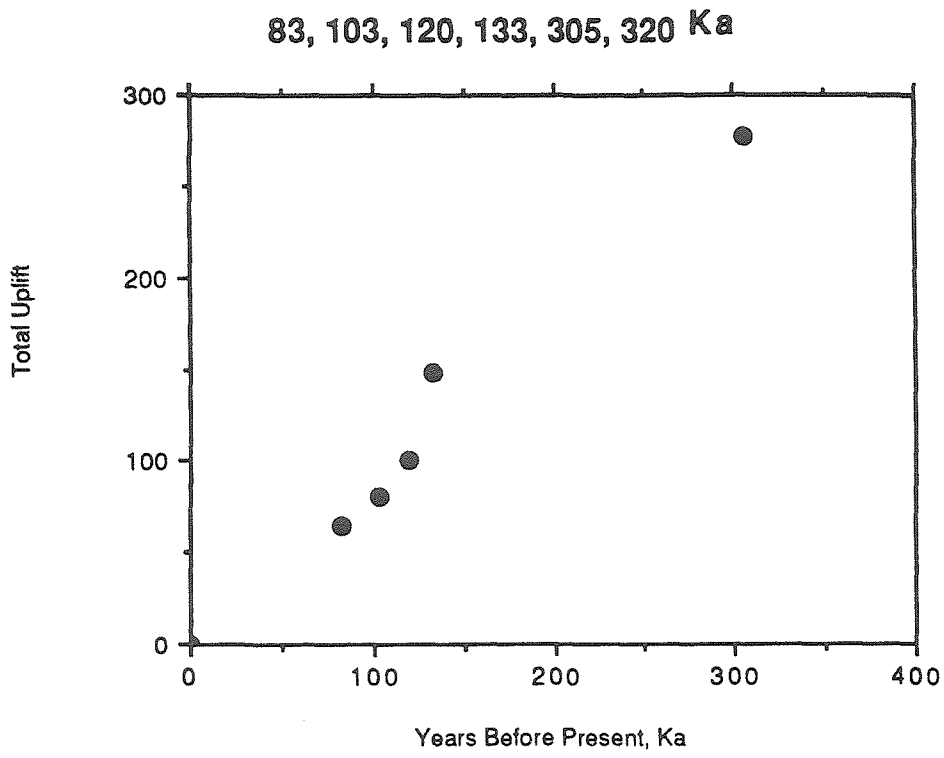


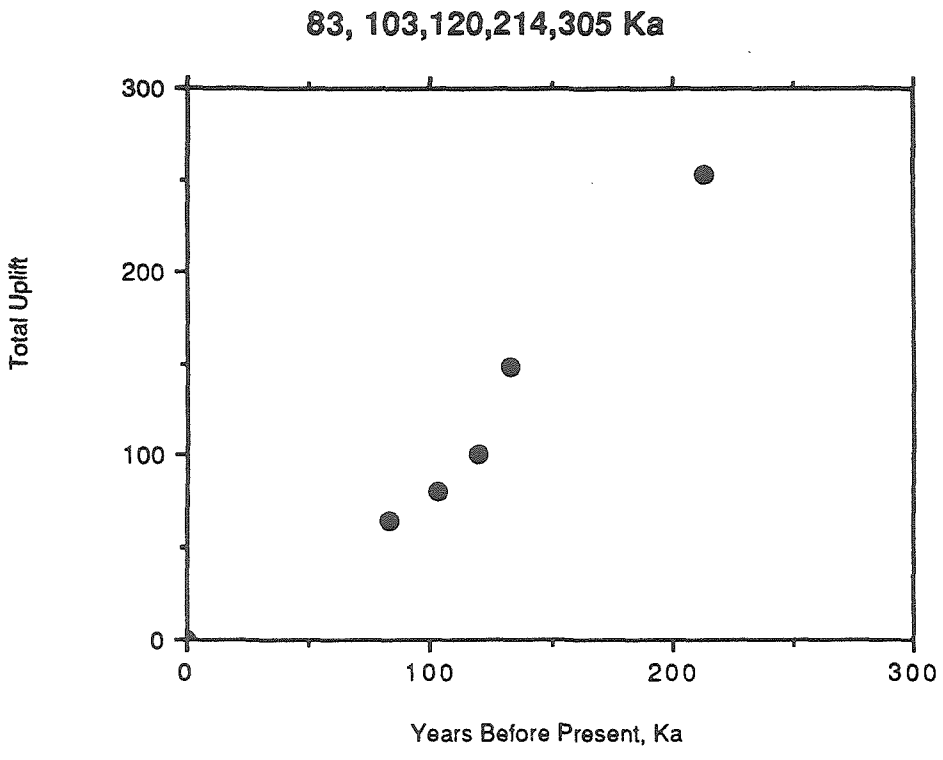




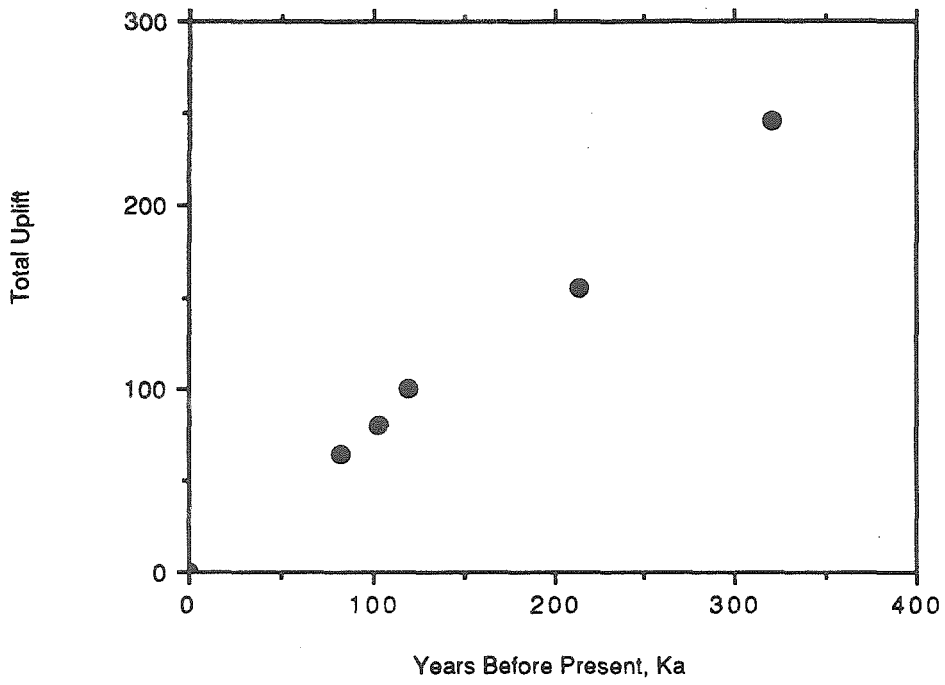




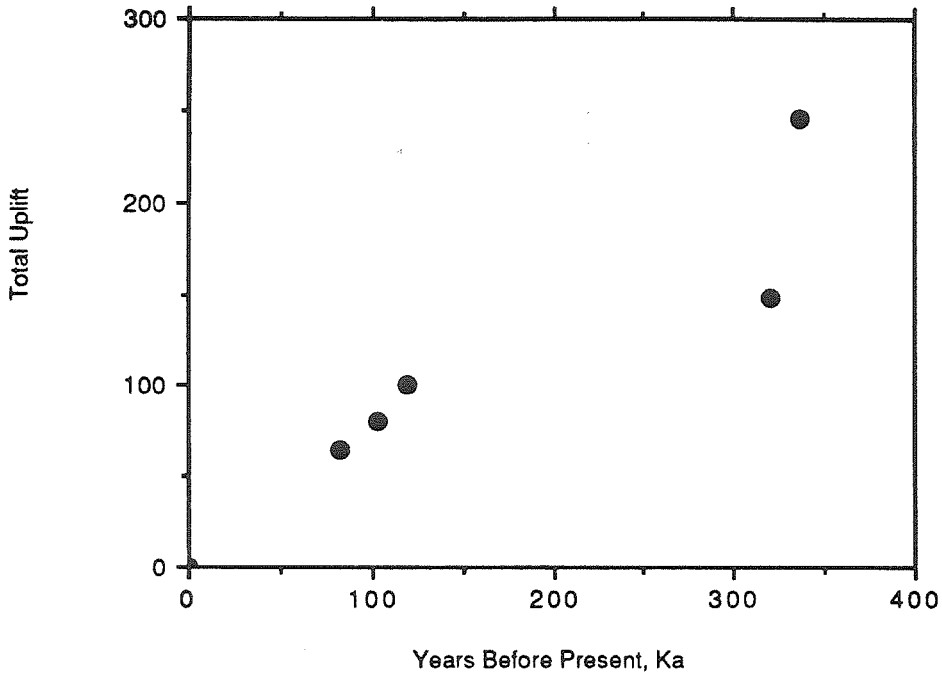


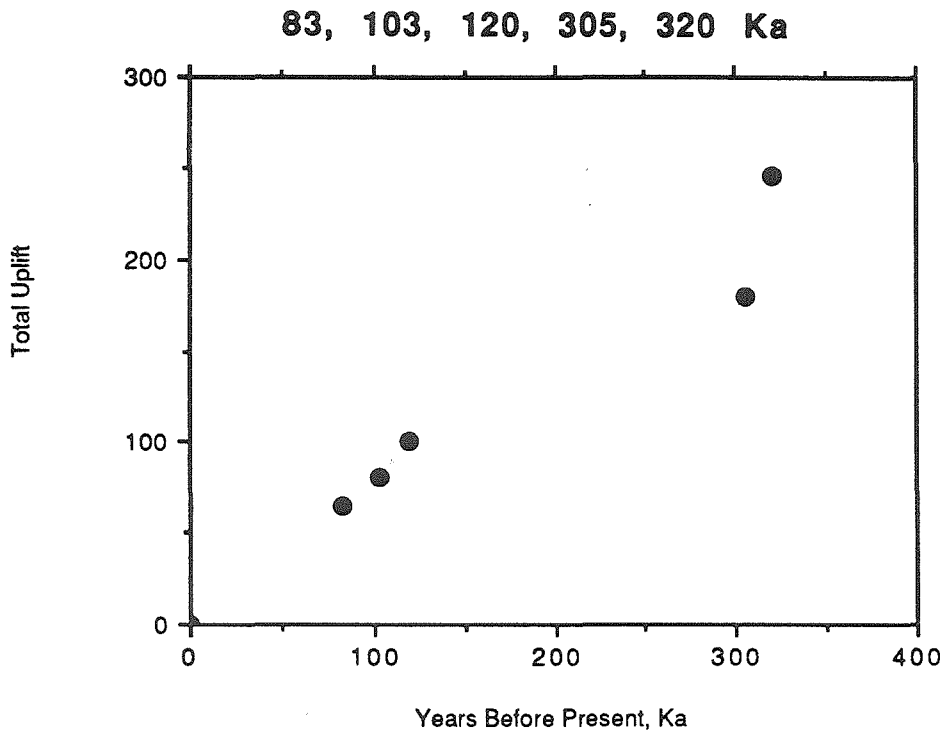


83, 103, 120, 214, 320 Ka

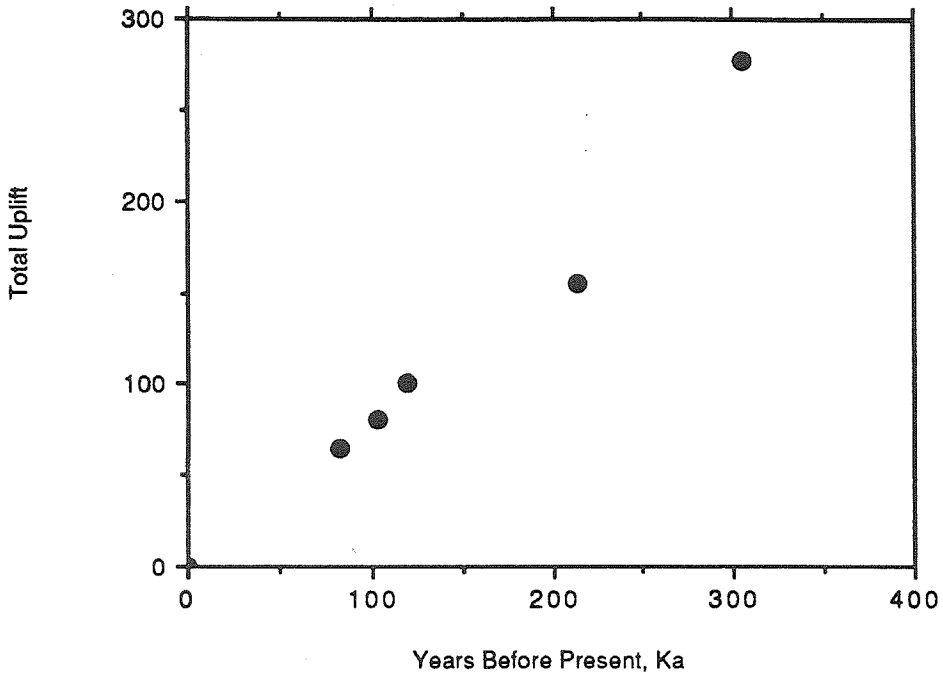


83, 103, 120, 320, 336 Ka

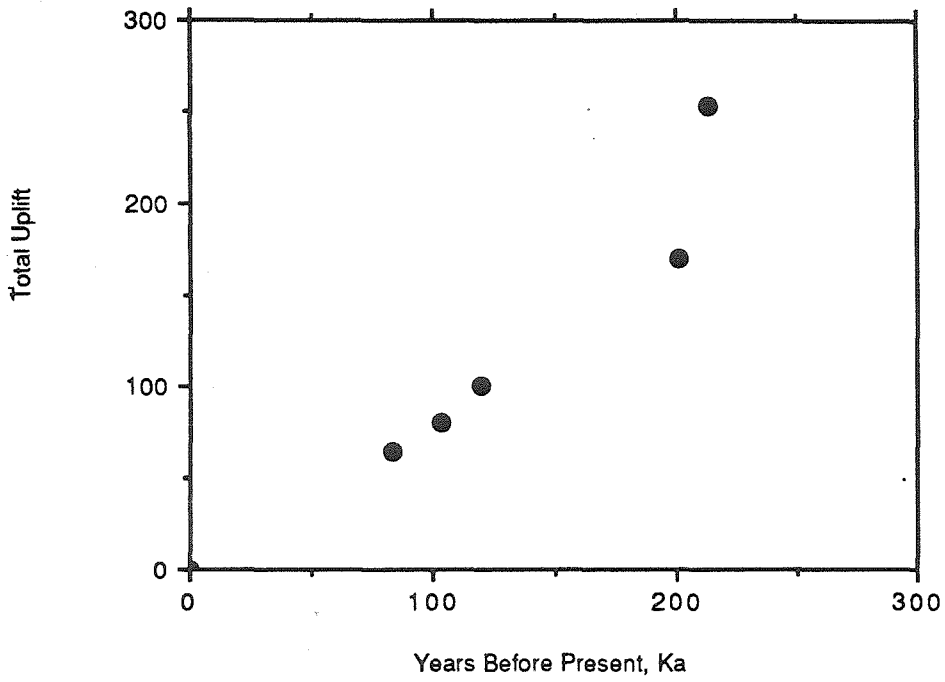




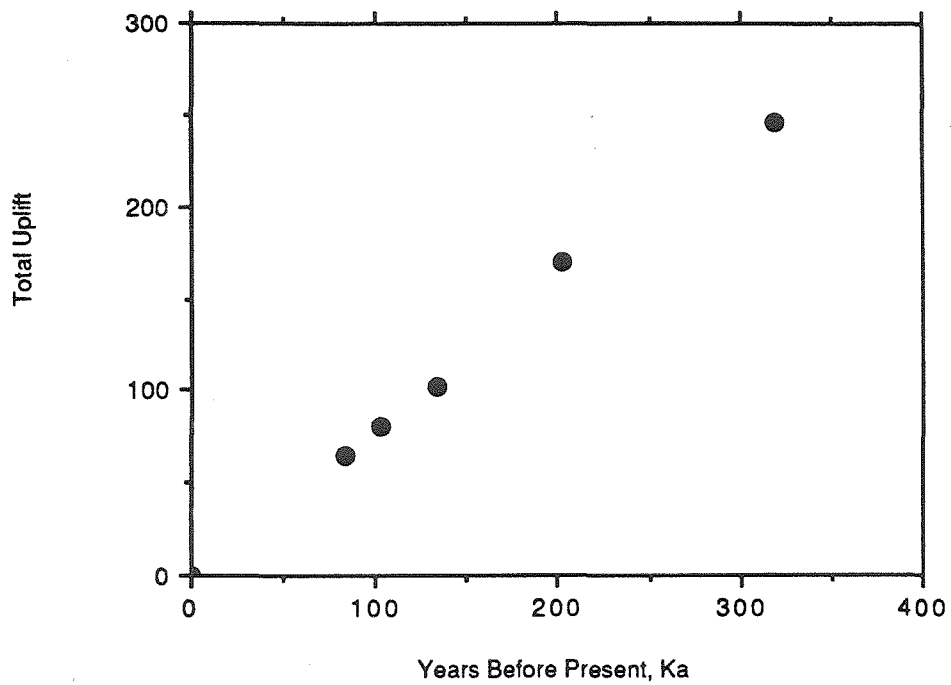
83, 103, 120, 214, 305 Ka



83, 103, 120, 202, 214 Ka



83, 103, 133, 202, 320 Ka



APPENDIX B: Correspondence

The following correspondence was received from C.W. Naeser and J.C. Ingle regarding samples collected from the Ohlson Ranch Formation.

To: Carol Prentice

From: C. W. Naeser

C. W. Naeser

Fission-track age report

Fri, May 13, 1988

SAMPLE	DF-	MINERAL	NUMBER GRAINS	ρ_s	FOSSIL	ρ_i	INDUCED	s'	NEUTRON	COUNTED	Ma	$\pm 2\sigma$
				$\times 10^6$ t/cm ²	TRACKS	$\times 10^6$ t/cm ²	TRACKS		DOSE $\times 10^{15}$ n/cm ²			
86-FR-1HP	5762	ZIRCON	6	0.533	74	9.46	657		0.988	2638	3.3	0.8

$\lambda_f = 7.03 \times 10^{-17} \text{ yr}^{-1}$ s' = STANDARD ERROR OF THE MEAN OF THE INDUCED COUNT (POPULATION RUNS ONLY)

DF = LABORATORY NUMBER ANALYZED BY: C. W. NAESER

COMMENTS:

STANFORD UNIVERSITY, STANFORD, CALIFORNIA 94305

JAMES C. INGLE
W. M. KECK PROFESSOR
OF EARTH SCIENCES

DEPARTMENT OF GEOLOGY
SCHOOL OF EARTH SCIENCES
(415) 723-2537

January 4th, 1987

Dr. Kerry Sieh
Division of Geological and Planetary Sciences
California Institute of Technology
Pasadena, California 91125

Dear Kerry:

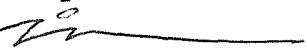
I processed your Point Arena samples for microfossils using kerosene and floating the washed residues in carbon tetrachloride. Only sample 86-PAOR-1 yielded foraminifera and one lone ostracod. The fauna in sample 86-PAOR-1 includes the following species of foraminifera;

Elphidium clavatum Cushman, *med. London & Tappan*
Buccella tenerrima (Bandy)
Cibicides fletcheri Galloway & Wissler
~~Cibicides frigidum (Cushman)~~
Dyocibicides biserialis Cushman & Valentine
Elphidiella hannai (Cushman & Grant)
Elphidium sp. (juvenile)
Globigerina bulloides d'Orbigny
Oolina costata (Williamson)
Pullenia cf. salisburyi Stewart & Stewart
Trifarina angulosa (Williamson)

All of these taxa are still living along the Pacific Coast of North America and are therefore not truly age diagnostic although they indicate a broad age of Pliocene to Recent. As I told you in our brief discussion a few weeks ago, I would anticipate a warm fauna in lower Pliocene deposits of this character. Thus, the age is likely upper Pliocene or Pleistocene. The species composition of the fauna is representative of an inner shelf setting and water depths of 60-10 m. Infact, the species mix is typical of inner shelf deposits off northern California today. However, it is apparent that dissolution has affected most of the specimens and it may well be possible that some species originally present are not represented in this assemblage. Although this faunas does not provide any really startling evidence of age or environment it does suggest useful faunas are present in the units you are working on in the Point Arena area.

My very best wishes to you and your family for a joyous 1987!

With very best wishes,



JAMES C. INGLE
W. M. KECK PROFESSOR
OF EARTH SCIENCES

DEPARTMENT OF GEOLOGY
SCHOOL OF EARTH SCIENCES
(415) 723-2537

February 12th, 1988

Ms. Carol Prentice
P. O. Box 727
Point Arena, California 95468

Dear Carol:

I enjoyed working with you this week and was pleased you were able to spend some time at Stanford. It was too bad that your Olson Ranch samples did not yield more foraminifera--however, the three that did contain useful assemblages. As you are aware, I have mounted representative foraminifera from sample 87-OR-51A on a glued and numbered faunal slide; the attached list provides the names of the species identified and their location on the slide. I did not arrange and mount specimens from samples 87-OR-51B and 54 but rather simply provide species lists from my analysis of your scatter mounts. All three faunal slides are enclosed with this letter.

The foraminiferal faunas in samples 87-OR-51A & B are more diverse than the fauna I analyzed earlier from sample 86-PAOR-1 as reported in my letter to Kerry Sieh dated January 4th, 1987. However, as is the case with 86-PAOR-1, the species present in samples 87-OR-51 A & B and 54 are all still living along the Pacific Coast of North America. Hence, they do not provide definitive biostratigraphic evidence of the age of the Olson Ranch Formation. Nevertheless, the faunas are clearly post-Miocene and are typical of Pliocene, Pleistocene, and Holocene shelf deposits in this region. More specifically, I would expect to see more warm water taxa in shelf deposits of early Pliocene age and higher percentages of truly cool water taxa than are present in your samples if they were late Pleistocene in age. Thus, the paleoceanographic character of your assemblages suggests a mid to late Pliocene age.

The abundances of Elphidium and Buccella and common occurrences of Cassidulina limabata and Florilus (Nonionella) basispinata point to deposition of your assemblages in an inner to mid shelf environment at water depths between 30 and 60 meters. In fact, your Olson Ranch assemblages are strikingly close in composition to Recent faunas characterizing the boundary between the Inner Shelf and Middle Shelf Assemblages off the Sonoma coast of northern California as reported by Quinterno and Gardner in Volume 17, pages 132-152 of the Journal of Foraminiferal Research (April 1987).

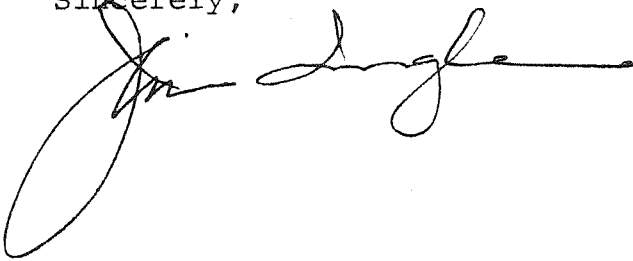
Ms. Carol Prentice
February 12th, 1988
Page 2

As we discussed, it might be very useful to analyze the foraminiferal faunas from the Quaternary marine terraces in the Point Arena area if you can find appropriate samples. Feel free to send material along as I would be very interested in analyzing such samples to confirm my notions about the differences between the Pleistocene and Pliocene faunas in this area.

The Quinterno and Garner (1987) paper I note above is one you might want to look at to obtain an idea of how modern faunas are distributed on the modern shelf of your area. Another classic reference is the 1953 paper by O.L. Bandy entitled "Ecology and paleoecology of some California foraminifera" in volume 27, pages 161-203 of the Journal of Paleontology.

The best of luck and success in your continuing studies of the Point Arena area. Come back and see us.

Sincerely,

A handwritten signature in black ink, appearing to be "Jim Douglas", written in a cursive style. The signature is positioned below the word "Sincerely," and above the "Enc." text.

Enc.

ANALYSIS OF FORAMINIFERA FROM THE OLSON RANCH FORMATION, POINT
ARENA, CALIFORNIA *

Sample 87 OR 51 A

Numbers below refer to square number on the prepared faunal slide.

1. Elphidium clavatum Cushman emend. Loeblich & Tappan
2. Buccella frigida (Cushman)
3. Buccella tennerima (Bandy)
4. Nonion sp.
5. Elphidium granulosus (Galloway & Wissler)
6. Cassidulina limbata Cushman & Hughes
7. Cassidulina tortuosa Cushman & Hughes
8. Trifarina (Angulogerina) baggi (Galloway & Wissler)
9. Buccella sp.
10. Bolivina vauhani Natland
11. Buliminella elegantissima (d'Orbigny)
12. Florilus (Nonionella) basispinata (Cushman & Moyer)
13. Elphidium clavatum Cushman emend. Loeblich & Tappan
14. Lagena acuticosta Reuss
15. Planulina depressa (d'Orbigny)
16. Elphidium cf. incertum Williamson
17. Cibicides fletcheri Galloway & Wissler
18. Cibicides lobatus (d'Orbigny)
19. Globigerina quinqueloba Natland
20. Discorbis sp.
21. Globigerina bulloides d'Orbigny
22. Textularia sp.
23. Florilus (Nonionella) miocenica stella (Cushman & Moyer)
24. Cassidulina sp.

Sample 87 OR 51 B

- Bolivina vauhani Natland
Buccella frigida (Cushman)
Buccella sp.
Buccella tennerima (Bandy)
Buliminella elegantissima (d'Orbigny)
Cassidulina bradshawi Uchio
Cassidulina limbata Cushman & Hughes
Cibicides fletcheri Galloway & Wissler
Cibicides lobatus (d'Orbigny)
Discorbis sp.
Elphidium clavatum Cushman emend. Loeblich & Tappan
Fissurina lucida (Williamson)
Florilus (Nonionella) basispinata (Cushman & Moyer)
Florilus (Nonionella) miocenica stella (Cushman & Moyer)
Fursenkoina (Virgulina) bramletti (Galloway & Moyer)
Globigerina bulloides d'Orbigny
Lagena acuticosta Reuss
Oolina catenulata (Williamson)

* Analysis by J.C. Ingle, Stanford University

Sample 87 OR 54

Buccella frigida (Cushman)

Buliminella elegantissima (d'Orbigny)

Cassidulina sp.

Elphidium clavatum Cushman emend. Loeblich & Tappan

Elphidium incertum Williamson

Florilus (Nonionella) basispinata (Cushman & Moyer)

Globigerina bulloides d'Orbigny

Oolina catenulata (Williamson)

Trifarina (Angulogerina) baggi (Galloway & Wissler)